2020:00505- Unrestricted

Report

AniConFilm

Subtitle

Author(s)
From SINTEF AS: Astrid Sofie Vardøy, Kristine Kaspersen, Branson Belle, Jon Tschudi and Grégory Bouquet
From CondAlign AS: Marie-Audrey Raux, Phillip Mayhew and Henrik Hemmen

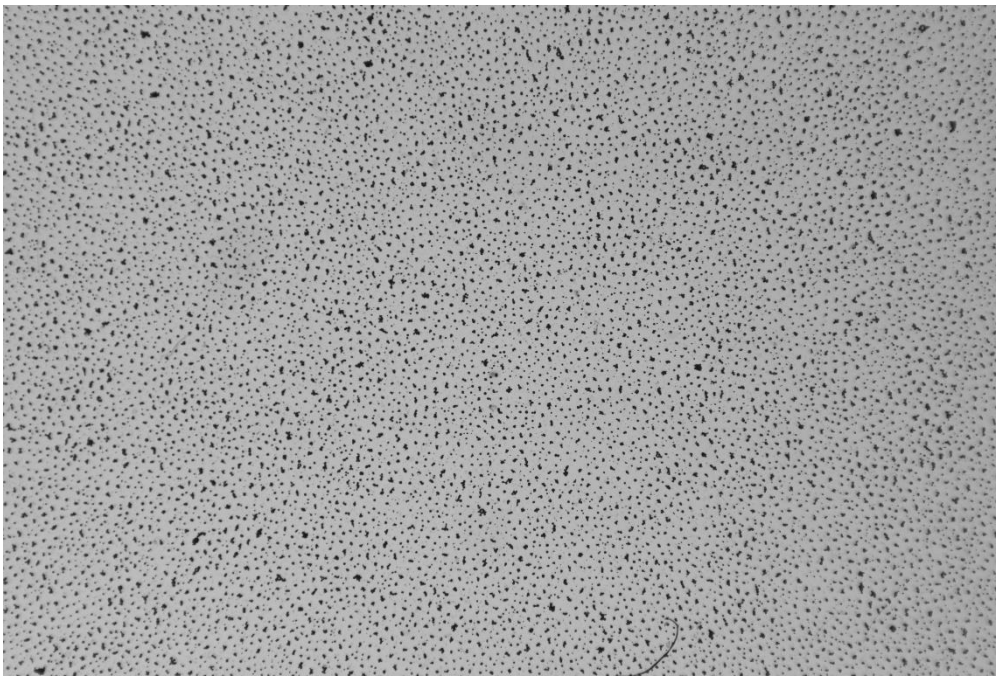

SINTEF Digital
Optics
2020-05-19

SINTEF

SINTEF Digital
SINTEF Digital
Address
Postboks 124 Blindern
NO-0314 Oslo
NORWAY
Switchboard: +47 40005100

info@sintef.no

Enterprise /VAT No
NO 919 303 808 MVA

Report

AniConFilm

Subtitle

KEYWORDS:
Anisotropic Conductive Film,
Conductivity,
Scanning Electron Microscopy,
Optic,
Machine Vision,
On-line monitoring

VERSION
1

DATE
2020-05-19

AUTHOR(S)
From SINTEF AS: Astrid Sofie Vardøy, Kristine Kaspersen, Branson Belle, Jon Tschudi and Grégory Bouquet
From CondAlign AS: Marie-Audrey Raux, Phillip Mayhew and Henrik Hemmen

CLIENT(S)
Forskningrådet

CLIENT'S REF.
Aase Marie Hundere Turid
Grøtli Aalholm

PROJECT NO.
102018757

NUMBER OF PAGES/APPENDICES:
97 + Appendices

ABSTRACT

Abstract heading

Anisotropic conductive materials (ACF) are film-type conductive adhesives allowing electrical and mechanical connection. They are used in applications like display production, printable flexible electronics, thermal interface materials. One of the consortium members, CondAlign AS, has developed a process that uses electric fields to align and distribute particles in polymer films. This allows production of ACFs with added functionality and reduced cost compared to other technologies. Today, quality inspection of the fabricated sample is only performed offline and is time consuming. There was a need for developing both offline and online characterization tool to achieve automatic and continuous production of CondAlign s ACF. The project developed a novel, automatic roll-to-roll (R2R) process, with increased production efficiency, for continuous production of anisotropic conductive films (ACF) for electronics and biomedical applications.

PREPARED BY
Gregory Bouquet

SIGNATURE

CHECKED BY
Branson Belle

SIGNATURE

APPROVED BY
Mats Carlin

SIGNATURE

REPORT NO. 2020:00505
ISBN 978-82-14-06503-9
CLASSIFICATION Unrestricted
CLASSIFICATION THIS PAGE Unrestricted

Document history

VERSION	DATE	VERSION DESCRIPTION
Version No. 1	2020-05-19	"[Version description.Use TAB for new line]"

SINTEF

Table of contents

APPENDICES

Impact of the project

The main impacts of the project can be summarised as follows:

1. Anisotropic Conductive Film (ACF) films manufactured by CondAlign were used by SINTEF to design and build an industrial imaging setup and develop an image analysis software
2. An online Imaging system for monitoring the quality of Condalign's R2R process was installed in the CondAlign´s Roll to Roll (R2R) line at the end of February 2020.
3. The CondAlign team was trained by SINTEF in using the camera system inline and can now use it as part of their production line going forward.
4. Inline tests, early March 2020, successfully compared ACF films during production. The optical differentiation system enabled comparing aligned and non-aligned samples without stopping the process line which increased the process continuity for long stretches of samples. Furthermore, the optical system can also differentiate the degree of alignment within the same sample which can be used as a quality test for continuous film production.
5. CondAlign is entering a temporary production for one of its licenced partners and the use of this new optical system will enable continuous production of long lengths of aligned films whilst monitoring the quality of the film. It will decrease the production time for the same amount of material and allow CA to have more R2R resources for new customers and projects.
6. New off-line measurement tools as well as experiment procedure (**D**esign **O**f **E**xperiment) have been established to better characterize ACF samples and improve the manufacturing process of CondAlign
7. The university of Iasi and All Green AS have performed simulation and characterization of ACF using advanced characterization techniques.

1 Introduction

This report summarises two years of research in the AniConFilm project. The partners in the consortium consist of CondAlign and SINTEF from Norway, University of Iasi and All Green AS from Romania. The main contributing partners are specified in each chapter title or are described in the short introductory text. The document consists of a main body and several attached appendices.

This introduction gives a short overview of the background of the project (1.1), which challenges were met at the outset of the project (1.2) and a short description of the structure and summary of the project (1.3).

1.1 Background:

The main objective of this project is to develop a manufacturing process for continuous production of anisotropic conductive films (ACF) for electronics and biomedical applications.

Anisotropic Conductive Films (ACF) are used in many applications, where a mechanical, thermal and/or electronic connection is needed between electronic components, (see Figure 1-1 for an example of application to ultra-fine pitch bonding). The advantage of using ACF's compared to traditional solder is that the mechanical properties of the joint can be tuned through careful selection of the polymer matrix and more importantly, the ACF can be applied as a global film without the need for high resolution deposition techniques since conductivity is only achieved in the vertical direction.

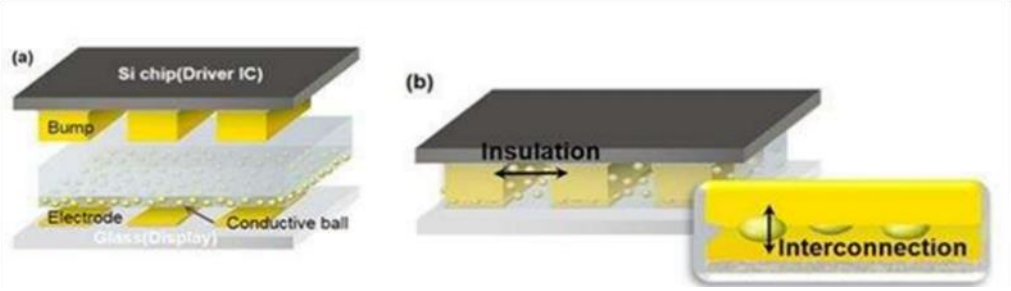

Figure 1-1: Ultra Fine pitch bonding process between bump and electrode using ACF used for the Korea Advanced Institute of Science and Technology (KAIST)

The innovation is based on patented production technology developed by CondAlign [1], in which an electric field is applied to a liquid polymer mixture containing nano/microparticles. The electric field induces electric dipoles in the particles, causing the particles to align into chains, a phenomenon called dielectrophoresis [2], see Figure 1-2 and appendix A.

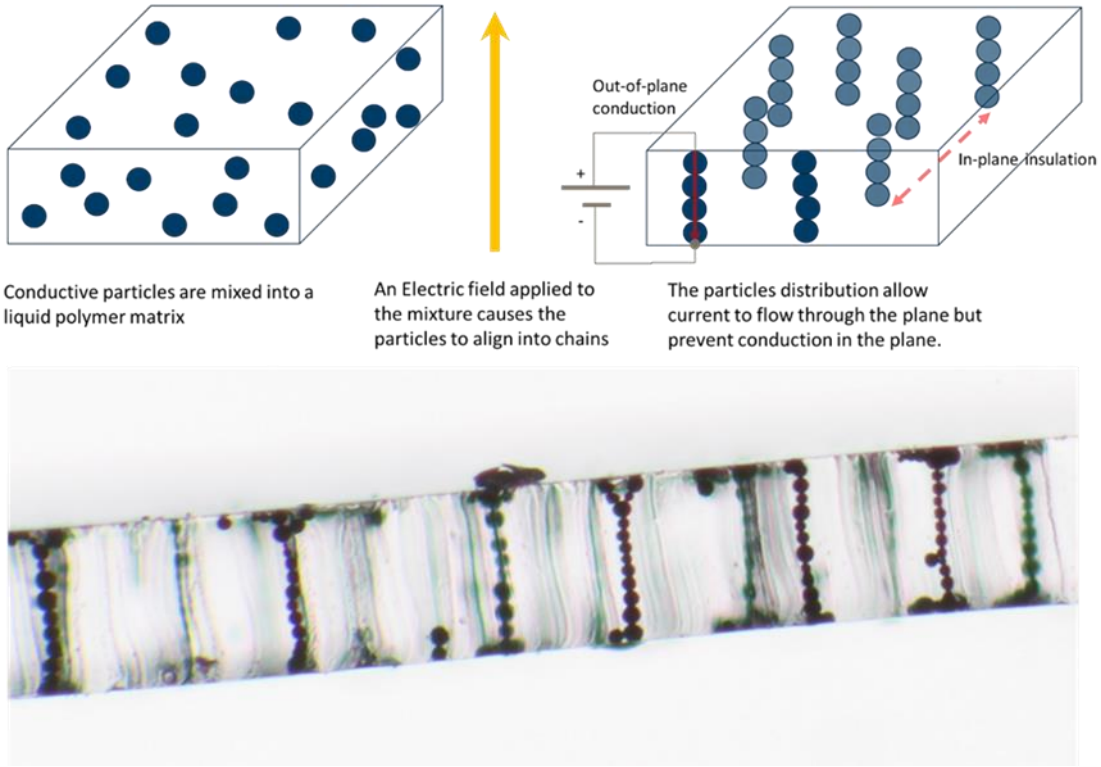

Figure 1-2: Top figure, principle for alignment of particles into chains under the effect of an electric field. Bottom figure, cross section view of an ACF manufactured by CondAlign, showing the particle chains through the film after alignment. Picture courtesy of CondAlign

The chains form permanent pathways through the material, which opens for many potential applications including ECG electrodes (Figure 1-3) and anisotropic conductive films for electronics applications. The alignment typically introduces anisotropy to the finished materials. As an example, a polymer film with metallic particles aligned along the film thickness can have resistivity ten orders of magnitude lower in the direction along the chains than perpendicular to them. Active arrangement of the particles also entail that desired film properties can be achieved with less filler material added to the films. This allows more of the

pure polymer properties to be retained, such as flexibility, transparency, softness, etc while reducing costs as filler materials are normally made of expensive metals (Ag, Au etc).

Figure 1-3: Red Dot™ Foam ECG Monitoring Electrode (3M, St. Paul, MN, USA). One of the envisaged applications of ACF is manufacturing of sticky cardiac electrodes or signal receptive material that can easily stay on the body to capture electrical signals in the body. With sticky ACF, there is no need for hydrogel and electrodes can stay longer on the body. This opens for connected wearable patches enabling potentially long-term monitoring of patient

1.2 Challenges:

The fabrication process of anisotropic conductive film includes three main steps: 1) homogeneous dispersion of nano/micro-particles in a liquid polymer, 2) chain generation and 3) polymer curing for particle locking (see 3.1 for in depth description). After production, characterization tests consisting of electrical and microscopy measurements are performed to assess the quality of the manufactured product. At the outset of this project several challenges in the existing R2R line of CondAlign were identified:

1. Characterization tests are performed offline, are destructive, time consuming and therefore degrade the continuity of the fabrication process
2. Process parameters that influence the final resistivity of the manufactured ACF are not properly identified and therefore the production of ACF is suboptimal.
3. Stability and reproducibility of the web handling.
4. A single syringe pump used for dispensing material prevents continuous production.

In AniConFilm, we focused on finding solutions to challenges 1 and 2. A short description of the work approach is given in the next chapter.

1.3 Structure of the project and executive summary

The project was divided in five work packages (WP).

In WP2, the University of Iasi performed simulations to gain a better understanding of the effect of the particle on the absorption of the electromagnetic energy in ACF's (WP2 presented in 2).

In WP3 and WP4, ACF samples were manufactured with the CondAlign technology and using material from the university of Iasi. The effect of various particle types, dimension and shape, and electrical field parameters on the conductivity of the ACF samples were investigated.
SINTEF, in collaboration with CondAlign worked with establishing methods to measure physical characteristics of ACF's manufactured by CondAlign at various dimension scales:

1) set-ups for measuring macroscopic quantities offline, such as electrical conductivity under pressure (4.2.2) and image analysis algorithms to measure the degree of spatial organization based on microscopy images have been established (4.3).
2) Using SEM, we studied ACF samples at the nanometric scale (4.2.1) and showed physical contact between aligned particles.

The project entailed manufacturing many ACF samples with many varying process parameters. It is usually expensive and time consuming to test every process parameter one at a time. SINTEF and CondAlign have laid out a detailed experimental plan on how to change process parameters and measure changes in process responses in advance of the actual experiment. This procedure, called Design Of Experiment (DOE) is presented in 4.4. Using the DOE, a statistical model that links conductivity to process parameters (particle shape, film thickness, particle concentration) was established.

In WP5, SINTEF in collaboration with CondAlign have worked with optical characterization of the ACF. We have designed, developed and tested an optical system customized for inline imaging of particles. Unlike a laboratory microscope, the optical system developed in this project allows imaging on large area, with high enough optical resolution and short integration time. The optical system was optimized such that the image quality (Signal to noise ratio and optical resolution) was good enough for inline utilization on the R2R line of CondAlign. To qualify the optical system for inline application, we tested the sensitivity of the image analysis algorithm (developed in 4.3), to changes in optical resolution, signal to noise ratio and defocus. We showed that we successfully could use images from the optical system to quantify the spatial organization of the particles and as a consequence detect if ACF samples were aligned or not (i.e. detect if sample were conducting or not). This is presented in chapter 5

In WP6, SINTEF and CondAlign have installed and tested the optical set-up on CondAlign's process R2R line. Demonstration tests consisted in manufacturing various type of samples, acquiring data in real time and post processing data. Analysis results were investigated off-line just after sample fabrication. Successful separation between aligned and non-aligned were reported by the image analysis algorithm for every tested sample. A summary of this demonstration is presented in Chapter 6.

2 Simulation (work performed by the University of Iasi and All Green AS)

The phenomenon investigated was primarily the absorption of electromagnetic energy in the sample. To this end, the effect of an electromagnetic field on an ACF sample with metallic inclusions was simulated. The Specific Absorption Rate (SAR) which is defined as the rate at which energy is absorbed by the mass unit of material exposed to electromagnetic radiation has been calculated. SAR is expressed in W/kg. Absorption total rates and the peak local value of this rate (Peak Point SAR) have been calculated as an indication of the uniformity of energy absorption in the material.

The main conclusions of this theoretical analysis are:

- One observes a beneficial effect of inserting particles on the absorption capacity of the substrate material.
- An increase of up to 80% of the average dissipated power is observed. The material used for inserts is of great importance, with materials with highest permittivity and greatest possible losses being recommended. In the cases analysed, Type B inserts (ε_r = 12, tan δ = 0.09) have a double efficacy compared to the inserts type A (ε_r = 7, tan δ = 0.05) at any particle size.
- At high particle concentration, corresponding to smaller particle size (5µm), a more pronounced increase in energy absorption is observed.

Details about this work are given in appendix B. This work has been the subject of a publication by researcher from University of Iasi and All Green AS at the ISFEE-IEEE in Iasi in 2019.

3 Manufacturing

Three series of samples have been manufactured in this project. In two of those series, particle diameters range between 5 and 30 µm. In the third series, particles provided by the university of Iasi were used and their dimension was ~ 50 nm.

The ACF's were manufactured using CondAlign's technology, which means that particles were mixed into liquid polymer (1), then aligned along the Z-axis of the film using an electric field (2) and finally, the film was cured with UV-radiation (3).

We describe first the manufacturing of ACF particle with micrometric dimension in 3.1 and ACF with nanometric dimension in 3.2.

3.1 Manufacturing of ACF with micrometric particle

3.1.1 Homogenous dispersion of nano/microparticles in a liquid polymer

Four different types of films were made using four different particles with dimensions in the micrometre range:

- Type A: graphite particles - d_{50}=30 µm – flake particles
- Type B: silver coated glass particles - d_{50}=13 µm - spherical particles
- Type C: silver/nickel coated polymer - d_{50}=3 µm - spherical particles
- Type D: silver/nickel coated polymer - d_{50}=5 µm - spherical particles

Different concentrations of these particles, shown in Table 3-1, were dispersed in either a UV-curable polyurethane (NOA68 from Norland products Inc.) or a UV-curable acrylic (LR-18 from Kaneka Belgium NV) to study the effect on dispersion and alignment with increasing the particle loading.

Sample #	Type	Particles shape	Polymer	Loading of particles [vol%]
#A1	A	Flakes	NOA68	1
#A2				5
#A3				10
#B1	B	Spherical		1
#B2				5
#B3				10
#C	C	Spherical	Kaneka LR-18	21
#D	D	Spherical	Kaneka LR-18	16

Table 3-1: Overview of the different films made by CondAlign for analysis by Sintef.

During this project, the dispersion of the particles has been significantly improved from using a simple vortex for 1 minute to using a planetary centrifugal mixer ("Thinky mixer" ARV310), bought in September 2019 for better and more even dispersion of particles into the liquid matrix. The main useful features of the Thinky mixer for CondAlign are: uniform mixing of material in a short time; dispersion of particles without shearing; high reproducibility of dispersion; removal of air bubbles into the mixture (vacuum mode).

The following steps were performed to prepare the mixtures in sample types A and B: the polyurethane matrix and varying amounts of particles are added and quickly premixed by hand in a container. The container is then closed and placed into the Thinky mixer. The mixing parameters are first 30 sec at 600 RPM centrifuge without vacuum followed by 2 min at 2000 RPM under vacuum (0.2 kPa) to remove trapped air.

3.1.2 Chain generation

Aligned and cured sample films were made on CondAlign's pilot roll-to-roll machine shown schematically in Figure 3-1 (R2R). The general sample making process is as follows. Firstly, the sample is transferred to a syringe, with care taken to avoid creating air bubbles, and then placed into the dispenser. To create the film, the mixture is applied onto a moving flexible substrate and a second flexible substrate is laid over the top of the polymer creating a "sandwich" or laminate. This sandwich is then squeezed in a nip between two rollers to create a 50µm film. This laminate is conveyed between two parallel electrodes which are connected to an AC power source. The AC power source is composed of a high voltage amplifier (TReK Model PZD700A M/S) and a signal generator (BK precision 4010A 2MHz).

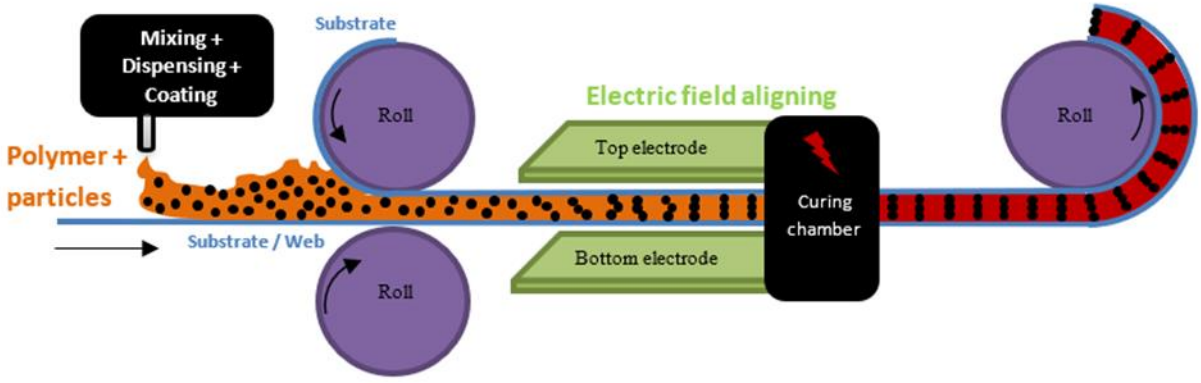

Figure 3-1: Scheme of the R2R line of CondAlign illustrating the successive step for the fabrication of the ACF.

For all samples described here, the velocity of the conveyer was set to less than 0.5 m/min with a 60 x 10 cm alignment area (length and width of the electrodes). This speed is necessary to achieve complete particle alignment.

3.1.3 Polymer curing for particle locking

After aligning the particles, the polymer film is UV-cured which quickly increases its viscosity, thereby locking the particles in their aligned state even when the film is conveyed beyond the electric field. The UV curing was done by two 400 W Cure King lamps (UV III systems Inc.), mounted in series. The UV curing chamber is air cooled to avoid excessive heat from the UV-bulbs, potentially damaging the polymer films or substrates.

3.2 ACF with 50 nm Ø particles

Two different types of films were made using two different particles with dimensions in the nanometer range. Those particles were synthetized by The Technology Institute of Iasi. CondAlign dispersed several times with an ultrasonic probe those nanoparticles in an UV-curable polyurethane polymer. The mixing of nanoparticles is crucial for making ACF with nanoparticles. Single nanoparticle must be dispersed into the matrix to allow the alignment of single particle and not cluster. Three successive ultrasonic mixing was necessary to remove partially cluster of iron nanoparticles (Figure 3-2)

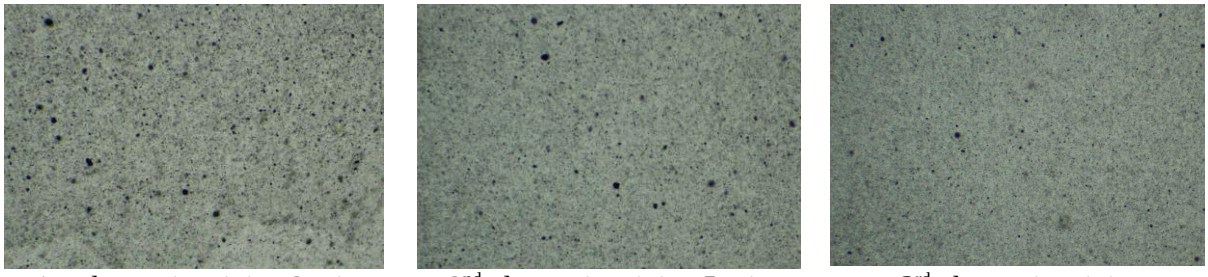

1st ultrasonic mixing 2 min | 2nd ultrasonic mixing 5 min | 3rd ultrasonic mixing

Figure 3-2: Top-view picture of 0.5 wt% iron nanoparticles in a polyurethane matrix with successive ultrasonic mixing. Film thickness is 50 µm.

Once the nanoparticles were dispersed in the polyurethane matrix, CondAlign applied their technology to the mixture to align in the z-axis the nanoparticles. We studied the alignment at different electric field powers for the iron particles. The difference between the electric field power was the frequency used for aligning defined as low – medium and high frequency. The particles responded and aligned at all frequencies but, the best alignment is obtained with a medium frequency Figure 3-2-2.

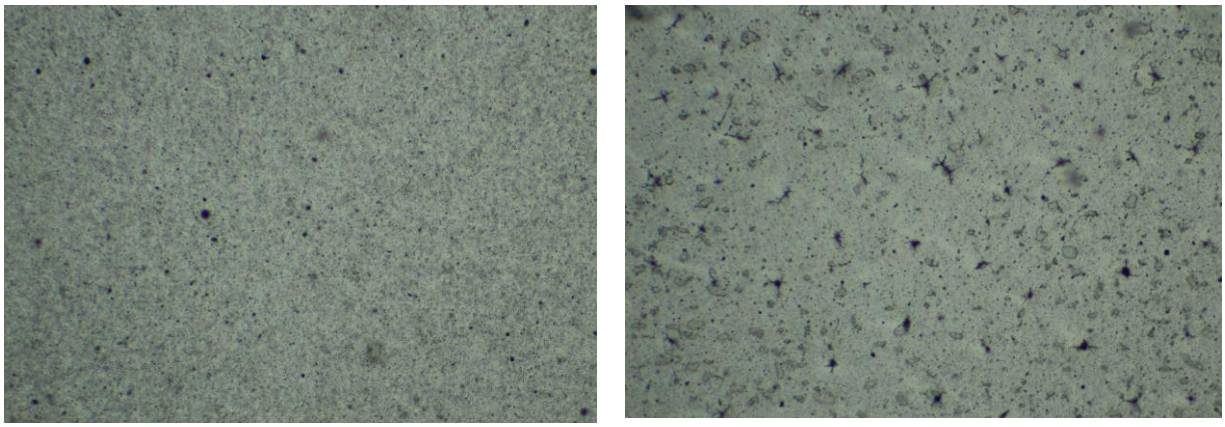

Non-aligned sample | Aligned sample

Figure 3-3: Top view pictures of a 0.5 wt% iron nanoparticles film in the polyurethane matrix. Non-aligned sample on the left and aligned samples on the right. Film thickness is 50 µm.

3.3 Conclusion

The particle with diameter >5 µm can be dispersed and aligned in a polymer matrix. A preliminary study of the conductivity showed that the samples are conductive.

The particle with 50 nm diameter can be partially dispersed in a polymer matrix and aligned but the samples are not conductive. That can be explained by the fact that the total resistance of the chains increases when the number of particles increases. In a film of 50 µm, the number of nanoparticles per chain is colossal thus, the interfacial resistance observed at the interface between each particle leads to a non-conductive sample.

In light of this result, the rest of the project focused on ACF samples manufactured with particles with diameter > 5 micrometre.

4 Characterization methods

In this chapter, we were interested in obtaining information about the correlation between microscopic parameters like contact between particles, particle shape, particle material, viscosity and macroscopic parameters like conductivity and geometrical arrangement of the particles. The objective is to better understand the alignment of the particles and optimize the manufacturing process. The various characterization methods used -SEM, optical microscopy, conductivity - are meant to provide information of the conductivity at various degree of spatial resolution (nm, um and mm).

SEM measurement provides spatial information at the nanometre level. This can be used to inspect the geometry of the sample, e.g. alignment of the particles, how well the particles are dispersed in the polymer matrix in non-aligned samples, particle size distribution, etc. It can provide information about inter particle contact in aligned samples, and also if a chain is conductive or not. This is the only characterization technique that can provide conductivity information at the single chain level available to the project during the project period. Results of characterization using SEM are presented in 4.1 and 4.2.1 on thermally and electrically conductive samples respectively.

The traditional way of measuring the conductivity of the ACF is by resistivity measurement. Localized resistivity measurement gives information about the local conductivity of the sample. This is an indirect measurement of e.g. the degree of alignment of the particles, inter particle contact and particle conductivity. Large and low resistivity measured on non-aligned and aligned sample respectively, is an indication of successful manufacturing process. A new set-up for measuring conductivity of ACF is presented in 4.2.2. It allows for localized (3by 3 mm^2) measurement of conductivity under various level of pressure. The set-up is used to characterize sample of type A and B with various particles loading.

Traditional optical microscopy will provide information at the micrometre level about the arrangement of the particles. In nonaligned samples, the position distribution of the particle is random after curing. In aligned samples, due to inter-repulsion between the particle chains, the chains tend to adopt hexagonal patterns. Measuring the degree of order in the microscope images is an indirect way of measuring the degree of alignment of the particles. In 4.3, we present an image analysis algorithm that allows to quantify the degree of spatial order in an ACF sample. The algorithm is then applied to the sample of type A and B and various measures are defined to characterize the spatial organization of the particles.

As studying the effect of changing each process parameter on film properties like conductivity and level of alignment would be extremely costly in term of manufacturing and experimental time, we present a design of experiment (DOE) in 4.4 whose objective is to identify process parameters of importance in advance of the actual experiment. A set of ACF samples are manufactured by CondAlign and the measurement techniques developed in 4.2, 4.3 are used to characterize the conductivity and the optical organization of ACF samples. Models linking the conductivity and process parameters are established.

4.1 SEM on thermally conductive particles (CondAlign)

CondAlign made elastomer-filled ceramics pads. Classical microscopy is not possible with these samples because of the high loading and because the ceramics particles are translucent. CondAlign can indirectly evaluate the alignment by comparing the thermal conductivity of each pad to a corresponding non-aligned sample. However, these results do not give detailed information about the orientation of the ceramic particles. We therefore wanted to perform SEM-imaging, which provides important information on the interface polymer/particles and orientation of the particles.

By orienting the longitudinal axes of hexagonal boron nitride (hBN), we exploit its anisotropic property. hBN is a platelet-shaped particle with a highly anisotropic thermal property. The in-plane thermal conductivity is reported at about 400 W/mK, whereas the through-plane thermal conductivity is around 2 W/mK. SEM cross-section imaging of those ceramic pads were done by the Technical Institute of Iasi and, allowed us to verify the orientation of boron nitride platelet (Figure 4-1-1).

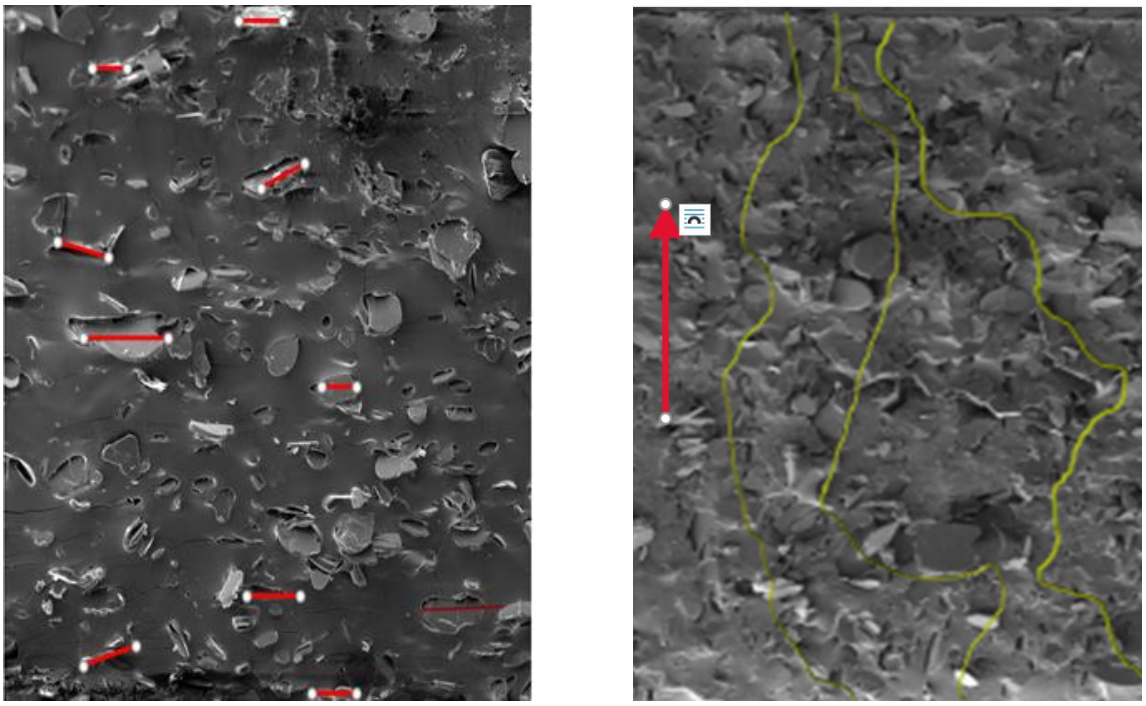

a- Non-aligned sample b- Aligned sample

Figure 4-1: Cross-sectional SEM-images of 10 vol% hBN fillers in silicone. a) cured silicone pad with stochastic orientation. Most of the hBN fillers are oriented perpendicular to the Z-axis, indicated by the red lines. b) cured silicone pad with electrically oriented particles. The Z-axis of samples, which is also the direction of the applied electric field is shown by the arrow. Most of the hBN fillers are oriented parallel to the Z-axis, thereby increasing the thermal conductivity along this direction by creating path across the sample (green line).

4.2 Characterization of electrically conductive particles

Electrically conductive particles manufactured by CondAlign were characterized at SINTEF by SEM (4.2.1), by a new set-up for measuring local electrical conductivity under pressure (4.2.2) and by optical microscopy (4.3).

4.2.1 SEM characterization

A FEI Nova NanoSEM 650 Scanning Electron Microcscope (SEM) has been used to acquire high magnification and resolution images of the conductive particle loaded polymer films.

4.2.1.1 Cross sectional Analysis

Cross sectional samples were prepared to observe the alignment of particles along the Z axis of the film. To create these cross sections, a section of the polymer film was embedded into an epoxy block shown in Figure 4-2. The epoxy block was then grinded and polished until chains of conductive particles were revealed. After polishing, a thin layer of carbon was deposited on the surface of the cross section to create a conductive surface, necessary for SEM analysis.

Figure 4-2: Epoxy block used to embed samples for cross sectional imaging

The cross-sectional analysis was carried out at 30 kV to give the incoming electrons a higher penetration depth and thus more information from within the sample as opposed to the surface information obtained from lower acceleration voltages. Figure 4-3 shows a stitch of SEM images totalling 5 mm of sample B3 Aligned. The white specs are metal coated glass spheres which are aligned due to the applied electric field during curing. Once aligned, these metal particles provide a path for electrons thereby creating a conductive polymer film.

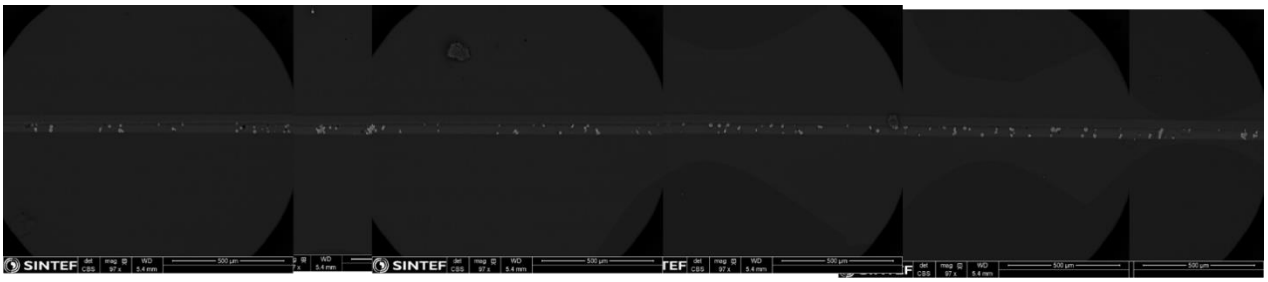

Figure 4-3: 5mm length of cross section for sample B3 Aligned.

Upon closer inspection of the cross section, areas with well aligned particles can be observed as shown in Figure 4-4. As observed, the particles do not sit directly on top of each other but meander in both the x and y direction. This is because the total film thickness is not an exact multiple of the particle diameter. They are therefore forced into an offset to achieve the alignment. Although it appears, that the particles do not touch, they are indeed in contact. Further polishing is required to reveal the exact contact point.

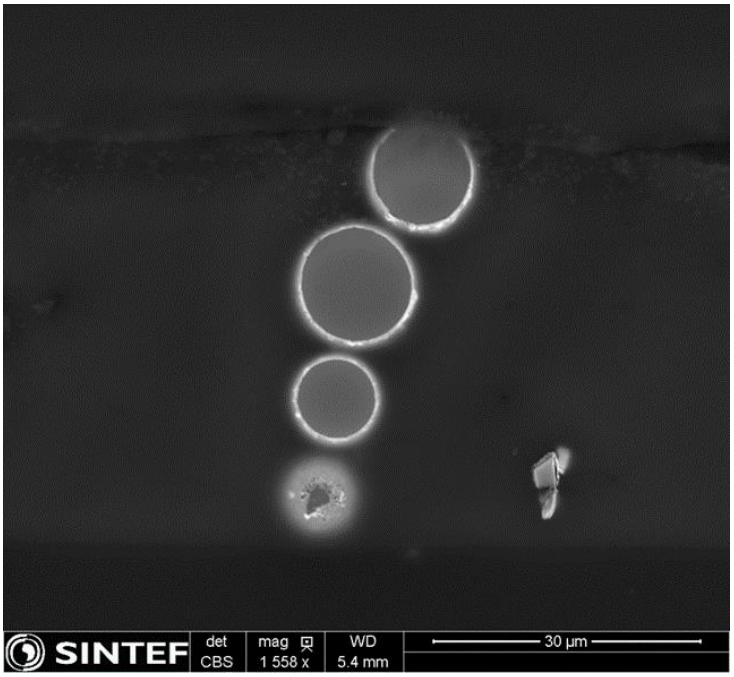

Figure 4-4: Close up of an area of well aligned particles

Figure 4-5 shows particles in contact thereby creating a path for electrons to flow from the top surface of the polymer to the bottom surface.

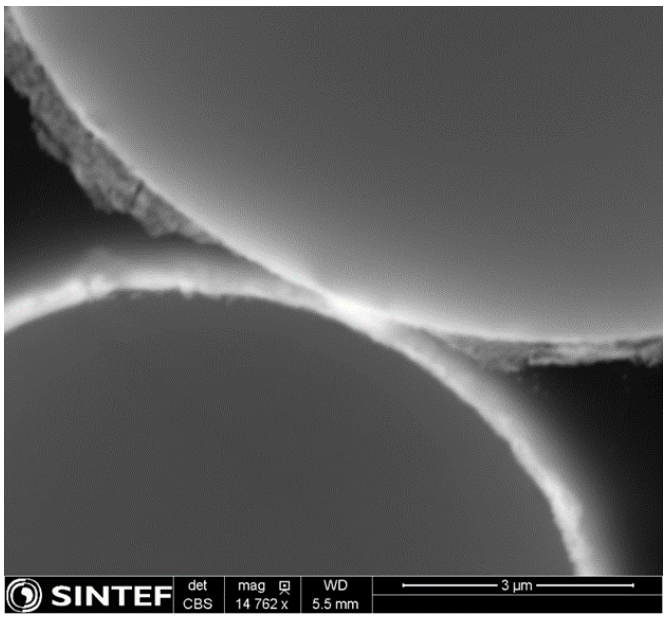

Figure 4-5: SEM image of particles in contact

4.2.1.2 Plan view

Both aligned and unaligned samples were observed in the SEM from the top of the samples in a plan view. Electrons are accelerated through high voltage and directed at the sample's surface. Insulated or charged surfaces repel these electrons making it difficult to analyse the surface of the sample (unless water vapour is sprayed in the chamber to improve conductivity of insulating surfaces). Conductive samples attract electrons

to the samples surface such that secondary electrons can be emitted to a detector and an image reconstructed. The table below shows images of samples A1, A2 A3, B1, B2 and B3; aligned and non-aligned.

	Aligned	Non-Aligned
A1	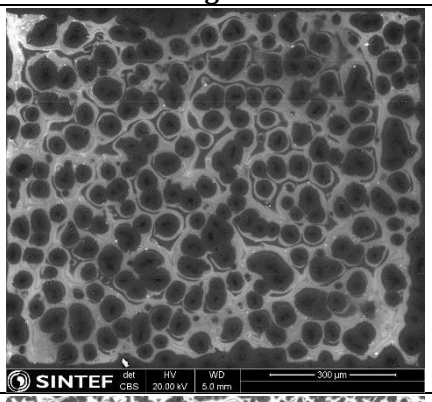	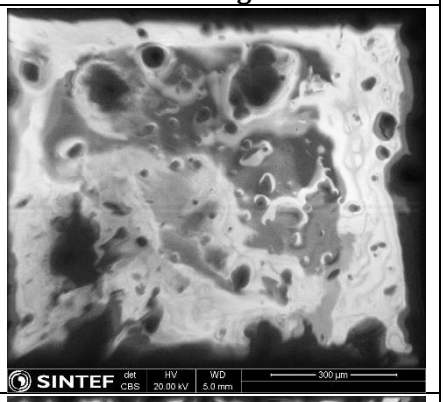
A2	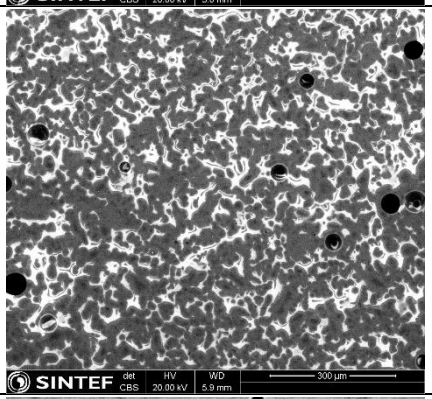	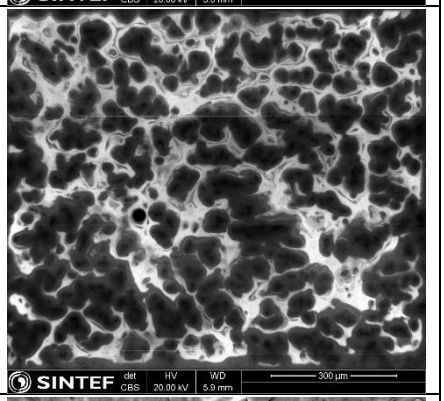
A3	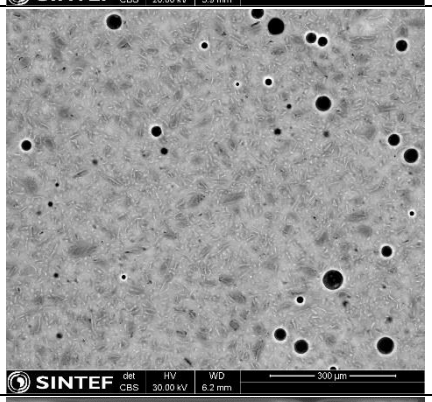	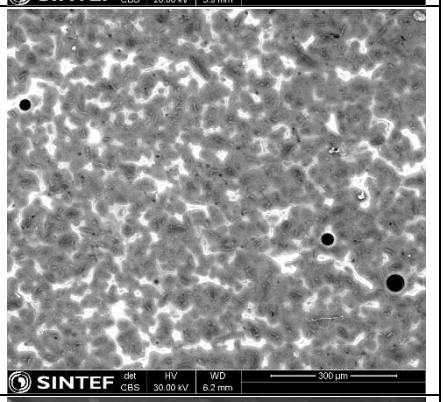
B1		

B2	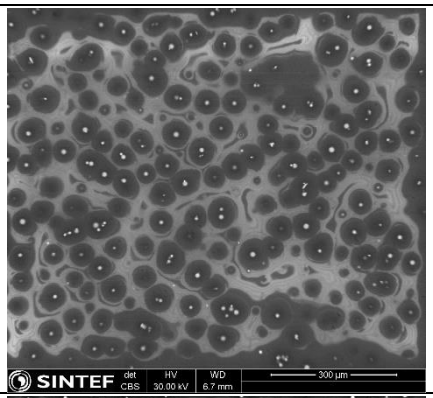	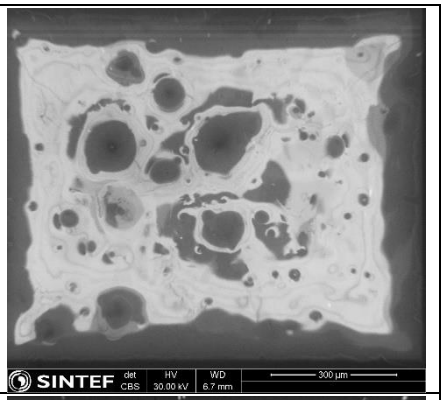
B3	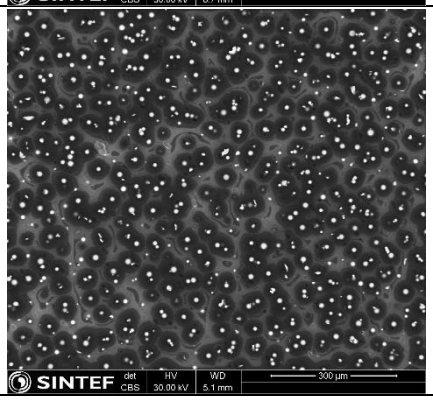	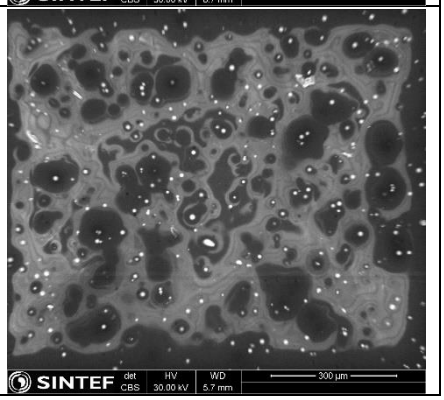

As observed, the aligned samples are qualitatively conductive compared to the non-conductive samples. This is noticeable by the ease of focusing on the samples surface as well as the conductive areas (normally darker contrast) compared to the non-conductive areas (normally lighter contrast). It should be noted however that in the B series the light contrast dots are the conductive spherical particles. They appear light in contrast due to the mass of the metal coating the glass spheres.

The table below shows plan views of conductive samples C and D.

C - conductive	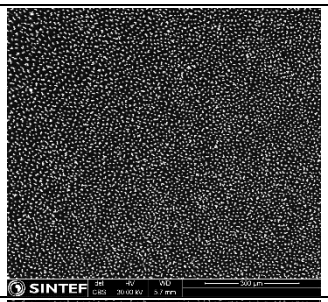	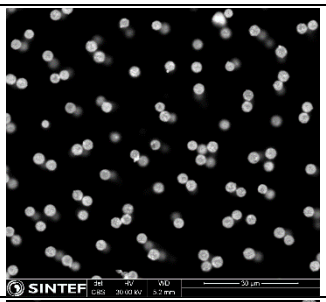	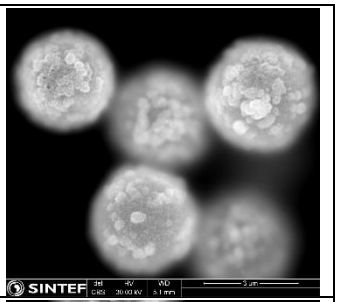
D - conductive	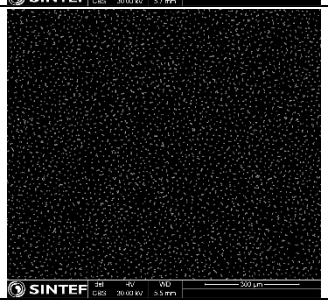	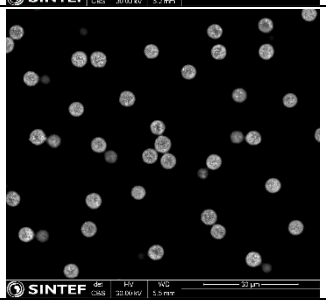	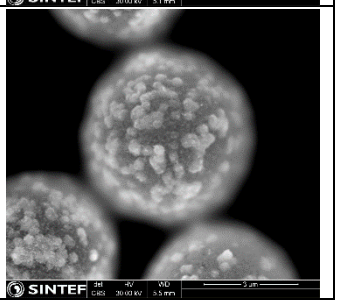

Conclusions:

- From the SEM analysis, it is possible to observe the alignment of particles into conductive chains
- It is also possible to observe the connection between individual particles. Although it is not feasible to determine the exact nature of the material between particles and whether the contact tunnels through a monolayer of polymer, the particles appear to be intimate contact
- SEM can be used to view the samples in plan view. Conductive samples do not charge whereas samples with non-aligned particles charge.

4.2.2 Electrical characterization

The resistivity of the electrically conductive samples was evaluated as a function of applied pressure. In all cases, a 4-point probe setup was used to ensure contact resistance was not included in the reported values.

4.2.2.1 Measurement Setup

The resistivity measurements were carried out using a Keithley 2450 in 4-point probe measurement mode. The resistivity was measured once per second for approximately 200 seconds, and the average of these measurements is reported. "Bad measurements" (due primarily to inaccurate sample placement) were taken out before averaging. The polymer samples were placed between a gold-plated Si wafer and a gold-plated copper block. The size of the polymer sample under investigation was larger than the copper block but smaller than the Si wafer. The measurement area was therefore defined by the copper block (3 x 3 mm). Weights were added to the copper block so that resistivity at different pressure could be measured. The setup is highlighted in Figure 4-6.

A small detail in the measurement setup was changed between measurements of the aligned A and B samples (shown to the left in Figure 4-6), and the remaining measurements (shown to the right in the same figure). In the latter, the gold-plated copper block was glued directly to the rod where weights were added to make sure the top and bottom electrodes were parallel.

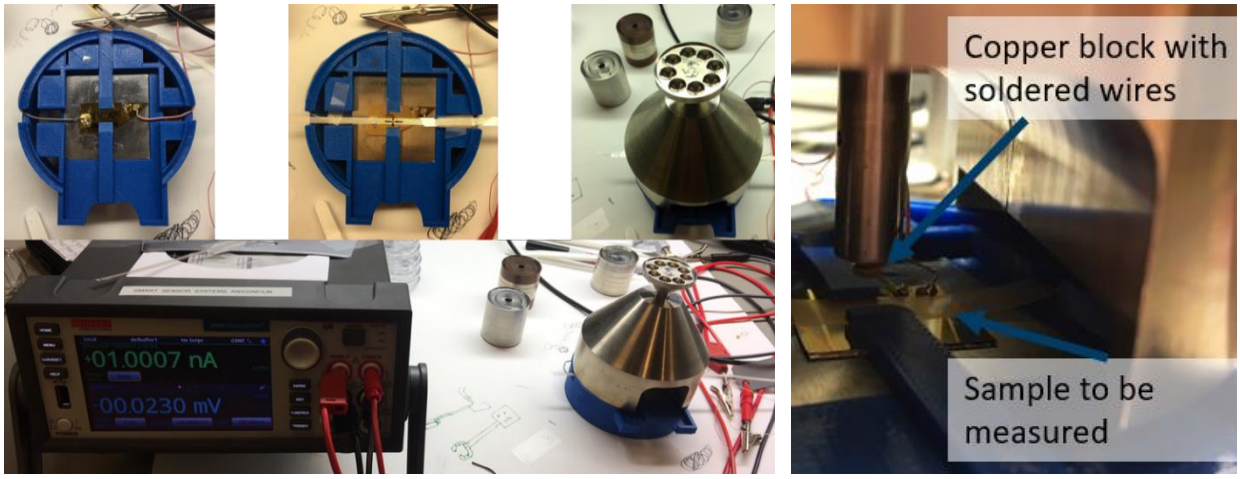

Figure 4-6: Resistivity measurement setup. To the right is a detailed view of how the top electrode was glued directly to the rod for measurements of C1, D1 and non-aligned samples.

4.2.2.2 Resistivity measurements

The table below shows the resistivity measurements carried out both by CondAlign (using a different setup), and by SINTEF. For the measurements performed at SINTEF pressures of 0.14, 0.57 and 1.36 MPa have been chosen for this summary table. The thickness of A and B films was assumed to be 45 µm, while C1 was assumed to be 12 µm thick and D1 was assumed to be 25 µm thick.

Table 4-1: Overview of electrical measurements performed by Condalign and SINTEF. For the measurements at SINTEF we have chosen to show the results from applied low, medium and high pressure. Open spaces correspond to missing measurements, while "Open circuit" has been used for the measurements of very high resistance/open circuit i.e. no measurement.

		0,14 MPa pressure		0,57 MPa pressure		1,36 MPa pressure	
Sample	CondAlign (Ohm.m)	Spot A (Ohm.m)	Spot B (Ohm.m)	Spot A (Ohm.m)	Spot B (Ohm.m)	Spot A (Ohm.m)	Spot B (Ohm.m)
A1a	230	18	38	16	37	14	17
A2a	39	229	170	40	34	16	15
A3a	170	28	16	15	9	11	6
B1a	*10000*	*Open circuit*	*3,0E+08*	*Open circuit*	*2,5E+06*	*Open circuit*	*0,39*
B2a	0,62	0,7	2,7	0,3	0,3	0,2	0,3
B3a	0,09	5,5	12	1,9	1,1	0,8	1,3
C1a		1,8		0,04		0,1	
D1a		0,5		0,5		2,0	
A1b	*1,6E+07*	*Open circuit*				*Open circuit*	
A2b	*1,6E+07*	*Open circuit*				*274*	
A3b	2,3E+03	150				51	
B1b	*4,5E+08*	*Open circuit*				*Open circuit*	
B2b	*4,5E+08*	*Open circuit*				*Open circuit*	
B3b	*Open circuit*	*Open circuit*				*Open circuit*	

From Table 4-1 it is seen that most aligned samples are electrically conductive, while most non-aligned samples were hardly electrically conductive even at a high applied pressure. An exception was B1a which had a very high resistivity at low pressure, but broke down and became electrically conductive when a higher pressure was applied. The samples B2a, C1a and D1a were highly conductive.

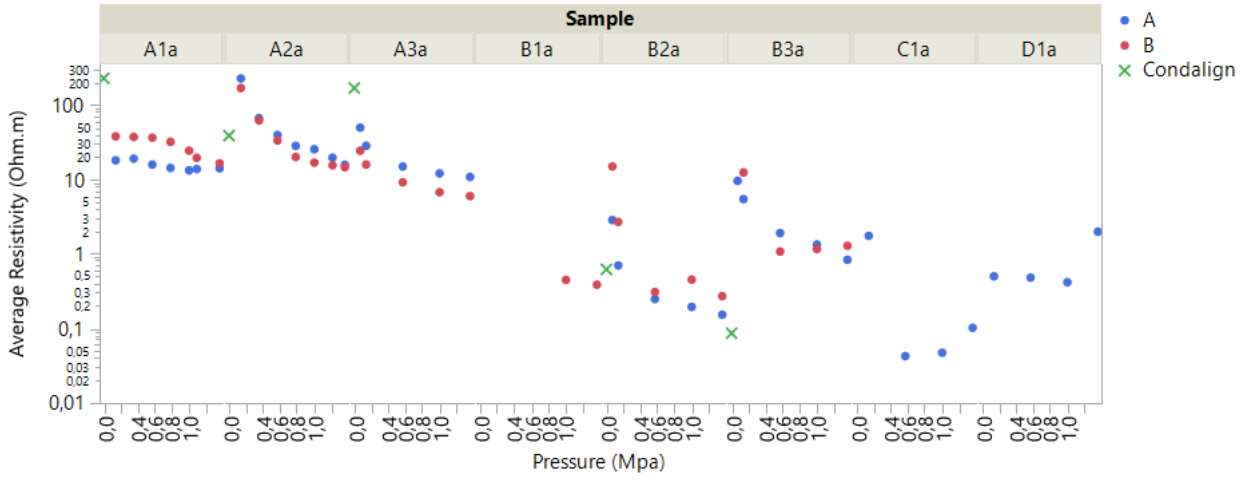

Figure 4-7: Plot showing the measured resistivity (Ohm.m) as a function of pressure for the aligned samples. Two spots have been measured for most samples, A and B. In addition, the measurement by Condalign is included as a cross.

Figure 4-7 shows the measured resistivity as a function of pressure for the aligned samples. Most samples have a reduction in resistivity when a higher pressure is applied, and some samples are only electrically conductive under applied pressure (e.g. B1a). However, this was not the case for samples C1a and D1a. C1a had a

reduction in resistivity from 1.8 Ohm.m to 0.04 Ohm.m when increasing the pressure from 0.14 to 0.57 MPa, but was rather stable with a slight increase when adding more pressure. D1a had a rather stable resistivity for pressures between 0.14 and 1 MPa, before it increased from 0.4 to 2.0 Ohm.m when the pressure was increased to 1.36 MPa.

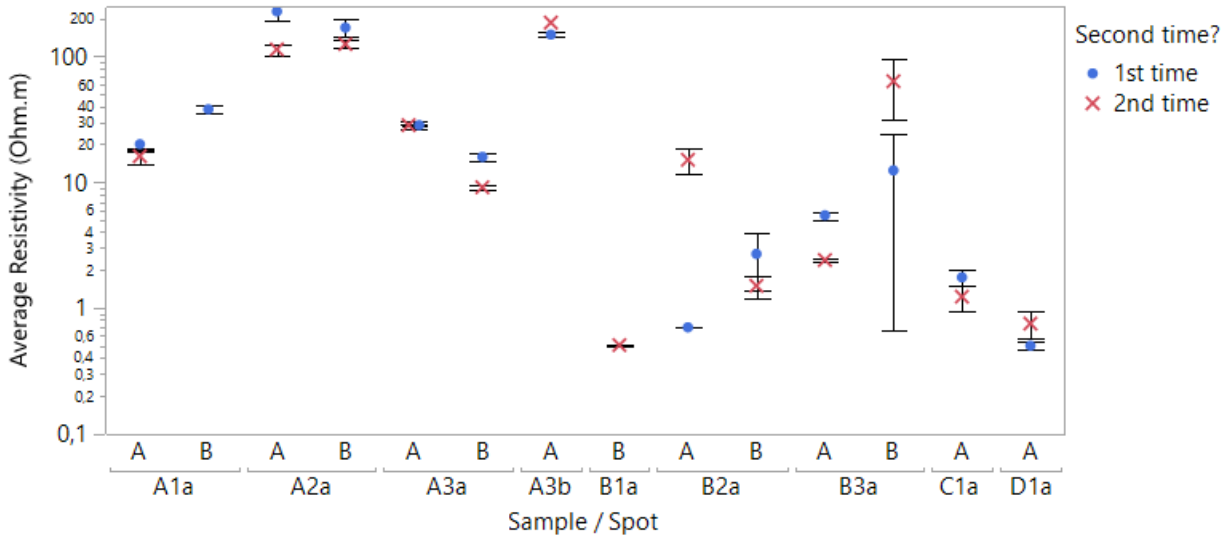

Figure 4-8: Plot showing the 1st and 2nd measurement at 0.14 MPa of measurement spots ("A" and "B"). The 1st measurement is performed on a "fresh" sample, while the 2nd measurement is performed after the pressure series where the sample has been exposed to up to 1.36 MPa pressure. The error bars indicate +/- 1 standard deviation of the measurement series (i.e. approx. 200 measurements).

In addition to the measurements shown in Table 4-1 and Figure 4-7, a second measurement was performed at 0.14 MPa for most samples after the pressure series to look for any hysteresis. Figure 4-8 shows the average resistivity measured the 1st and 2nd time at spot "A" and "B" on the measured samples[1]. The very resistive measurements approaching "open circuit" are not included. As can be seen most samples had a reduced resistivity after exposure to high pressure, however the reduction in resistance varies between samples and there are some exceptions where the resistance measured the 2nd time was higher than the 1st time.

In conclusion there was a large difference in the resistivity measured on aligned and non-aligned samples of which the aligned samples showed a much-improved electrical conductivity compared to the non-aligned samples. The applied pressure during measurement influences the measured resistivity, typically giving an improved electrical conductivity at higher applied pressure. To some extent the film is also altered after exposure to high pressure; a slightly changed measurement was obtained for most samples when measurements at low pressure were repeated a second time.
It is difficult to conclude which pressure is the most suitable as a "reference pressure", and this will also depend on the application. However, from the obtained data it seems like a pressure of approximately 0.14 MPa is needed to get good enough contact between the film and the electrode in this setup, so measurements below this pressure is not recommended.

4.3 Optical characterization

Studies of spatial organization of micro suspension under the effect of an electrical field are numerous. [5] used microscope optical images to study the low volume fraction and electric field phase behaviour of a

[1] A1a spot B was only measured once. B1a spot B was only electrically conductive after being exposed to high pressure.

Brownian colloidal suspension. [6] investigated the long-time dynamics and pattern formation in semi dilute suspensions of colloidal spheres in a viscous electrolyte under a uniform electric field using numerical simulations. [7] performed optical microscopy and dielectric monitoring of anisotropic epoxy/BaTiO3 composite formation tailored by dielectrophoresis. In all these works, optical microscopy is mostly used for obtaining qualitative information about the spatial organization of particles. In some studies Fourier Transform is performed on microscopy images to obtain more quantitative information about the mean distance between particles in an ordered phase [5], [6].

We are interested in finding algorithms that gives quantitative information about the spatial organization of particles and that are suitable to be used in a real time imaging system. The research was performed in two steps. In the first part of the project we established algorithms for separating aligned from non-aligned samples using high resolution microscopy images. This step is described in this sub-chapter. In the second part, described in see chapter 5, we develop and customized an optical system for application to the R2R line of CondAlign.

4.3.1 Experimental procedure

Images were acquired with an Olympus BX60 microscope at 6.3 magnification and using backlight illumination (see appendix D.1). Each film (A1-A3, B1-B3) was imaged at three different focus positions (top, centre, bottom) for the first data set. The image size was 1476 x 2048 pixels with three colour channels (RGB). The resolution was approximately 0.5 µm per pixel. Figure 4-9 shows example images of each film type.

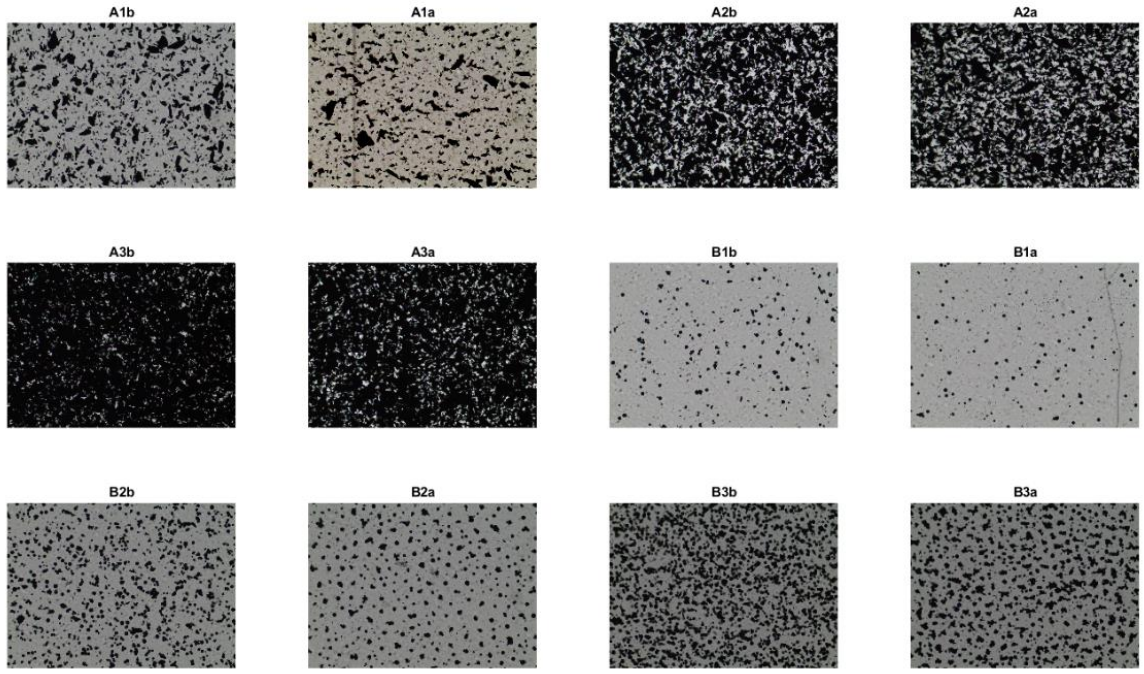

Figure 4-9 The different film types that were imaged in the initial experiment. The first letter (A/B) indicated the particle type (flake/circular), the number indicates particle density (low to high) and the last letter indicates whether the image is taken before (b) or after (a) alignment. Film B2 (bottom row to the left) was also imaged in the second experiment described below.

4.3.2 Image analysis

We first present a method based on two dimensional FFT in 4.3.2.1 and then a more robust method based on a line-by-line analysis in 4.3.2.2.

4.3.2.1 FFT based

Looking at the image of the different sample types in Figure 4-9, we can observe clear differences between the spatial organization of aligned and of non-aligned samples. The non-aligned samples present a non-ordered structure with no well-defined symmetry directions while for aligned samples, structure with higher degree of symmetries can be observed. This is more obvious for samples of type B, where aligned samples have crystal lookalike structures. A consequence of the increase in the degree of organization, seems to be that the mean value of the inter particle distances increases. We attempted applying a 2D Fourier transform of the images of sample before and after alignment, but the results were not convincing. An example for Sample B1, B2 and B3 is shown on Figure 4-10 after circumferential averaging. The radial Fourier transform shows broad peaks at spatial frequency of ~25 mm^{-1} for sample B2, which means an average inter-chain distance of ~40 um. The peak for B3 seems to have a slighter higher peak centre frequency but the calculated difference with sample B2 is negligible, while it can be seen from the image that there are clear differences in the inter-particle distance between the two samples. For B1, no real peak can be distinguished. For samples A, applying a 2D Fourier transform did not bring any useful information about periodical structure in the organization of the sample.

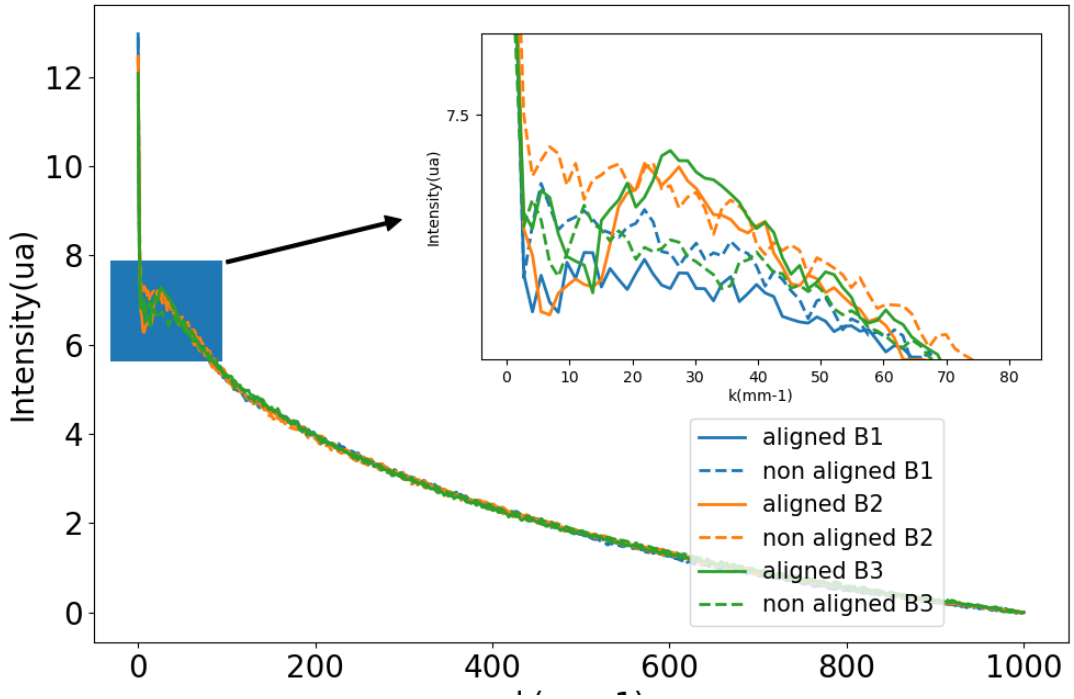

Figure 4-10: absolute value of FFT for images of sample B1, B2 and B3 after circumferential averaging

The poor information brought by applying FFT here can be attributed to the low size of the sample in term of pixel number and thus the low number of particle clusters taken into account in the calculation. In addition, FFT is computing intensive and is not well adapted for real-time analysis. We then present another algorithmic approach to obtain quantitative information about the spatial organization of in the sample.

4.3.2.2 Line by line analysis

As an alternative to FFT based analysis, we developed an algorithm that is based on segmentation of the image. The main steps of the segmentation are as follows:

1) Filtering of the image, *I*, with a relatively large, sliding mean filter (100x100 pixels) to find the average background level, I_{bg}.
2) Computation of a threshold image defined by $I_{thres} = a * I_{bg} * (1 + 0.5*PrctSat)$, where the factor a = 0.85 and *PrctSat* is the percentage of pixels that are saturated (pixel value = 255) in the image. The reasoning behind adding the *PrctSat* factor is to adjust for clipping of background level values if the

image has many saturated pixels. In practice this factor is only used for some of the static images, since saturation is not a problem with the roll-to-roll images where we need to use very short exposure time to avoid motion blur.

3) Segmentation of each pixel as foreground (= particles) or background defined by $I_{fg} = I < I_{thres}$.
4) Optional removal of small regions (< 3x3 pixels). This step is only used for the first setup where we used a lens that gives high spatial resolution. For the roll-to-roll images we use lower spatial resolution in order to cover the whole film width, so for these images we use the raw segmentation result.

After segmentation, we process the image row by row to compute a set of statistical measures for the particle distribution. Analysing image rows instead of using blob analysis reduces computational complexity. The rationale behind this simplification is that the particles are expected to have equivalent distributions in all directions, so we do not gain much extra information by analysing the particles in more than one direction. Row-based analysis also allows for simpler and more consistent analysis of films with high particle coverage, where the segmentation would have to be inverted in order to achieve separated regions (since the particles can be connected throughout the whole image, with only "islands" of background in between).

The computed measures are:

- **Particle coverage (coveragePrct):** Percentage of pixels segmented as particles relative to the total number of image pixels. This measure is expected to decrease when the particles are aligned, since there will be fewer visible particles when they are aligned perpendicularly to the image plane. For the example image in Figure 4-11, we get particle coverage = 100*(2+4+1+4+3+2+3+1+1)/(9*5) = 46.67 %.
- **Mean image intensity:** The mean value of the pixel intensity within the analysed image region. For images with fixed camera parameters and identical illumination, this measure will be related to the particle coverage, so we expect the mean intensity to increase when the samples are aligned.
- **Percentage of coloured pixels (coloredPrct):** The number of pixels where not all three colour channels (R, G, B) have the same segmentation result (i.e. some colours are segmented as foreground and others as background for the same pixel). This feature has higher values for nonaligned images because uneven colour segmentation typically occurs when the particles are out of focus, which happens when we have visible pixels that are not near the top of the film. After alignment these particles should ideally not be visible since we should only see the top of the particle chain. This measure is only computed for the first setup where we used an RGB camera.
- **Mean difference between the colour channels (imColorsumMean):** This is computed as the mean of the sum of the absolute differences between the pixels in the different colour channels (R-B, B-G, G-R) divided by the total number of pixels in the image. This measure is related to the other colour-based measure, and only computed for the first setup with an RGB camera.
- **Summed edge intensity (imQual)**: This feature is computed as the sum of the spatial (x,y) gradient at all pixel positions where the gradient is larger than 0.5 x mean of all gradients in the image. This is a measure of the image quality in terms of sharpness/degree of particles that are within the focus plane of the camera. This measure behaves differently for round particles and flaky particles. For the round particles we get a lower value for aligned films because there are more edges in the non-aligned samples (correlated with particle coverage). For the flaky particles, however, we get a higher value for the aligned samples. This is probably because these samples have very high particle coverage even after alignment, which means that the degree of sharpness of the edges contributes more to the edge intensity measure than the number of edges. For flaky particles, the aligned samples have sharper edges between background and particles, and therefore the mean edge intensity is higher than for the non-aligned samples.

- **Mean particle size**: This measure is computed as the mean value of the length of all consecutive runs of pixels segmented as particles, except the first and last sequence of each row, which are rejected to avoid errors if the film is partially outside the imaged region. An example is provided in Figure 4-11. The run length for each sequence is marked at the beginning of each sequence. For the particles, shown in white, we have a total of nine sequences, and the sum of the sequence lengths is 2+4+1+4+3+2+3+1+1 = 21, so we get an average particle size of 21/9 = 3. This measure is expected to decrease when the particles are aligned since there will be fewer clusters of overlapping particles after alignment. Since we compute this measure for all parts of the particles (and not just the largest measure for each particle), we will generally get a value that is related to, but lower than the actual particle diameter.
- **Mean background size**: This measure is computed in the same way as the average particle size, only using background pixels instead of particle pixels. For the example below, we get an average background size of (1+6+3+1+2+1+3+3+3+1)/10 = 2.4.
- **Maximum background size**: This measure is computed as the largest consecutive run of background pixels. For the example below, the maximum background size is 6.
- **Standard deviation of mean particle size and background size**: In addition to computing the mean value, we also compute the standard deviation of all the input values to the mean value computations. For the particle size example, we get std([2, 4, 1, 4, 3, 2, 3, 1, 1]) = 1.22.

1	2		6					
4				3			1	1
4				2		3		
1	2		3			3		
3			1	3			1	1

Figure 4-11 Illustration of input to the computation of average particle size and average background size. Pixels segmented as particles are shown in white and background pixels are shown in blue. The number indicates the number of consecutive pixels with the same segmentation result, which is used as input for computation of mean particle size and mean background size.

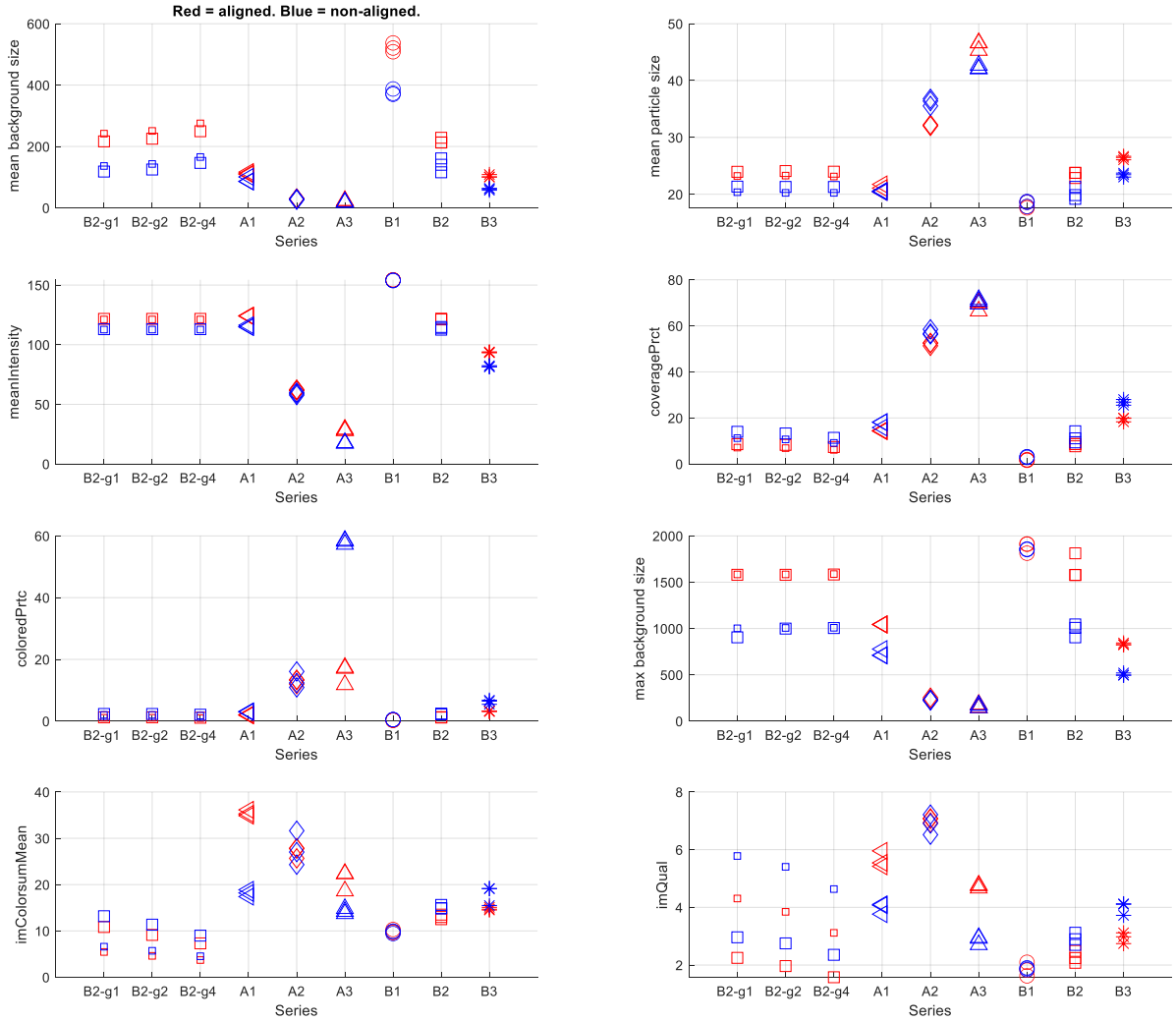

Figure 4-12 Analysis results (in pixels and percentages) for the different image series that were acquired with the first setup (RGB camera). Film B2 has been tested with subsampled and smoothed images to simulate poorer image resolution. These are the first three results (B2-g1, B2-g2, B2-g4), followed by the results for all the films at the initial resolution (A1-B3). Images taken before alignment are shown with blue markers, and after alignment are shown with red markers.

Table 4-2 is a summary of the analysis results for the aligned and non-aligned samples. It shows the distance between the mean value of all measures before and after alignment relative to the sum of the standard deviations of the measures; abs(meanA-meanB)/(stdA+stdB), i.e. the contrast to noise ratio of the measure. The color-coding indicates values > 2*std (light yellow), >3*std (dark yellow), > 5*std (green). In addition, images of sample B2 were convoluted with a 2D gaussian with various widths (sigma = 1, 2, 4) to degrade the original optical resolution. The aim was to test the impact of resolution degradation on the algorithm.

The main conclusion that we can draw from Figure 4-12 and Table 4-2 is that it is possible to separate aligned from non-aligned samples based on at least one of the measures, e.g. mean background size for B1, image quality for A1 etc. Note that the threshold between aligned and non-aligned is not the same between the series and that not all measures give good separation for all the series. For example, a very good separation (more than 11 std) is obtained with imColorsumMean for sample A1, but with other particles this is not a good

measure[2]. Measures still give good separation with degradation of original resolution up to 2 um per pixel. For the blob measures we get different results depending on how much we erode (N x N pixels). For the films with high particle density, we need to use a higher value for N to get separation between the particle clusters, whereas for low particle density we get better results with a small N (too many particles are removed for high N).The table below shows the distance between the mean value of all measures before and after alignment relative to the sum of the standard deviations of the measures; abs(meanA-meanB)/(stdA+stdB), i.e. the contrast to noise ratio of the measure. The color-coding indicates values > 2*std (light yellow), >3*std (dark yellow), > 5*std (green).

Table 4-2: distance between the mean value of all measures before and after alignment relative to the sum of the standard deviations of the measures

	B2g1	B2g2	B2g4	A1	A2	A3	B1	B2	B3
mean particle size	0.14	0.15	0.14	0.8	5.73	3.49	0.37	2.09	4.55
mean background size	0.52	0.51	0.47	1.75	0.95	1.34	6.14	2.5	5.47
std particle size	0.22	0.12	0.63	12.14	4.91	1.78	0.49	0.88	11.44
std background size	2.94	3.06	3.42	2.31	1.79	0.83	3.02	2.18	5.1
max background size	8.8	74.5	102.35	7.85	0.81	0.15	0.4	3.24	13.32
coveragePrct	1.6	1.55	1.44	2.05	2.74	0.53	4.08	1.09	3.44
coloredPrtc	3.44	3.44	3.13	5.74	0.07	11.18	5.85	6.94	4.08
Image quality	0.32	0.37	0.42	3.53	0.35	9.89	0.1	1.52	2.49
Mean image intensity	14.4	14.49	14.48	8.89	2.11	13.71	2	5.14	13.67
imColorsumMean	0.97	0.52	0.43	11.18	1.06	1.17	0.76	0.07	0.29

We can see that for some of the measures, the contrast to noise ratio increases, (resp decreases) with the particle concentration. This is the case e.g. for the measure *mean particle size*, *image quality* and *mean image intensity* and samples B, or *std particle size*, *max background size* for sample A. *mean particle size* is a measure of the particle cluster size. Its increase with particle concentration means that the more particle we have in a sample of type B (given a particle size and film thickness), the larger the cluster will be in average. Similar arguments can be given for *std particle size*, one will observe larger variation in the cluster size as the particle concentration increases in sample of type B. One hypothesis about this behaviour could be that above a certain concentration, when there are enough particle to create a given number of chains, the particles in excess around a given chain will have a tendency to agglomerate on the top and bottom of existing chains instead of creating new chains.

but the threshold between aligned and non-aligned is not the same between the series, and not all measures give good separation for all the series. For the blob measures we get different results depending on how much we erode (N x N pixels). For the films with high particle density, we need to use a higher value for N

[2] We believe that due to chromatic dispersion in the lens, light from different depths are focused on the three colour channels of the camera giving us images of particles at three depths. In sample A, the flakes particles aligned in very disordered chains and no real two-dimensional patterns appears under electric field. A hypothesis is that information about alignment in this sample type is depth dependent and that "imColorsumMean" is a good quantifier for this information.

to get separation between the particle clusters, whereas for low particle density we get better results with a small N (too many particles are removed for high N).
The major observations are:

- It is possible to separate aligned from non-aligned samples based on at least one of the measures, e.g. mean background size for B1, edge intensity for A1 etc.
- Not all measures give good separation for all the series. For example, a very good separation (more than 11 std) is obtained with imColorsumMean for sample A1, but with other particles this is not a good measure.
- Measures still give good separation with degradation of original resolution up to 2 µm per pixel

4.3.3 Conclusion:

On high resolution microscopy images, the FFT based algorithm offers qualitative information about the spatial organization for two of the samples of type B but fails to give any useful information for sample of type A. Obtaining quantitative information about the degree of alignment is also challenging even for well-organized sample like sample B2 and B3.

We have then established an image analysis algorithm based on segmentation of the images that can distinguish between aligned and non-aligned samples and unlike the FFT algorithm can give quantitative information about the degree of alignment of the particles. The resolution must be high enough to distinguish the distances between particles or clusters of particles and distinguish between relative size of particle clusters.

The algorithm is based on a set of statistical measures of geometric parameters measuring how particle's clusters and chains organizes themselves spatially. We found that for each sample, there is always at least one measure that quantifies the separation between aligned and non-aligned with a good degree of confidence.

In 5, an optical system optimized for online application to the R2R system is developed. We establish how robust the algorithm is when the resolution of the imaging system degrades.

4.4 Design of experiment

In this chapter, we summarize the results from the Design of experiment performed in the AniConFilm project. Data are gathered both from the measurements performed at SINTEF, but also from the reports that CondAlign wrote about how the samples were prepared.

4.4.1 Introduction to Design of experiment

Design of Experiments (DOE) is a way of planning experiments so that the data obtained can be analyzed to yield valid and objective conclusions i.e. the laying out of a detailed experimental plan for how to change process parameters and measure changes in process responses in advance of the actual experiment [9], [10]. Typically, in the lack of a DOE, process parameters are tested one at a time, with several potential disadvantages: 1) The risk that combining the individually identified best input parameters does not result in the best combined output i.e. that there are interactions between the tested parameters. 2) Wrong conclusions are drawn due to a lack of randomization of the tests allowing random variations, e.g. operator, influence on the test result, and 3) testing the process parameters one at a time is very time consuming if there are several parameters to be tested.

Optimal DOE, i.e. experimental designs that are optimal with respect to a chosen statistical criterion, is a general and flexible method for applying design of experiments [11]. It suggests an optimal DOE for the specific experimental challenge by taking the relevant input parameters, the planned data analysis, and the resources available into account and allows parameters to be estimated without bias, with a minimum variance and a minimum number of test runs.

The goal of this study was to understand which parameters contribute the most to the conductivity of the electrically conductive films, and to identify optimal parameter settings for maximizing the electrical conductivity. In order to evaluate this, an optimal DOE was used.

Prior to designing the experiment, the following steps were performed: 1) Identification of a standard test to evaluate an improvement or degradation of the electrical conductivity. 2) Identification of the most critical parameters during the sample assembly, decision of parameters to study and parameters that should be kept constant and/or recorded. 3) Identification of the constraints of the experiment, i.e. constraints concerning combinations of parameters and the number of tests which could reasonably be carried out during the DOE. 4) Definition of the DOE, i.e. the number and randomization of the runs comprising the experiment.

4.4.2 Methods

4.4.2.1 Design of Experiment

The optimal DOE was designed by first identifying the test method which would be used to detect any improvement or degrading of the electrical conductivity; it was decided to measure the electrical resistance of the films under various applied pressures.

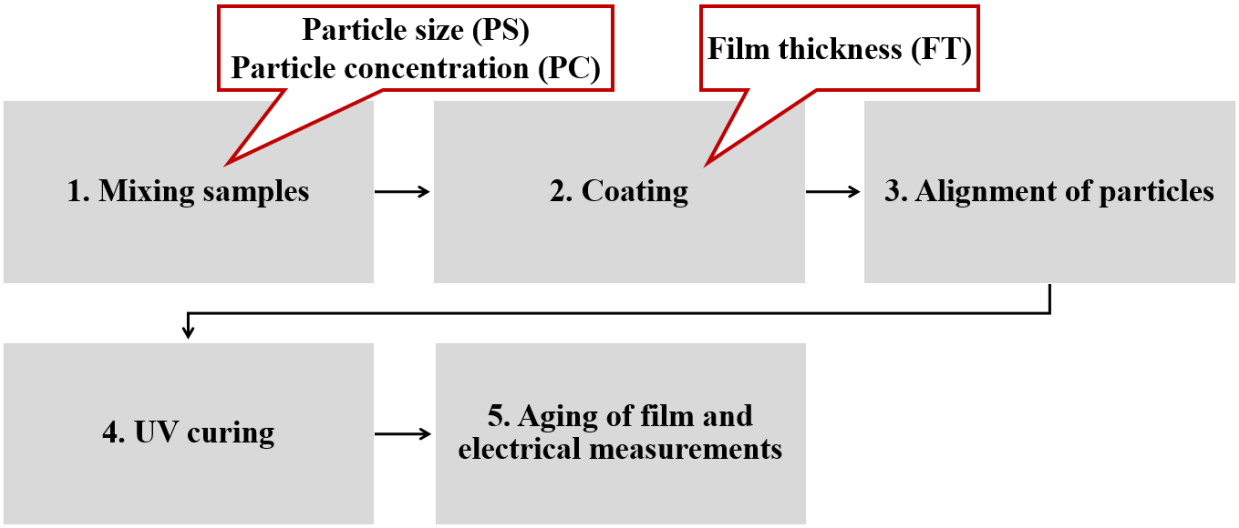

Figure 4-13: Process overview of the making of CondAlign conductive films

Secondly, the parameters to study were identified by first understanding the process used for making the conductive films and then identifying the parameters that were expected to influence the electrical conductivity of the films the most: Particle size (PS), Particle concentration (PC), and Film thickness (FT). The process for making the conductive films is shown in Figure 4-13 where the parameters under study are highlighted. In addition to the parameters under study, each process step has a variety of parameters which were controlled and kept constant during the assembly.

The parameters under study were varied within a range where it was expected to get conductive samples. The PC was treated as a continuous variable, since the volume % can be changed continuously, while the PS and FT were treated as discrete variables since the values these parameters could take were determined by the available particles and by the height of spacers available in order to determine the film thickness. All

parameters under study were considered easy to change between runs, so the order of the sample preparation could be fully randomized. See overview of parameters under study in Table 4-3.

Table 4-3: The parameters under study

Parameter	Abbr.	Unit	-1	+1	Parameter type	Ease of change
Particle concentration	PC	Volume %	2	10	Continuous	Easy
Particle size	PS	µm	13	97	Discrete*	Easy
Film thickness	FT	µm	50	191	Discrete**	Easy

After identifying the parameters under study and the parameter ranges, the constraints for the experiment was identified. There is a constraint for the combination of parameters since the particle size (PS) cannot be larger than roughly half the film thickness (FT) in order to form conductive chains during the alignment of the particles. However, we would like to allow e.g. 97 µm particles in a 191 µm thick film. The disallowed combinations were thus set to PS > 0.6 FT.
It was also decided that10 samples including the measurements and analysis were within the cost and time budget for this experiment.

Based on this, an optimal DOE was suggested using the software JMP 14 from SAS. A D-optimal design was chosen in order to obtain precise estimates of the effects. The goal was to maximize conductivity, and since it was a goal to detect non-linear behaviour of factors (if present) each parameter was set to have three levels. All parameters (factors) were modelled as discrete numeric factors. The resulting randomized design is shown in Table 4-4.

Table 4-4:The optimal DOE used in this study.

Sample name	Run Order	PC (Vol%)	PS (µm)	FT (µm)
DOE_1	1	2	98	191
DOE_2	2	2	50	102
DOE_3	3	10	13	191
DOE_4	4	10	50	102
DOE_5	5	10	13	50
DOE_6	6	2	13	191
DOE_7	7	5	50	191
DOE_8	8	2	13	50
DOE_9	9	10	98	191
DOE_10	10	5	13	102

The quality of a design can be evaluated by examining the average variance of prediction for the design, and whether there are any correlations between the parameters under study in the design. The average variance of prediction, which should be as low as possible, for this design was 0.7 which is regarded an acceptable variance. Some correlations between parameters PS and FT were observed due to the constraint of disallowed

combinations. If budget had allowed, these correlations could be better understood by augmenting the design to include more runs and possible more values of both PS and FT.

4.4.2.2 Assembly of samples

The samples for the DOE (1 and 2) are made by a stationary setup and not in the roll to roll. One sample was prepared per.

Details of how the samples for the DOE were made is given in the appendix F:

- 20190319-DOE samples making (F.1)
- 20190611-DOE samples making – 2nd DOE (F.2)

The particle concentration (PC) was varied by changing the volume percent of particles in the matrix in the mixing of the samples (step 1). A bulk density for each of the particles (PS = 12, PS = 50 and PS = 100) was calculated by taking into consideration the density of the glass bead (2.5g/cm^3), and the amount of silver coating around the glass beads (assumed density 10.5g/cm^3). The resulting bulk density varied from 2.66 g/cm^3 for the largest glass beads to 3.78 g/cm^3 for the smallest beads. The particle size (PS) was varied by choosing particles of three different sizes. The film thickness (FT) was varied by using different heights of spacers between the liners used to apply an electrical field followed by the UV-curing of the conductive films.

4.4.3 Characterization

4.4.3.1 Initial characterization of films

The sample thickness was determined by a mechanical micrometer at CondAlign, measuring across the thickness of the film. Verification of alignment was done heuristically by confirming the presence of particle chains in an optical microsocope.

4.4.3.2 Electrical characterization

Electrical characterization was performed by placing the conductive films between two electrodes and then measuring the resistivity across the films (in z-direction) using a Keithley 2450.

The top electrode consisted of a copper block with dimensions 3*3*1.5 mm^3 which was electroplated with gold in order to ensure good and reproducible electrical conductivity over time i.e. no oxidation. The bottom electrode consisted of an electroplated gold pad on a PCB. Both this pad, and the sample to be measured, were larger than the copper block, such that the measurement area was defined by the copper block (3*3 mm^2).

Two wires were soldered onto each of the electrodes allowing for 4-point measurements and thus ensuring that the contact resistance was not included in the reported values. By adding weights to the top electrode, the resistivity could also be measured at different applied pressures. All samples were measured at pressures of 0.14 MPa, 0.57 MPa and 1.36 MPa. Starting with the lowest pressure.

The resistivity was measured once a second for approximately 200 seconds, and the average of these measurements is reported. In order to convert the raw measurement of resistance to resistivity, the resistance values were multiplied with the measurement area and divided by the theoretical film thickness (given by the DOE).

Some samples appeared "stickier" than others, these samples were softly laminated to the bottom electrode in order to reduce the chance of air pockets between the film and the electrodes to influence the measurement. After the electrical measurements, an imprint could usually be seen in the film where the top electrode had been placed. The measured area could then be marked with a marker, and subsequently be imaged by optical microscopy.

4.4.3.3 Imaging of areas after electrical characterization

4.4.4 Results

4.4.4.1 Electrical characterization

All the samples from the DOE were measured electrically as a function of applied pressure as described above. Two or three spots were measured for each sample (run). The overview of all measurements, including both conductive and non-conductive values, can be seen in Figure 4-14.

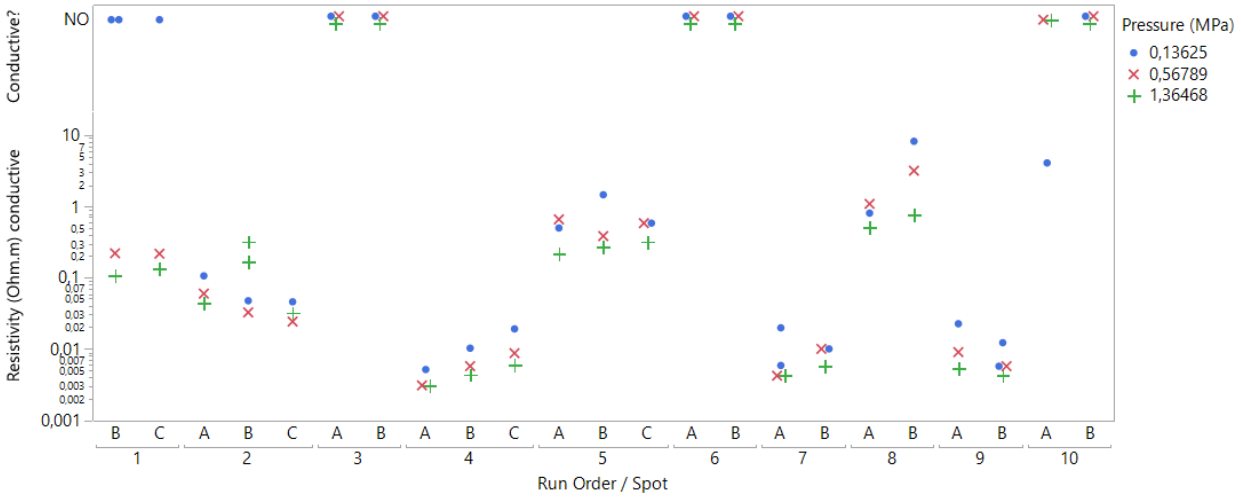

Figure 4-14: Overview of all measurements performed on the DOE samples. The run order (1-10) and spot (A-C) is given on the x-axis, while the resistivity is given on the y-axis. The non-conductive measurements (resistivity > 20 kOhm*m) are shown as "Conductive? NO" on the top of the y-axis. The pressure applied during measurement is shown by the marker colour and shape: 0.14 MPa = blue dot, 0.57 MPa = red x, 1.36 MPa = green cross.

All measurements which are shown as "conductive" have a resistivity of < 10 Ohm*m, while the lowest resistivity which has been defined as "non-conductive" was 20 292 Ohm*m. This gives an abrupt shift between the conductive and non-conductive samples:

- Samples 2, 4, 7 and 9 have low resistivity for all measured spots, and for all applied pressures.
- Samples 5 and 8 also have a consistently low resistivity for all measured spots, but with slightly higher resistivity values.
- Sample 1 has a bit special behavior, here only measurements performed under an applied pressure of 0.57 MPa or 1.36 MPa give conductive results.
- Samples 3, 6 and 10 all give non-conductive measurements except for sample 10 which has one conductive measurement.

This is summarized in Table 4-5, where the sample (run), the parameter settings, whether the sample is electrically conductive and the minimum and maximum of the measured resistivity values is shown. In the table there is also included an additional column FT/PS which tells approximately how many particles are needed in order to form an electrically conductive chain through the sample.

Table 4-5: Sample names, parameter setting and resulting electrical conductivity.

Sample name	Run Order	PC (Vol%)	PS (µm)	FT (µm)	FT/PS	Electrically conductive?	Resistivity, min/max (Ohm*m)
DOE_1	1	2	98	191	2	Under pressure	0.106 / -
DOE_2	2	2	50	102	2	Yes	0.024 / 0.320
DOE_3	3	10	13	191	15	-	
DOE_4	4	10	50	102	2	Yes	0.003 / 0.019
DOE_5	5	10	13	50	4	Yes	0.214 / 1.460
DOE_6	6	2	13	191	15	-	
DOE_7	7	5	50	191	4	Yes	0.004 / 0.020
DOE_8	8	2	13	50	4	Yes	0.504 / 8.213
DOE_9	9	10	98	191	2	Yes	0.004 / 0.023
DOE_10	10	5	13	102	8	- one exception	4.082 / -

4.4.5 Optical imaging

Images of the DOE Samples were acquired using an optical system described in 5.1.1. The images are shown in the Table 4-6.

Table 4-6: Optical images of each sample

Sample (run)	PC (Vol%)	PS (µm)	FT (µm)	FT/PS	Electrically conductive?	Optical image, captured by in-line prototype
1	2	98	191	2	Under pressure	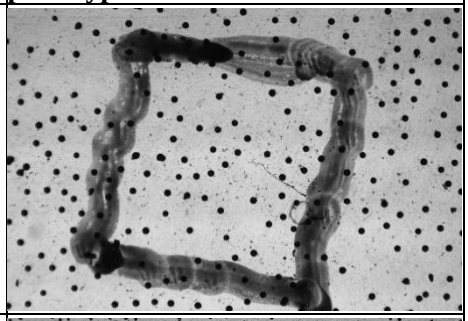
2	2	50	102	2	Yes	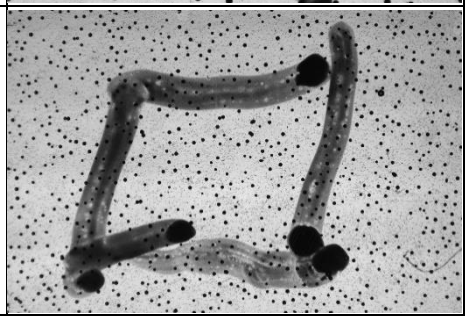

3	10	13	191	15	-	
4	10	50	102	2	Yes	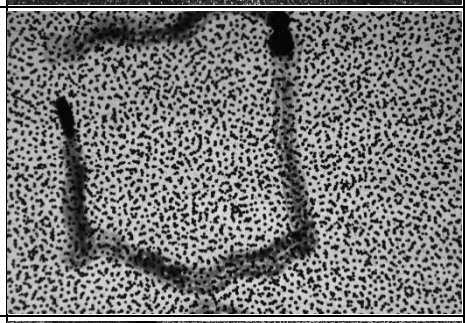
5	10	13	50	4	Yes	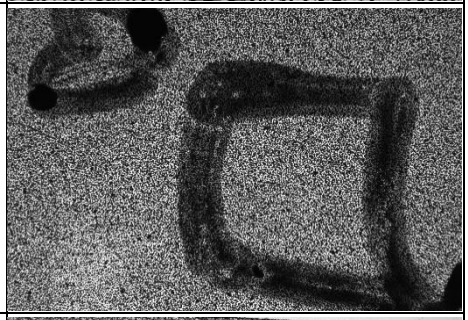
6	2	13	191	15	-	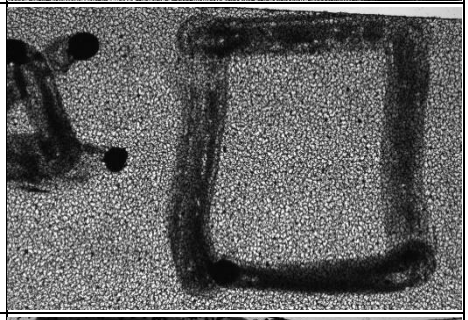
7	5	50	191	4	Yes	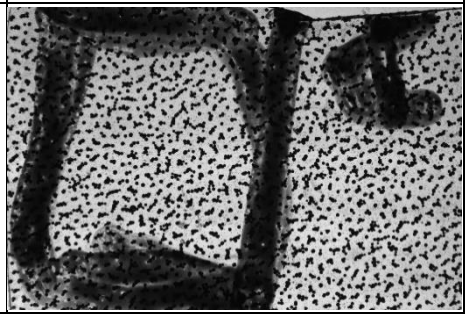

8	2	13	50	4	Yes	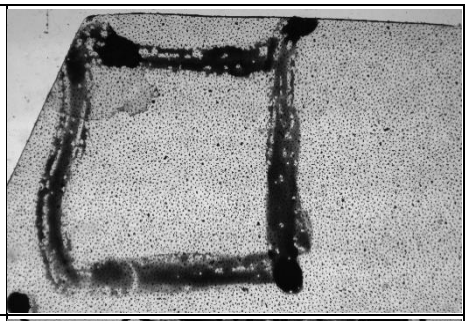
9	10	98	191	2	Yes	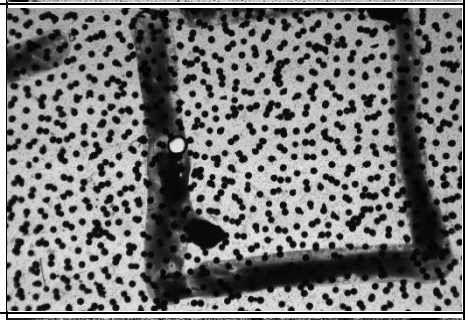
10	5	13	102	8	- one exception	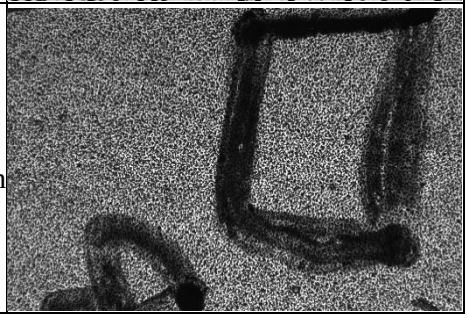

4.4.6 Data analysis and discussion

4.4.6.1 Electrical characterization

When looking at the measured electrical resistivities, there seem to be two trends in the data

- It seems like the most important factor in order to determine the conductivity of the samples is the ratio FT/PS which indicates how many particles are needed to form a conductive chain, see Table 4-5. From these measurements, it seems that to form conductive chains with 8 or more particles is very challenging – and the samples which require formation of long chains, i.e. > 4 particles, are indeed not electrically conductive (sample 3, 6 and 10).
- For most spot measurements the resistance is reduced by increased pressure, but there are also some exceptions where the resistivity is higher for higher applied pressures. The clearest example of this trend is for sample 1 where only measurements under an applied pressure (0.57 MPa or 1.36 MPa) allows for electricity to conduct. When we investigated this particular sample in microscope (with high magnification) it seemed like some polymer was covering most of the particles, and this could explain why this sample needs some pressure to push aside the electrically insulating matrix and be electrically conductive.

In order to get an impression on how (and whether) the individual parameters influence the measured resistivity, the absolute resistivity has been plotted as a function of the parameters PC, PS and FT in Figure 4-15. In addition, the ratio of FT/PS has been included in one plot, and the applied pressure during

measurements in another plot. The resistivity of has been set to maximum 10 Ohm.m such that all non-conductive samples are shown as 10 Ohm.m.

From these plots it seems like there is a correlation between the PS and the resistivity, i.e. that larger particles give a lower resistivity, and similarly there might be a correlation between the FT and the resistivity. However, the only plot that indicates a clear correlation is the factor FT/PS with the resistivity. There does not seem to be an overall correlation between the applied pressure during measurements and the resistivity.

The weakness of looking at the parameters individually like this is that effects can be camouflaged if several parameter settings are influencing the resulting resistivity in different directions at the same time. To work around this, a regression model was created and analysed.

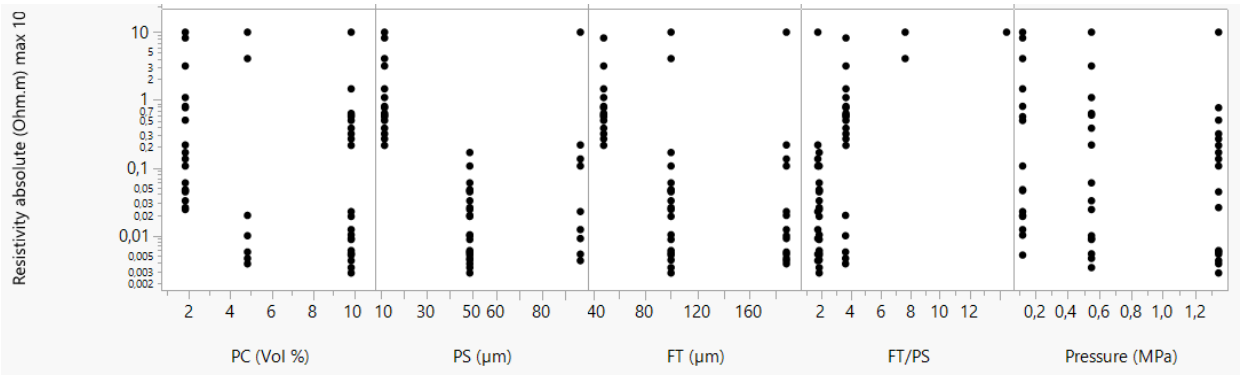

Figure 4-15: The measured absolute resistivity is plotted as function of the individual parameters PC, PS, and FT. In addition, the ratio of FT/PS has been included, and the pressure applied during the measurement. The maximum resistivity is set to 10 Ohm.m, i.e. all the non-conductive measurements are set to 10 Ohm.m.

4.4.6.2 Data analysis

The raw data from the resistivity measurements is as mentioned above binary; the measurements of conductive samples give accurate and reliable values while the measurements of non-conductive samples give very high values in Ohm and it seems random whether they are with a positive or negative sign. To handle this in the data analysis i.e. the regression model, the non-conductive samples are all set to 10 Ohm.m.

The measured data was fit to a linear Standard Least Squares regression model using the same software as used for the design of the optimal DOE.

Model 1, only physical parameters

PC (Vol%), PS (µm) and FT (µm) found in Table 4-4 were set as main parameters. The resulting regression model was used to test the influence of the individual parameters and to predict what would be the outcome with specific combinations of parameters. The linear regression model used was:

$$\textit{Measured resistivity} = \beta 0 + \beta 1\ PC + \beta 2\ PS + \beta 3\ FT + \varepsilon$$

where the β's are constants which are found by using a standard least squares method, PC, PS and FT are the parameters that were varied, and ε is the remaining variation in our data which cannot be explained by the model, i.e. an error term. Before suggesting this model, it was also tested whether the applied pressure during the electrical measurement, and/or the interactions between the main parameters would give significant contributions to the model. This was however not the case.

This model gave a Rsquare Adj of 0.557424, which indicates how much of the variation in the measured data which can be explained by the suggested model. The root mean square error (RMSE) was 2.9432. This gives

an indication of magnitude of the error of the estimated resistivity. However, PC did not give a significant contribution to the model, and by removing also this term we got a model with an Rsquare Adj value of 0.5476 and an RMSE of 2.9757. The values of β0, β2 and β3 for this model are shown in Table 4-7.

Table 4-7: Values and standard errors for the constants in Model 1.

Constant	*Value*	*Std. Error*
β_0	0.6952	0.8901
β_2	-0.1082	0.0131
β_3	0.0527	0.0071

In summary, a significant reduction in measured resistivity was observed when:

- The particle size was increased
- The film thickness was decreased

The particle concentration or pressure applied during the electrical measurement did not give significant contributions to the model.

A possible explanation for the decrease of the resistance as the number of particle increase is as follow: Decreasing particle size and increasing film thickness means more particles aligned in chain for a given film thickness. resistance in a chain of particles is due to the resistance in the volume of the particles and the contact between particles. As the number of particles increases, so do the number of contact points, and an assumption is that this contribution dominates the total resistance when the number of particles increases.

Model 2, including the ratio FT/PS

From the plots shown in Figure 4-15 it seemed like the ratio FT/PS could explain a lot of the variance observed in the measured resistivity. Therefore, a model was also suggested where FT/PS was included as a parameter in addition to the parameters included in Model 1.

$$\textit{Measured resistivity} = \beta 0 + \beta 1\ PC + \beta 2\ PS + \beta 3\ FT + \beta 4\ FT/PS + \varepsilon$$

where the β's are constants which are found by using a standard least squares method, PC, PS and FT are the parameters that were varied in the experiment, the ratio FT/PS is included as it has shown to influence the resistivity, and ε is the remaining variation in our data which cannot be explained by the model, i.e. an error term. Again, the contribution of the pressure applied during the electrical measurements did not show any significant contribution to the model, neither did the interactions between the remaining parameters.

This model gave an Rsquare Adj of 0.7343 and an RMSE of 2.2803, i.e. this explains more of the variation in the measured data than Model 1, and the error of the estimate has been reduced. The values of β0, β1, β2, β3 and β4 for this model are shown in Table 4-8.

Table 4-8: Values and standard errors for the constants in Model 2.

Constant	*Value*	*Std. Error*
β_0	-1.2690	0.9572
β_1	-0.1842	0.0754
β_2	0.0838	0.0305
β_3	-0.0369	0.0144
β_4	1.3009	0.1955

In summary, a significant reduction in measured resistivity was observed when:

- The particle concentration was increased (weak contribution)
- The particle size was decreased (*)
- The film thickness was increased (*)
- The ratio of film thickness over particle size was decreased (i.e. less particles are needed to form a conductive chain through the film)

Two of the observations above, marked with (*) are contradicting the results obtained for Model 1, and common sense, and this indicates that when introducing the parameter FT/PS it is better to remove these parameters from the model. See below.

The pressure applied during the electrical measurement did not give significant contributions to the model.

Similarly, the intercept is not giving a significant contribution and it can be seen that the standard error of β0 is in the same range as the value itself.

Based on the observations above, a simplified model was made where only the ratio FT/PS was included. This model still gave a very good fit, with an Rsquare Adj of 0.6957 and an RMSE of 2.4404 which means that for the samples included in this study the very simple expression shown below could be considered:

Measured resistivity = $\beta 0 + \beta 4$ FT/PS + ε

where β0 is a constant giving the intercept, β4 is a constant and ε is an error term. The values of these constants are given in Table 4-9. Note that the intercept, β0, now gave a significant contribution to the model.

Table 4-9: Values and standard errors for the constants in a simplified version of Model 2.

Constant	*Value*	*Std. Error*
β_0	-1.0882	0.4464
β_4	0.7967	0.0637

In summary, a significant reduction in measured resistivity was observed when the ratio between film thickness and particle size was decreased.

4.4.6.3 Correlation between resistivity and image analysis

The measures defined in 4.3 were calculated on the images of the DOE samples and compared with the measured resistivity. Figure 4-16: presents the results of this comparison.

Excluding the samples that are not conductive, we can see trends between the optical measures mean background size, CoveragePrct, max background size and entropy BW. Mean Background, size which is the measure of the average distance between particle cluster, increases as the resistivity increases. CoveragePrct, which measure the occupation percentage of particles decreases as the resistivity increases. Also, the entropy BW decreases as the resistivity decreases.
We saw previously that a model including the particle size and the film thickness explain the resistivity with a Rsquare of 70 % and that film with large particle and thin film had higher conductivity. An hypothesis for this behaviour, is that large particles will tend to occupy more area in the film so that for aligned sample and all other parameters constant, larger particle will lead both to increased conductivity and increases CoveragePrct. The meanBackground size decreasing as the resistivity decreases, can also be connected to a decrease of the inter distance between particle and particle cluster as the particle size increases when all other parameters are kept constant.

In conclusion, we can observe correlation between some of the optical measures and the measured resistivity, but further studies are needed to confirm those trends. Correlation studies should be performed within each type of samples by varying concentration, particle size and film thickness.

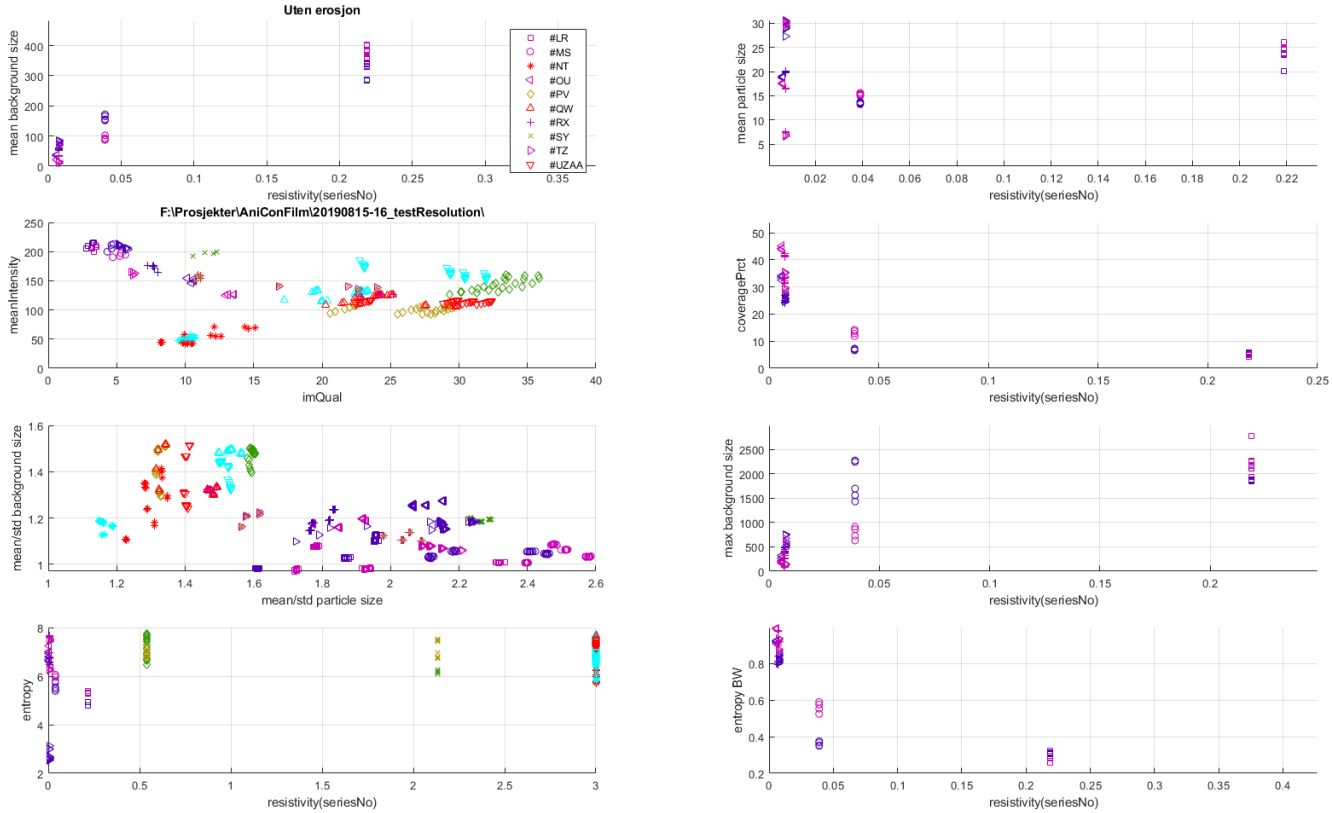

Figure 4-16: Comparison between resistivity and optical measures

4.4.7 Conclusion

An experiment was designed using optimal design of experiment in order to test how the resistivity of conductive films change as a function of particle concentration, particle size, and film thickness. The rest of the parameters during the production of these films were kept constant. The resulting conductive films had a large variation in measured resistivity; six out of ten films turned out to be electrically conductive.

To understand which parameters, contribute the most to the conductivity of the films, and how, two regression models were made:

- Model 1 explained approximately 55 % of the observed variation in measured resistivity and included only the physical parameters which were changed in the study. It was shown that a significant reduction in measured resistivity was observed when the particle size was increased and the film thickness was decreased.
- Model 2 explained approximately 70 % of the observed variation in measured resistivity and included the ratio of FT/PS as the only parameter. It was seen that a significant reduction in measured resistivity was observed when the ratio between film thickness and particle size was decreased.

We can observe correlation between some of the optical measures and the measured resistivity, but further studies are needed to confirm those trends. Correlation studies should be performed within each group of sample types by varying concentration, particle size and film thickness.

5 Establishment of industrial imaging set-up (SINTEF and CondAlign AS)

We have established in 4.3, an image analysis algorithm and defined a set of features that can be used to distinguish between aligned and non-aligned samples from ***high-resolution microscope images***. In conventional microscopy, high resolution microscopic images are synonymous of small field of view, i.e. inferior to 1 mm^2. Unless the field of view of a microscope system can be scanned over a large area, such a small FOV is not compatible with many real time R2R process applications where field of view of several cm^2, must be scanned during some millisecond. Although mechanical scanning of the field of view of an optical system is possible, it usually adds complexity and increases the cost of the imaging system. Another possibility is to use an optical system with as large a field of view as possible. In conventional optical systems, increasing field of view is synonymous with degrading the spatial resolution. In our application, we are dependent of a good enough optical resolution since we are interested in gathering information about particles with micrometric dimensions. It is thus necessary to find a trade-off between high optical resolution and large field of view in order to design an imaging system that is compatible with real time imaging of the CondAlign R2R process.

In this chapter, we evaluate experimentally and theoretically the robustness of the image analysis algorithm established in 4.3 for ***degraded optical resolution*** and assess for which optical resolution the image analysis algorithm will break-down eventually. This allows us eventually to customize an optical system for acquisition of images over film areas of ~4 cm by 4 cm and on samples moving at speed up to several 10 cm/min.

In 5.1, we describe lab experiments and simulations performed on static R2R samples using a 20 Mpixels industrial CMOS camera and lenses with medium magnification. The rationale behind these tests is to find out at which optical resolution the algorithm eventually breaks down. This also allow us to find the maximum field of view achievable. In 5.2, we establish an optical set using a lens with low resolution and large field of view to verify the finding of 4.3. We simulate the acquisition of images on a moving film by acquiring images with short exposure time and assess the impact of defocusing on the analysis results.

5.1 Finding the optimal optical resolution and field of view

In this chapter, we build optical systems with various optical resolution to assess the robustness of the image analysis algorithm against degradation of optical resolution. In 5.1.1, we build an optical system using a 20 Mp CMOS Camera and diffraction limited resolution lens with decreasing magnification (x5, x2 and x1) and test experimentally that the algorithm still allows differentiation between aligned and non-aligned samples for all the magnification. In 5.1.2, we then evaluate the performance of the image analysis algorithm on simulated low optical resolution images and find a threshold for which the algorithm eventually breaks down.

5.1.1 Optical system with medium optical resolution

We build an optical system using an industrial 20 Mpixel camera from FLIR and several diffraction limited lenses from Edmund optics. The camera and lenses are mounted on translation and rotation micrometric stages allowing to scan the field of view of the optical system in the plan of the ACF film. The samples are illuminated in transmission using a green LED light source. See appendix D.3 for a thorough description of this version of the optical system.

We assess the impact of the diffraction limited lenses on the image analysis algorithm. For that, we acquire images of B2 samples using the x1, x2, x5 magnification lenses. The achieved resolution and field of view are summarized in Table 5-1.

Table 5-1: Theoretical resolution and field of view of the optical system for magnification x1, x2 and x5

Magnification	Resolution (um)	Field of view (cm x cm)
5	0.6	0.325 x 0.2175
2	1.2	0.65 x 0.435
1	2.4	1.3 x 0.87

We run the algorithm established in 4.3 on the images. The analysis results for a selection of the measures established 4.3 are shown in Figure 5-1-Figure 5-3.

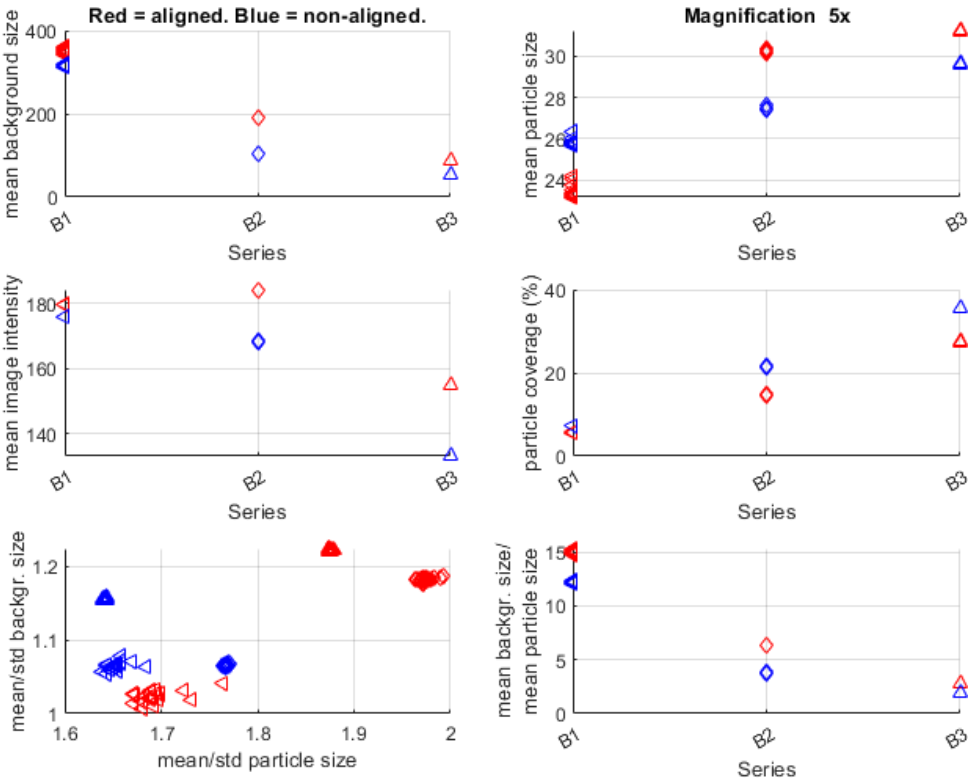

Figure 5-1: Results for images for 5X lens.

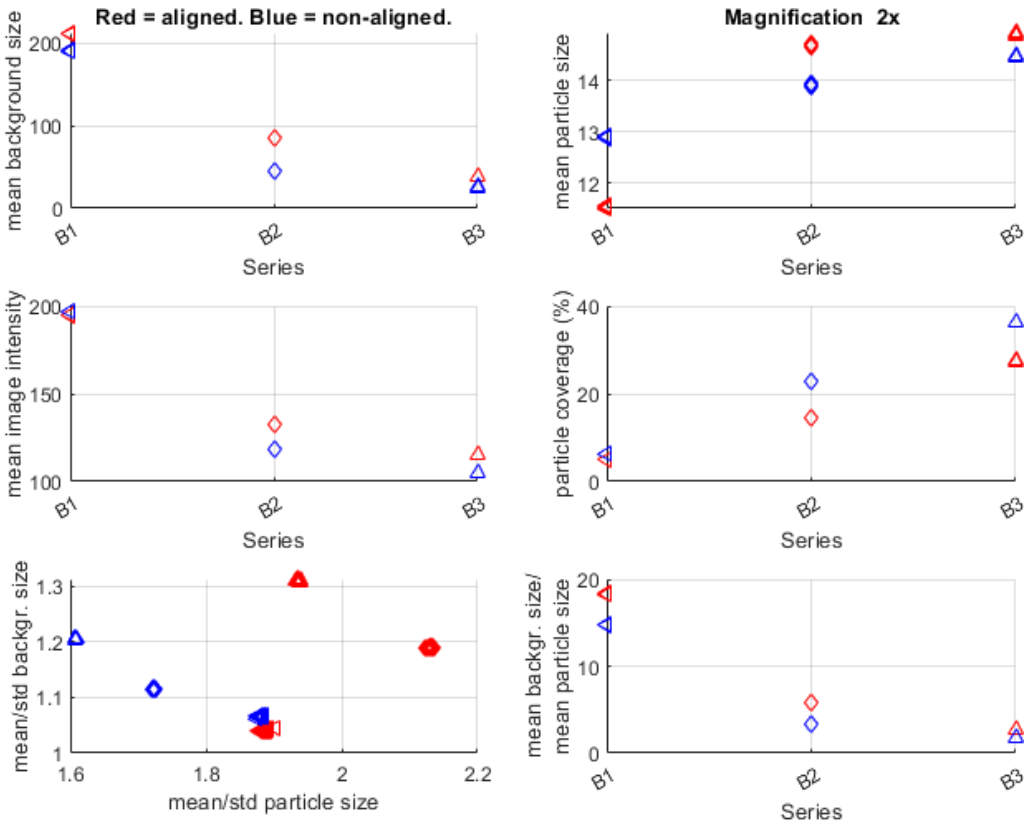

Figure 5-2: Results for images for 2X lens.

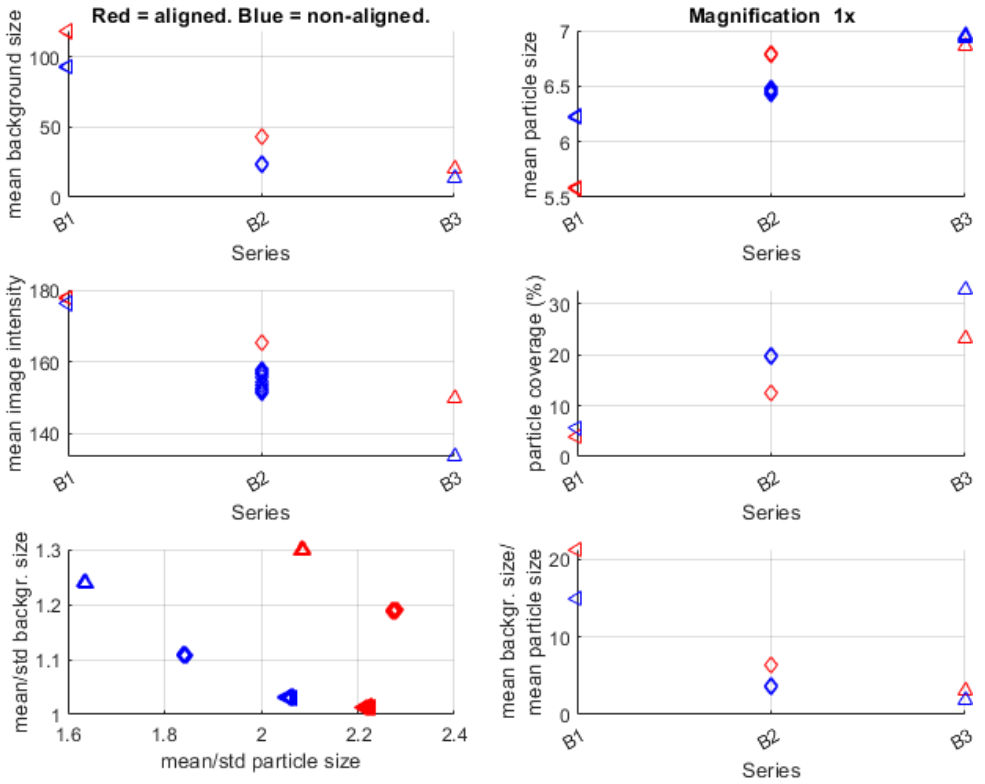

Figure 5-3: Results for images for 1X lens.

Discussion:

- X 5 is close to the magnification used in the microscopic imaging set up.
- For all magnification, we have a net separation between a set of measures for non-aligned and aligned sample
- Extensive measures like mean background size or mean particle size decreases as the resolution decreases. Since the measures are given in pixels and the number of pixels is reduced this is logical. Intensive measures like ratio of mean background size and mean particle size stays approximately constant, illustrating logically the goodness of those measures for quantifying the degree of alignment.
- We note that the sample, B1 shows most variation in the plot CNR background size as function of CNR particle size as the magnification increases, followed by sample B2 and then B3. This is a consequence of the decreasing number of particles in the analysis window as the magnification increases (high resolution means small field of view and a reduced number of particle). This shows that at constant optical resolution, the algorithm performs all the best as the number of particles increases.

Conclusion.

We have demonstrated experimentally that down to x1, the algorithm manages perfectly well to separate aligned from non-aligned. The CNR for the measure tested in this experiment is higher for x1 than for higher magnifications regardless of sample concentration. Since the optical resolution at x1 is well under the mean size of the particle, the improvement of the results can be explained by a higher number of particles in the analysis windows. At x1 magnification, the field of view is approximately 1 cm^2. This is a factor ~20 away from the useful analysis area on the CondAlign R2R. In the next chapter, we evaluate further the effect of resolution downgrading on the analysis results.

5.1.2 Simulation of degraded optical resolution

In the previous chapter (5.1.1) we found that a x1 magnification lens give satisfactory separation results for three type samples, B1, B2 and B3. In this chapter, we evaluate further the consequences of degrading the optical resolution and establish a limit under which the algorithm breaks down. Since optical lenses are costly, we instead simulate the degradation of resolution using experimental acquired images.

We use a magnification x1 lens and acquire images of B1, B2 and B3 samples, aligned and non-aligned. We then simulate degraded resolution in software by down sampling the images obtained for magnification 1 image by various factors (2, 4, 8). This allows us to simulate magnifications of x0.5, x0.25 and x0.125. Table 5-2 shows the expected field of view and resolution for a given simulated magnification and Figure 5-4 shows examples of images with original and degraded resolution.

Table 5-2: Simulated magnification and corresponding optical resolution and field of view

Magnification	Resolution (um)	Field of view (cm x cm)
1	2.4	1.3 x 0.87
0.5	4.8	2.6 x 1.74
0.25	9.6.	5.2 x 3.48
0.125	19.2	10.4 x 6.96

We then ran the image analysis algorithm on the simulated images. The factor used to separate between particles and background was adjusted according to the amount of down sampling but was not changed between the image series. Figure 5-5, Figure 5-6, Figure 5-7and Figure 5-8 show results of analysis on x1, x0.5, 0.25 and 0.125 magnification.

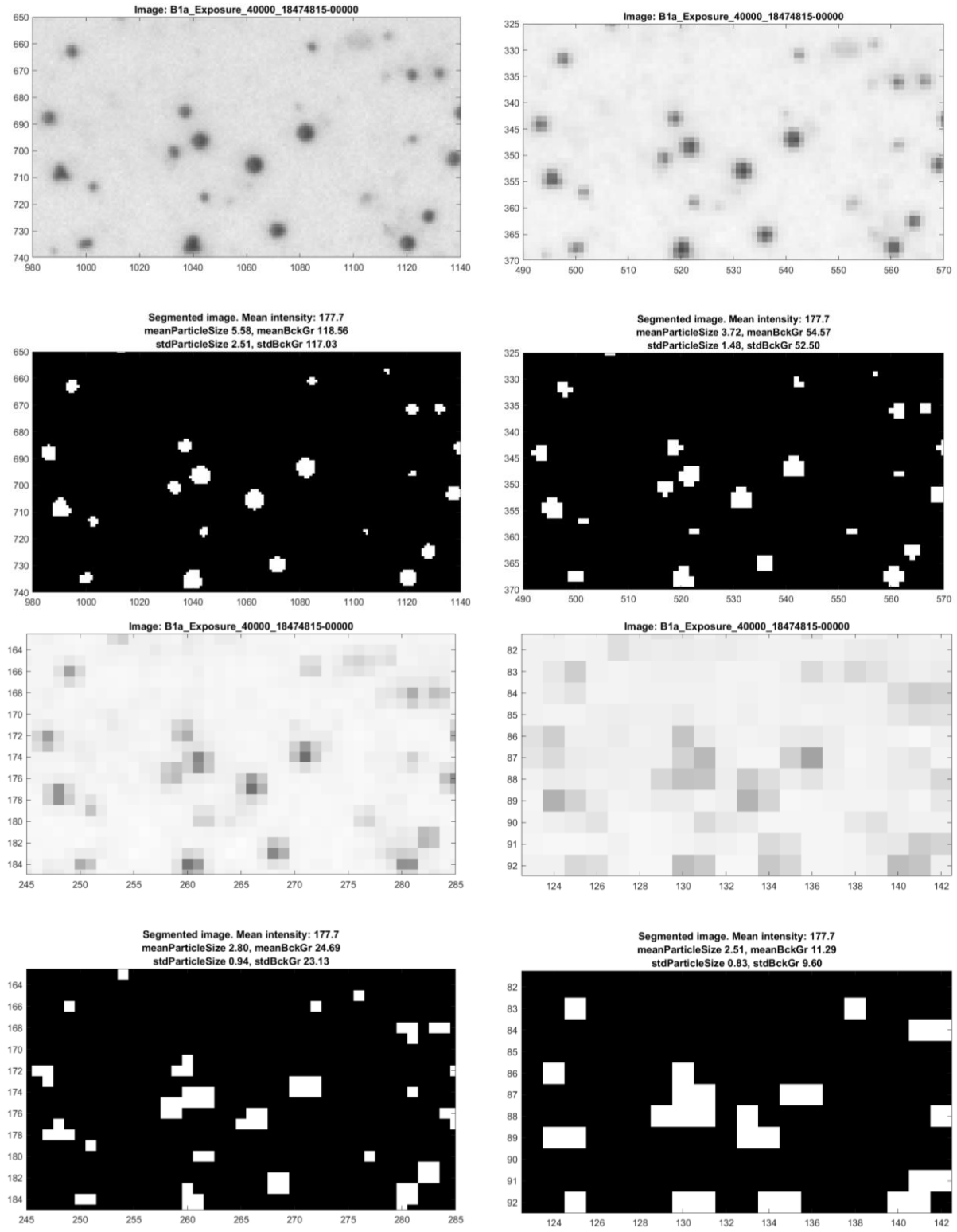

Figure 5-4: Examples of images and segmented particles for x1, x0.5, x0.25 and x0.125. The images illustrate how the optical resolution degrades and how the information about the shape of particles disappears as the resolution decreases.

For resolution down to 0.25, most of single particles and particle cluster present in the x1 images can still be identified and separated in the raw and segmented images. For 0.125 magnification, particle cluster tends to merge and information about the actual distribution of particles disappear, e.g. see how particles merge around pixels 174, 260 in the segmented images and how smaller or single particles disappears when transitioning from x0.2 to x0.125.

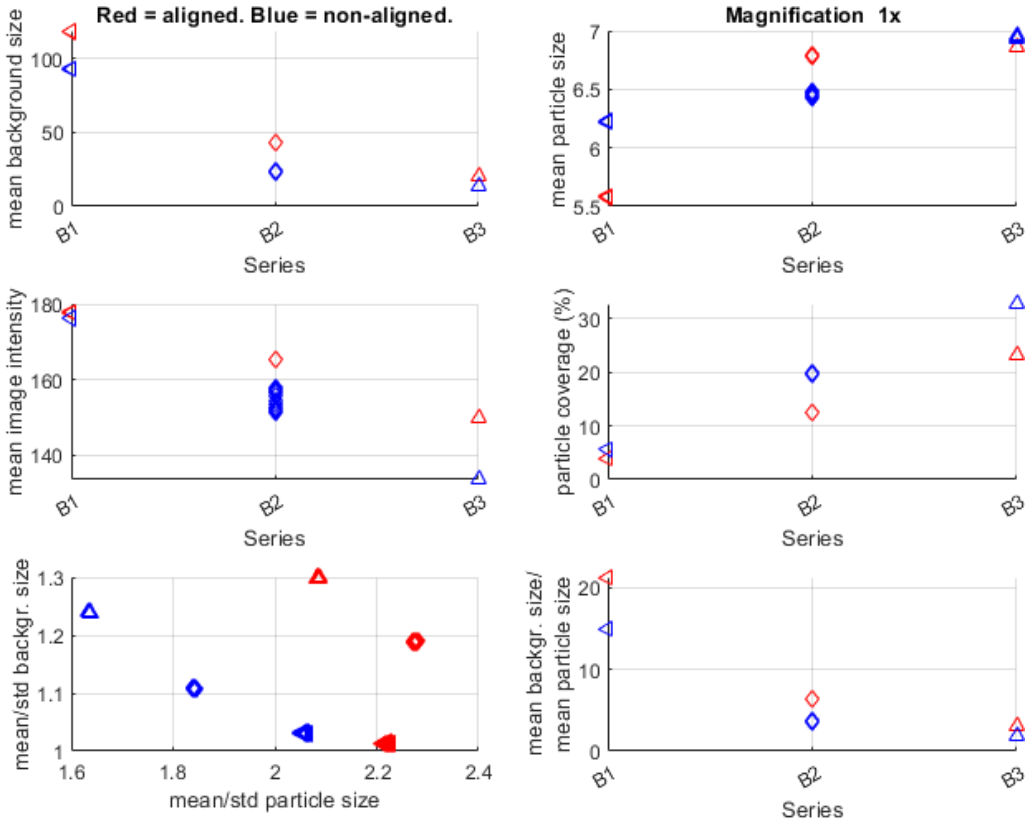

Figure 5-5: Analysis results for original 1x magnification images

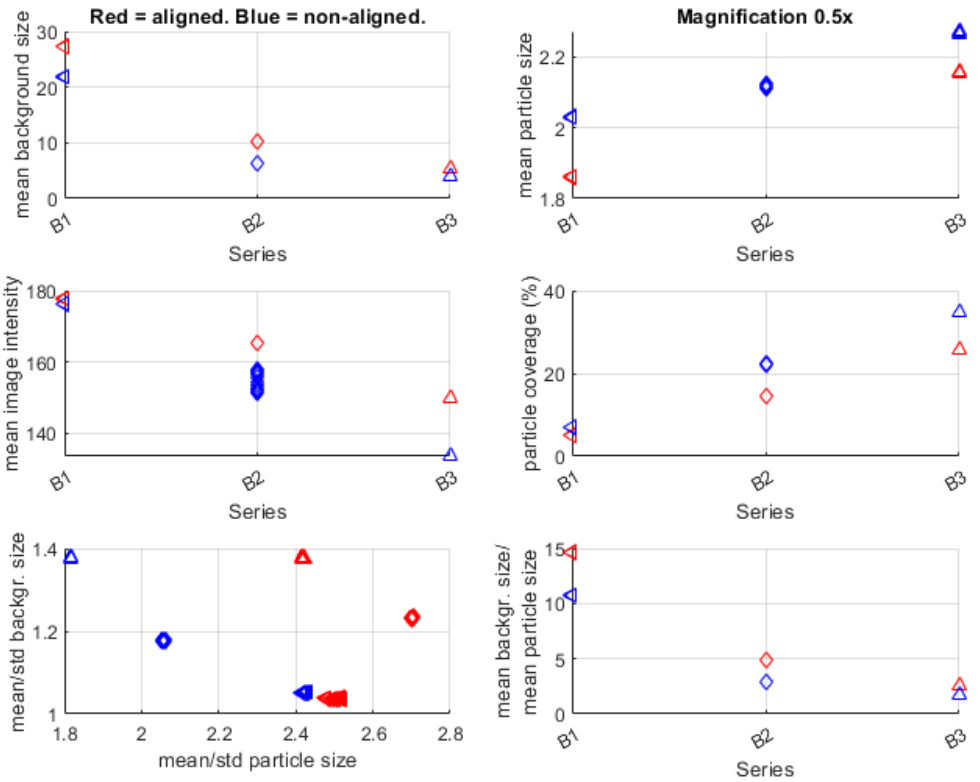

Figure 5-6: Analysis results for simulated 0.5x magnification images

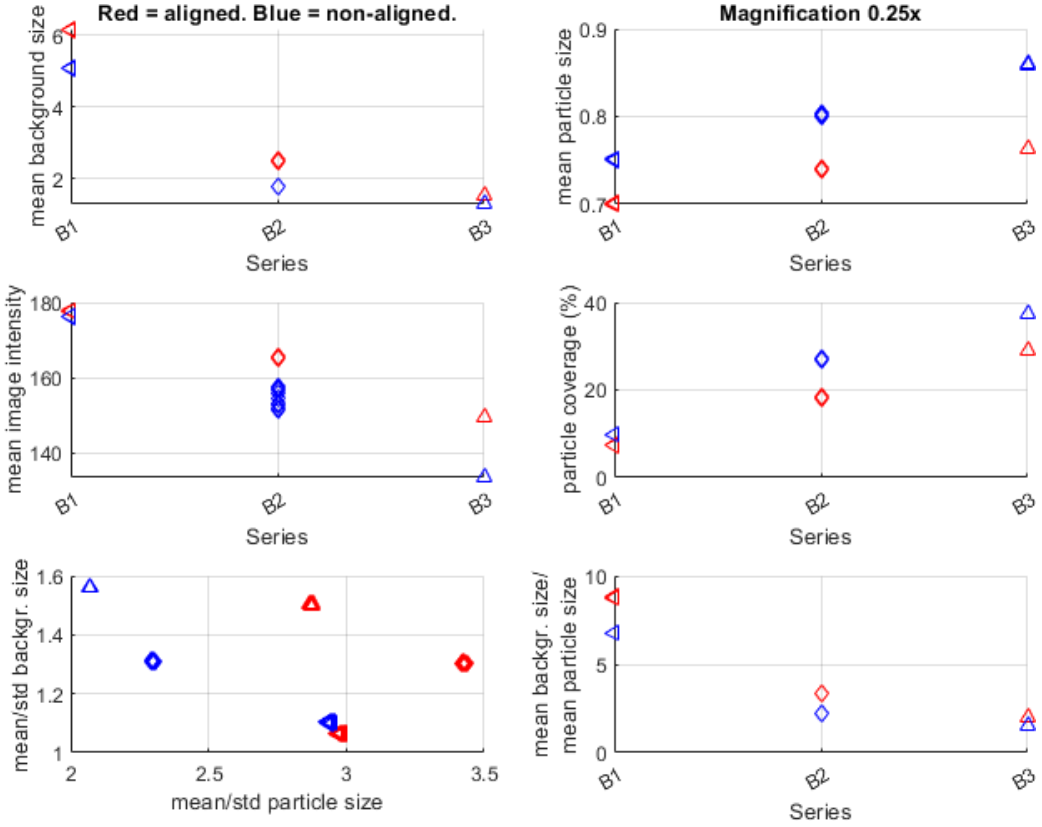

Figure 5-7: Analysis results for simulated 0.25x magnification images

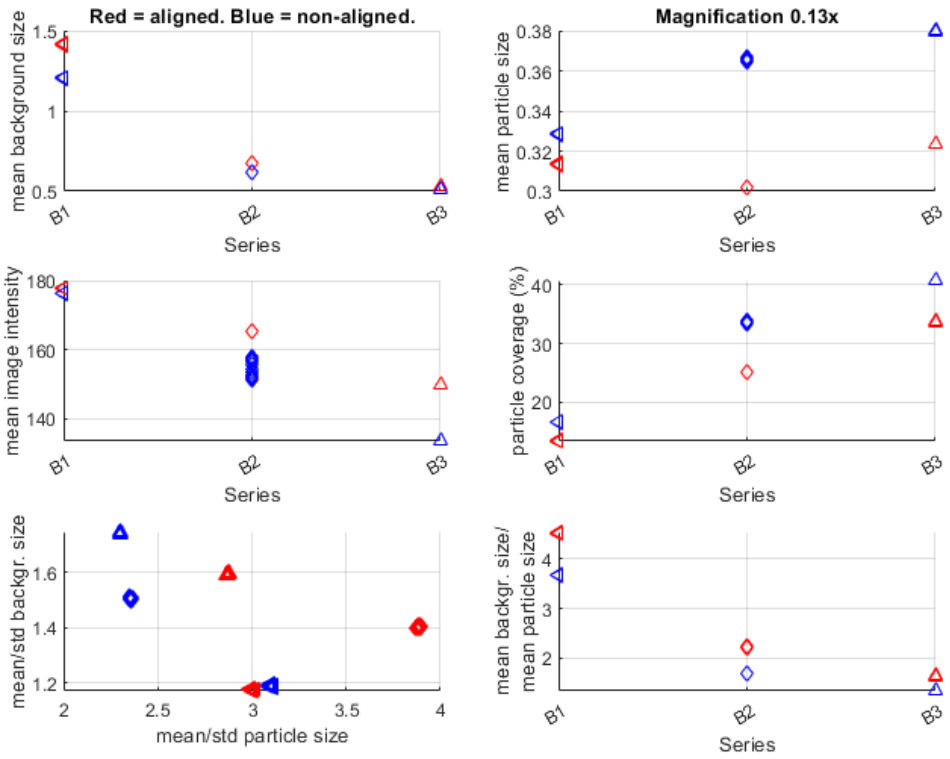

Figure 5-8: Analysis results for simulated 0.125x magnification images

We observe that for all the samples type and all magnification there is a net separation between the computed measures from aligned and non-aligned images (separation superior to the noise present in each measure). We can also see that the CNR

The algorithm seems thus very robust against degradation of the optical resolution. The results from this experiment allowed us to conclude that it is possible in theory to use lower resolution to infer the alignment of the particle. For a magnification of resp. 0.25, 0.125 the theoretical resolution equals resp. 12 um, 19.5 um, which corresponds approximately to the mean diameter value of the particles used in the samples of type B. We see on Figure 5-4 that for x0.2 and x0.125, information about the particle distribution starts to disappear.

At 0.2 magnification, the field of view equals approximately 6.5 cm x 4.35 cm which equals the widths of the ACD film on the existing R2R of CondAlign.

In conclusion, a magnification of 0.25 and an optical resolution of 12 um – 20 um should be thus satisfying both for inferring the alignment of the particle from a local region in the image and a region of interest that is large enough to inspect the whole film without need for mechanical scanning of the field of view .

5.2 Optical system with low resolution lens

In the previous step, the degradation of the optical resolution was constant over the image. Large field of views is synonym of images quality degradation when using conventional lens. In, conventional lenses, which have angular fields of view, when the distance between the object and the lens is increased, the magnification will decrease. The angular field of view also introduces perspectives error, which can result in inaccuracy when the object to lens distance changes. In so called telecentric lenses, the parallax error is reduced in comparison to standard lenses by having a constant, non-angular field of view; at any distance from the lens, a Telecentric Lens will always have the same field of view. Since we want the algorithm to give the same results for particles

in the centre of the field of view and at the periphery, a telecentric lenses seems recommended. We choose to pursue with a telecentric from Edmunds optic (0.25X 2/3" GoldTL™ Telecentric Lens) in the final version of the inline optical system. This lens was chosen because it has a magnification of 0.2 and a field of view close to 4 cm by 4 cm. This commercial lens possesses thus characteristics very close to the magnification and aperture identified in 5.1. This leads us to the design of a second version of the optical system. This new system consists in the 20 Mp FLIR camera and the telecentric lens from Edmunds optic. The system is described in more details in appendix D.4.

We evaluate the performance of this new system when varying the LED intensity from high to low value and keeping the integration time constant. This allows assessing the performance in high to low light conditions. In real life application, i.e. when acquiring images on moving particle in the R2R, the intensity of the LED will be chosen as high as possible. Low light conditions will thus be obtained when using short integration time, that are chosen to freeze the movement of the fast-moving particles. Varying the LED intensities at constant integration time will allow us to simulate the performances of the optical system in a laboratory setting.

The LED intensity is varied between 0 and 380 mA. Images of static sample B2 are acquired for each LED intensities and we run the image analysis algorithm. An example of image acquired with the optical system is given in Figure 5-9. Note that the size of the camera chip is larger than the field of view in the image plane but that we nevertheless acquire image of almost 100 % of the sample width.

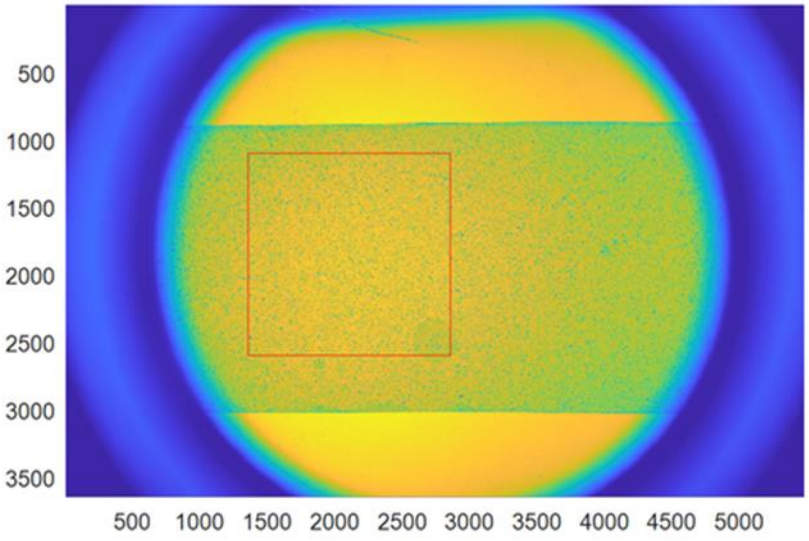

Figure 5-9: Example of image of one of the sample acquired by the optical system version 2. The field of view in the image plan is larger than the aperture of the lens. The effective field of view is a circle with a Ø~4 cm

We set the integration time of the camera to 2000 us. The results of the analysis for measure mean background size, mean particle size, meanIntensity, coveragePrct, max background size are show on Figure 5-10.

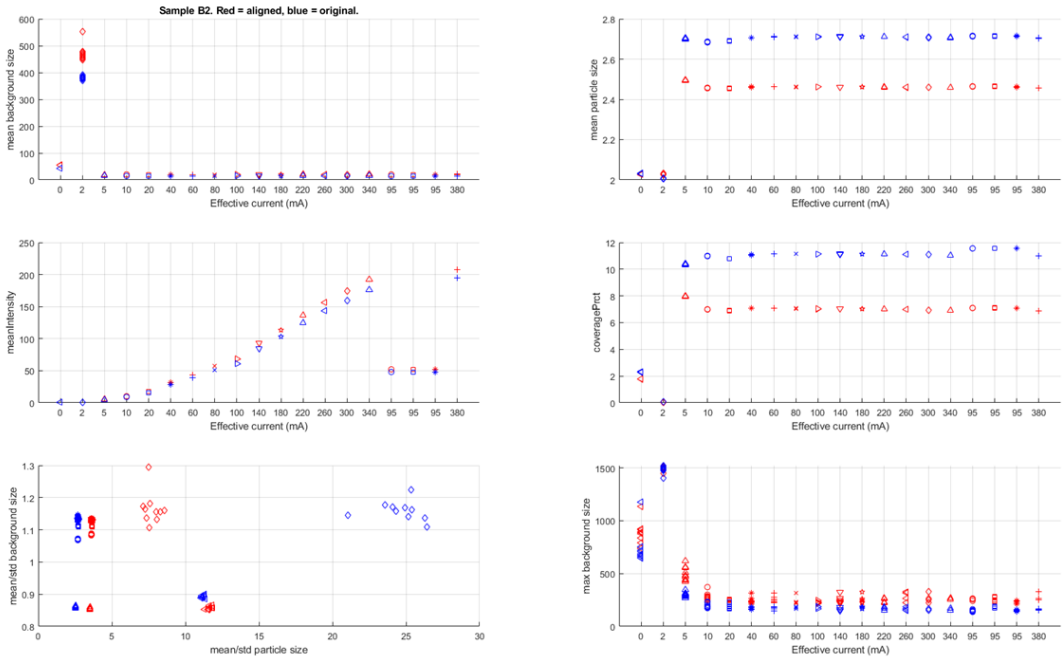

Figure 5-10: Evolution of the parameter "mean background size", "mean particle size", "meanIntensity", "coveragePrct", "max background size" as function of intensity of LED.

Observation: For the measure *mean particle size* and *coveragePrct*, the separation of the measure for aligned and non-aligned is constant and satisfying for LED current above or equal to 5 mA. There are fluctuations of the value of the measure of the order of 0.05 as the current in the LED varies but those variation are insignificant in comparison to the mean values for aligned and non-aligned and compared to the difference between aligned and non-aligned.

The measure *meanIntensity* gives also a good separation between aligned and non-aligned, but it increases logically with the LED intensity. For *max background size*, the separation between aligned and on aligned is not as convincing as those obtained with higher resolution lenses.

Discussion: The separation between aligned and nonaligned sample of type B2 is satisfying when using the telecentric lens. We thus verified experimentally that the algorithm can efficiently discriminate between aligned and non-aligned when applied to images with resolution compatible with utilization on the R2R of CondAlign.

We also find that the algorithm is robust against low light condition. Since we can control the intensity sent though our LED, low light condition will be obtained mainly when we use short integration time to freeze the movements of particle in a moving film. At low light condition, one of the main factor limiting the application of our algorithm is the photon shot noise At 2000 us integration time and 10 mA through the LED, we should obtain in theory the same pixel counts (~2000x10=20000 us.mA) and thus the same photon shot noise as for images that would be acquired with shorter exposure time but higher LED intensity. For a typical LED intensity of 360 mA, this exposure time amounts to 55 us (55x360 ~20000 us.mA). Since we manage to separate experimentally aligned from non-aligned even at LED intensity down to 10 mA, we should manage to separate aligned from non-aligned at 55 us exposure time and 360 mA LED intensity.

During 55 us, particles moving at 1 m/min have moved ~1 um. 1 um is small in comparison to the point spread function of the optical system (~12 um with our telecentric lens). The movements on the particle in a moving film should thus have little influence on the algorithm results, and the optical system should work efficiently even at film speed up to 1 m/min.

Conclusion:

- In conclusion, we find that the algorithm works for LED current down to 10. Some measures, e.g. the *mean particle size* and *coveragePrct*, have constant values whenever the LED intensity is superior to a threshold value (5 mA) and would be more adapted to application in environment with varying lighting conditions.
- We can also give degree of organisation with good confidence even when having low pixel counts. This mean that the new optical system combined with the algorithm should give us reliable results when used on the R2R line of CondAlign on moving samples.

5.3 Spectral characterization of polymers

Spectral characterizations of polymer were performed using a visible spectrometer to investigate whether spectral windows with high transmission exists. The results, described in detail in appendix E, show that the transmission spectra are rather flat between 300 and 600 nm and that any wavelength in that range can be used for imaging application.

6 Prototype testing on R2R (CondAlign AS and SINTEF)

In chapter 5, we described the design of an optical imaging system customized for real time imaging of particles on the R2R line. We now present the installation of the optical system on the R2R line as well as experiments performed on moving sample. We eventually demonstrate acquisition of images as samples are manufactured and close to real time analysis of the image using the algorithm developed in 4.3. This demonstration constitutes the final delivery in the AniConFilm project.

6.1 Set-up

Figure 6-1 and Figure 6-2 show the optical system installed on the R2R line at CondAlign facilities. The lens-camera system can be translated vertically and rotated using linear translation and rotation stages. The camera is fastened to the lens. A mount has been designed for mounting the lens to the translation stages. By doing so, we avoid tension on the c-mount of the camera and the lens-camera system is less subjected to vibration that would blur the images. The light source is located underneath the R2R film, at ~ 16 cm from the lens aperture (see Figure 6-2).

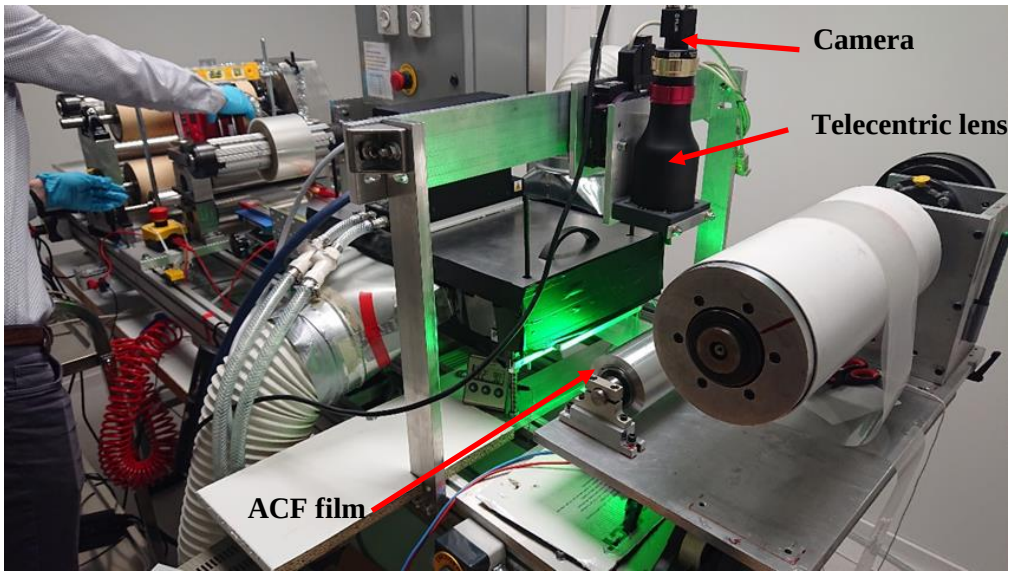

Figure 6-1: high-resolution imaging system installed on the R2R line. The telecentric lens is fastened to a metallic plate using a 3D printed holder. The camera is fastened to the lens. The lens-camera system can be translated and rotated using micrometric stages.

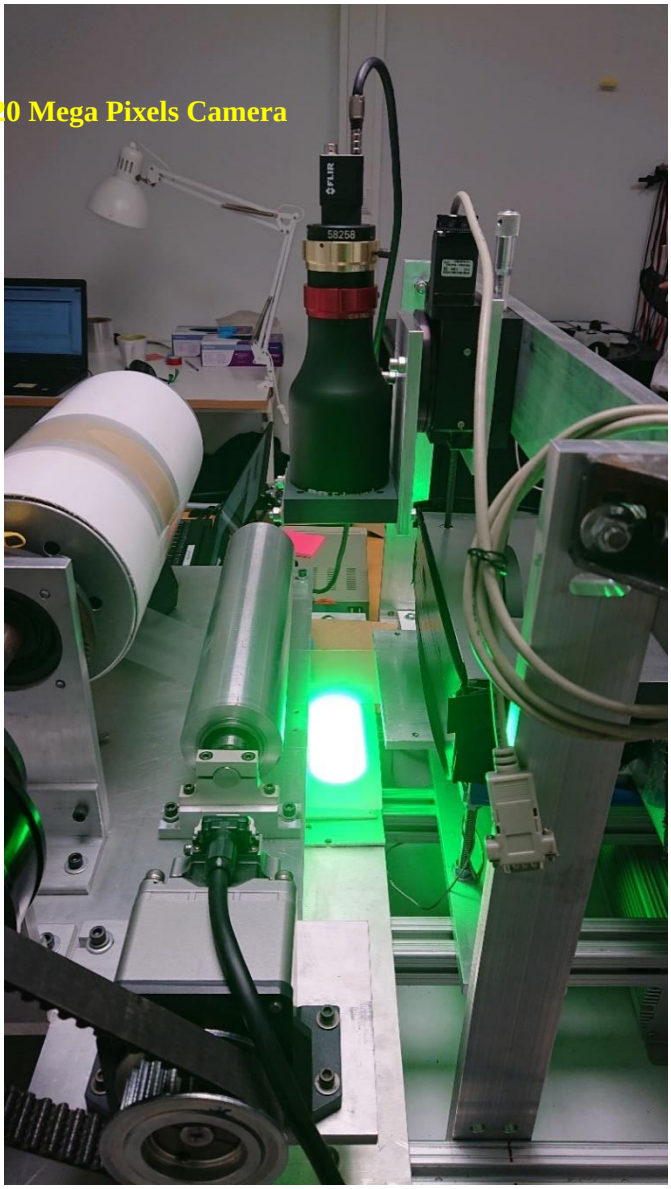

Figure 6-2: Side view of the imaging system installed on the R2R line. The light source is positioned under the ACF film. The distance from the light source to the lens aperture is ~15 cm. The field of view of the imaging system is roughly 4 cm by 4 cm.

The camera is connected to a PC, a customized application written in C++ allows controlling the settings of the camera (exposure time, gain) and the acquisition of images in sequences as the ACF film are manufactured.

6.2 Experiment and demonstration

We ran a series of measurement over three days. Mixture for sample of types A, B and F were prepared for the demonstration and ACF film were manufactured both aligned (electric field ON) and non-aligned (electric field OFF). The samples were imaged as they were fabricated, and the results were analysed off-line but almost simultaneously using Matlab. The results of the analysis are obtained after a few seconds of calculation. Table 6-1 List the sample prepared under the tests with their principal characteristics.

Table 6-1: Sample A and B characteristics

Sample #	Type	Particles shape	Polymer	Loading of particles [vol%]
#A1	A	Flakes	NOA68	1
#A2				5
#A3				10
#B1	B	Spherical		1
#B2				5
#B3				10
#B4				15
#B5				20

The sample were manufactured at 10 cm/min and 50 cm/minute web speed.

6.3 Analysis of grey scale image from final system/prototype demonstration

We present the results of real time measurement of the effect of the sample type and concentration in 6.3.1. In 6.3.2 we investigate the effect of the integration time on the image analysis results. Finally, in 6.3.3, we test the optical system and analysis algorithm om a film moving at 50 cm/min.

6.3.1 Results for samples A and B and as function of concentration, latest test (2020-03-11)

Figure 6-3, Figure 6-4 and Figure 6-5 summarize the results of the analysis for samples A while Figure 6-6, Figure 6-7 and Figure 6-8 summarizes the results of the analysis for samples B. We first observe that there is always a parameter giving a good separation between aligned and non-aligned sample both for sample A and B. This is well noticed on the plot of the SNR for background size as function of the SNR of the mean particle size, where the points cloud for aligned and non-aligned samples are separated by distance which are superior to several standard deviation (see subplot in bottom left in Figure 6-3 All A series and Figure 6-6 All B samples.). Interestingly the mean background size value for aligned and non-aligned sample seems to decrease as the inverse of the concentration of particles. This is in contrast with the mean image intensity, the mean particle size, and the particle coverage with seems to evolve linearly with the concentration, both for aligned and non-aligned samples

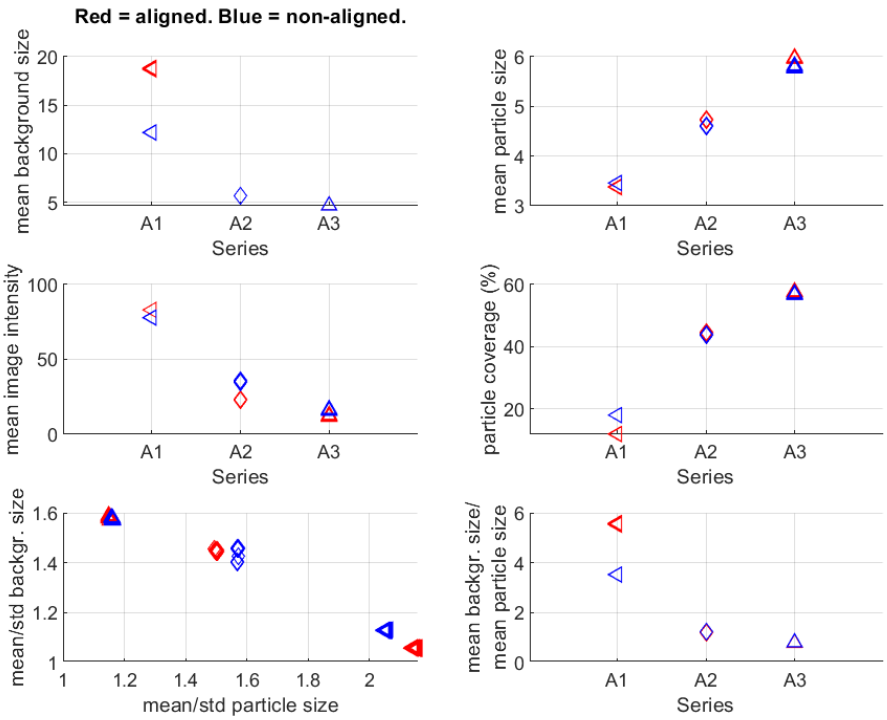

Figure 6-3 All A series

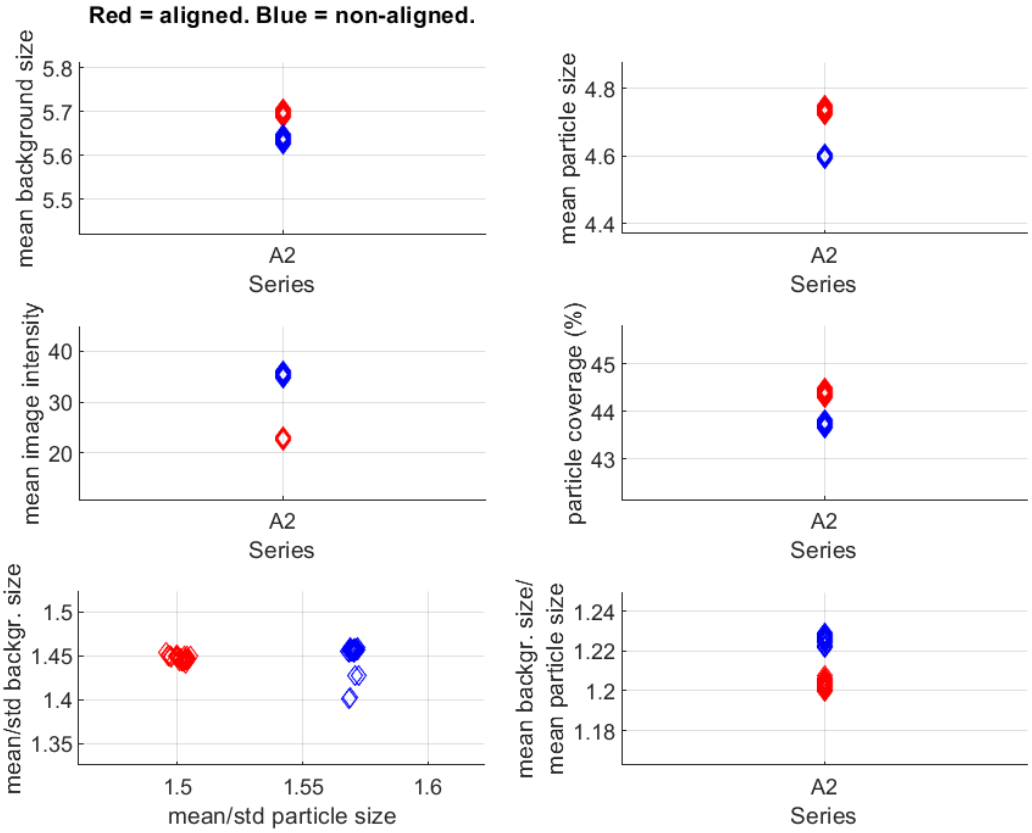

Figure 6-4 A2 zoomed

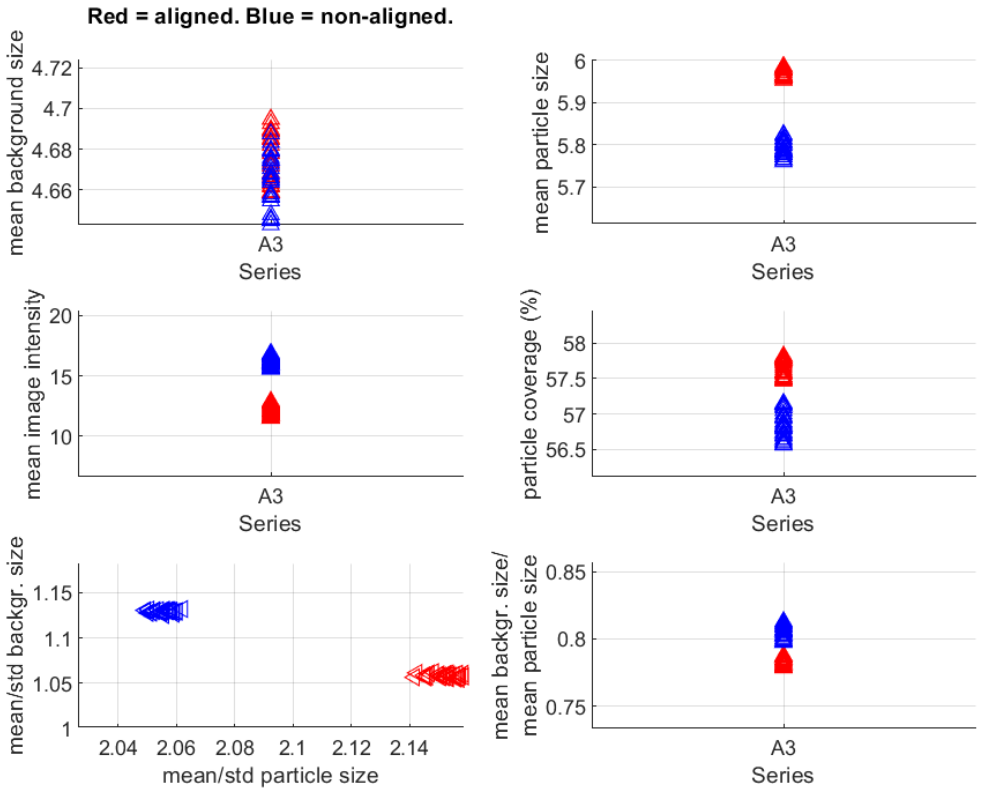

Figure 6-5 A3 zoomed

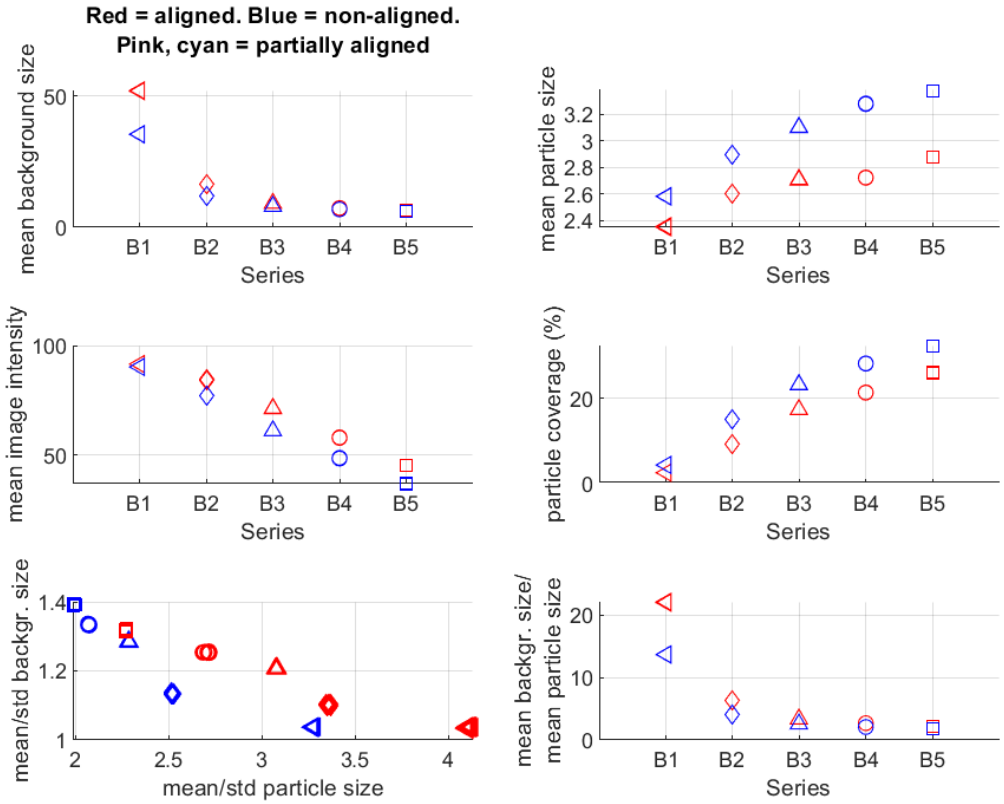

Figure 6-6 All B samples. Aligned samples are shown in red and non-aligned in blue.

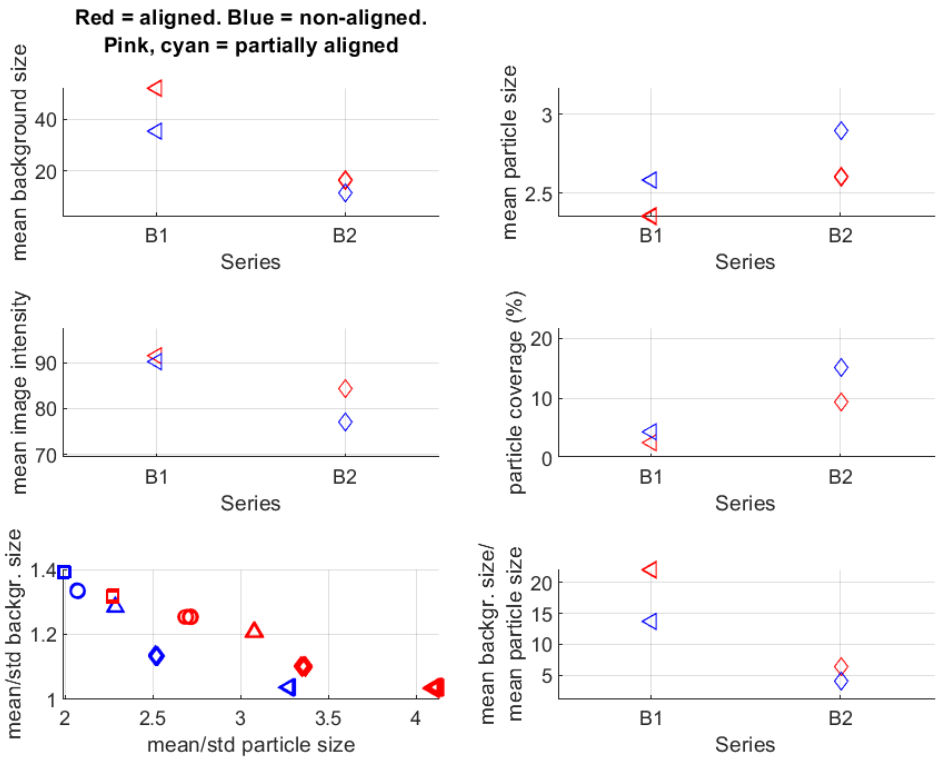

Figure 6-7 B1-B2 zoomed

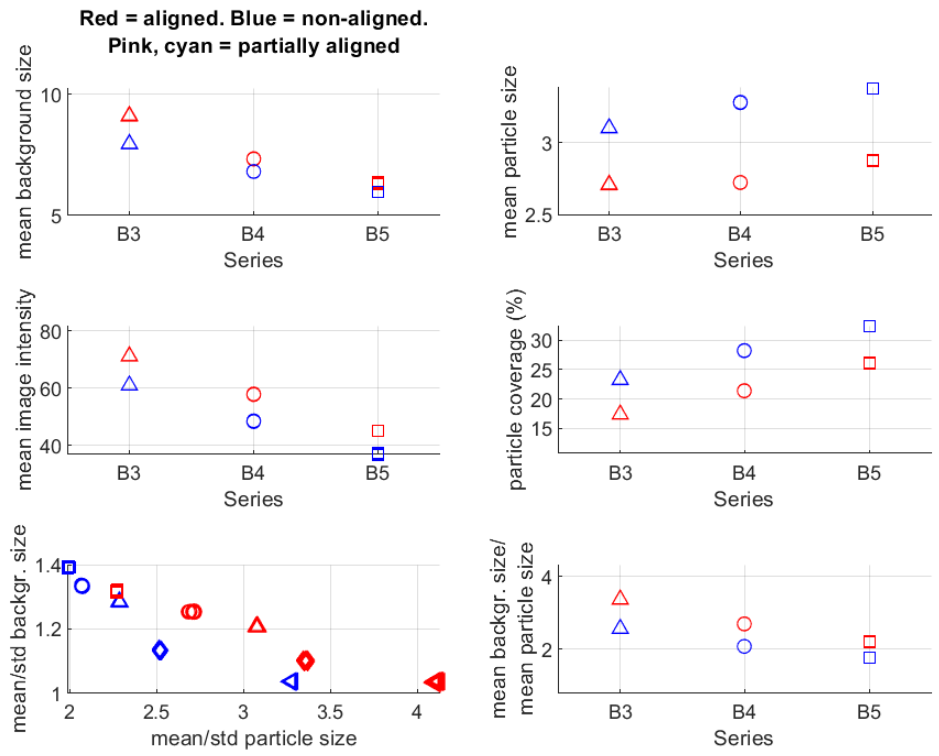

Figure 6-8 B3-B5 zoomed

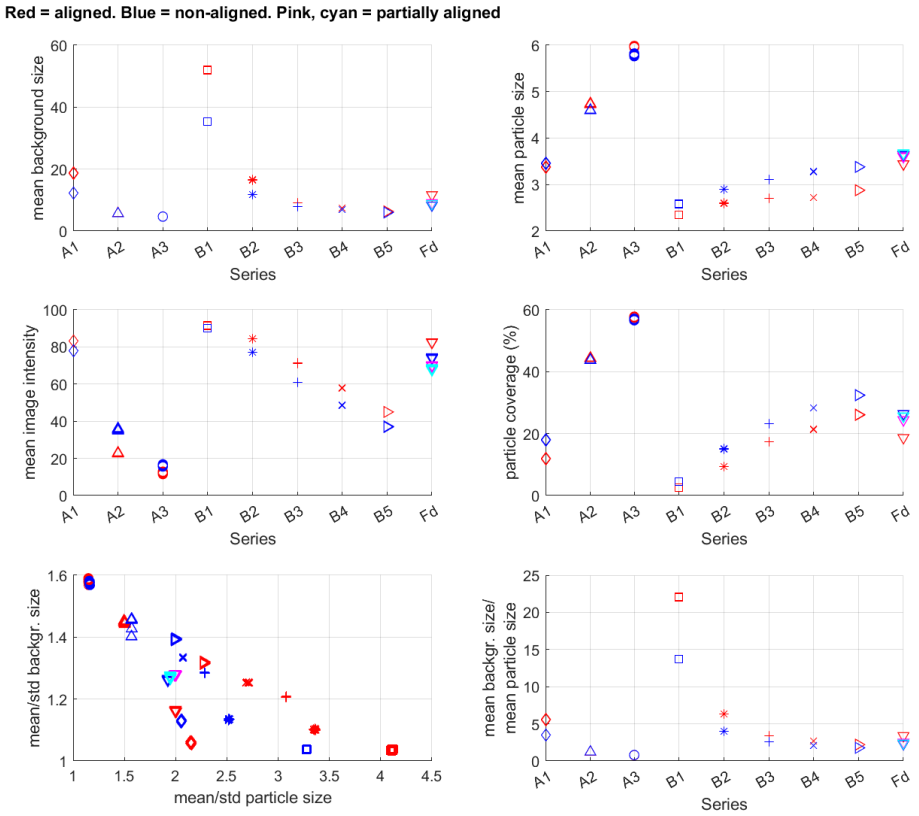

Figure 6-9 Results for all R2R images, second set of image series

6.3.2 Testing analysis results as function of integration time

During this test, sample B1, B2 and B3 were manufactured on the R2R with (aligned) and without (non-aligned) electric field. Images were acquired as the sample were manufactured and analysed offline. Figure 6-10, Figure 6-11: and Figure 6-12: shows the results for sample B1, B2 and B3. All the plots show the usual measure as function of integrations time, from 100 us to 500 us.

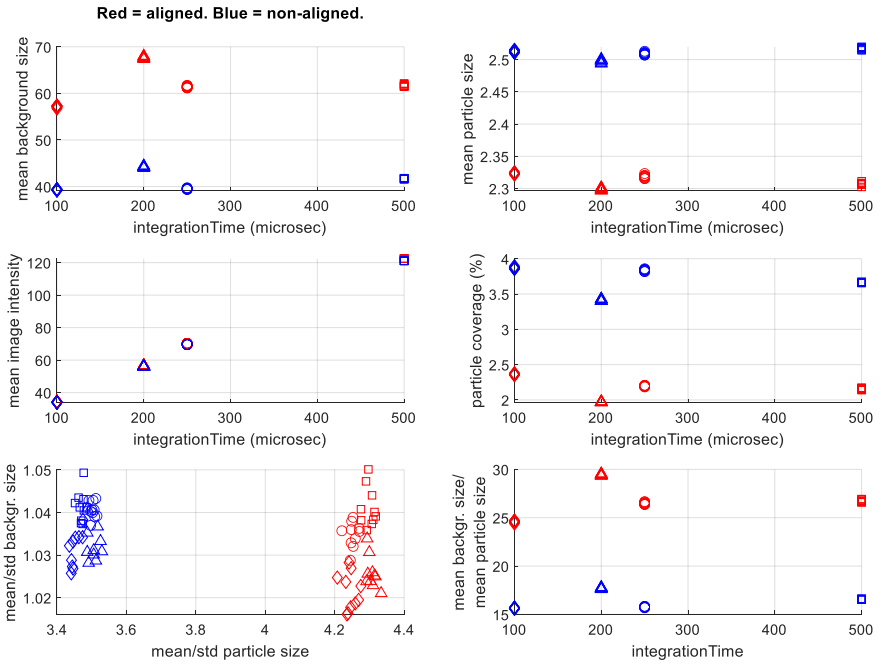

Figure 6-10: Sample B1 tested 2020-02-12. Measures plotted as a function of camera integration time

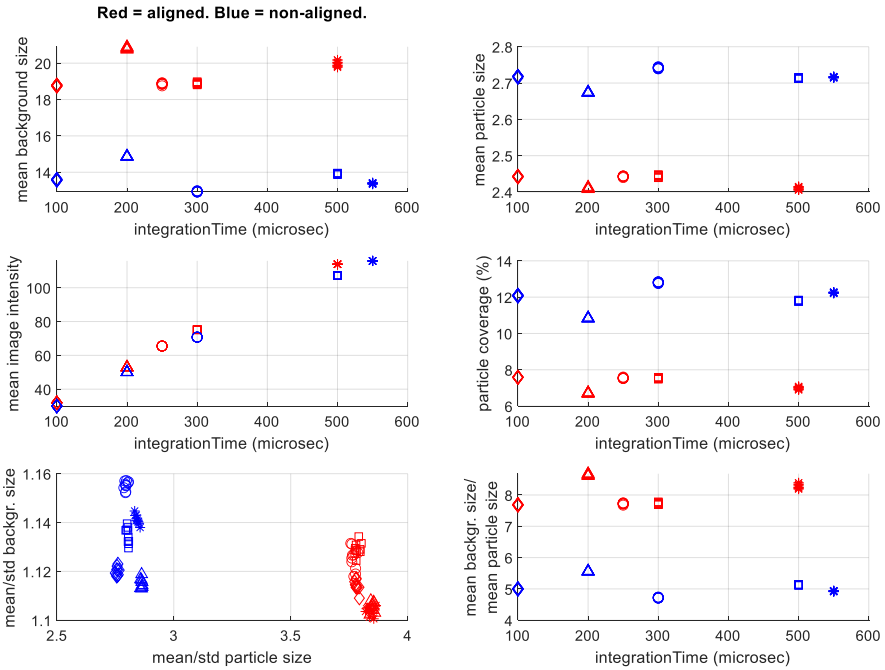

Figure 6-11: Sample B2 tested 2020-02-12. Measures plotted as a function of camera integration time

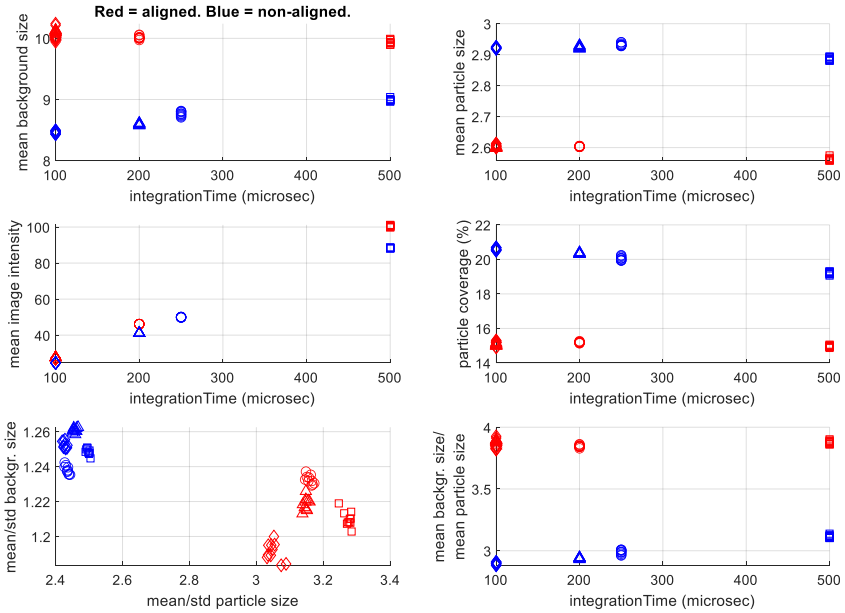

Figure 6-12: Sample B3 tested 2020-02-12. Measures plotted as a function of camera integration time

We can observe that good separation (approximately two time the dimension of the cloud size) between aligned and non-aligned sample is achieved for all three types of concentration (see bottom left subplot in Figure 6-10, Figure 6-11: and Figure 6-12:). We also observe that the integration time has little influence on measure like mean background size, mean particle size, particle coverage, although some variations are observed. The correlation between the results on the different sample is presumably a systematic effect of fabrication process. As the acquisition of the data with different integration time were acquired always following the same time sequence, we surely catch up a variation in the speed of the sample or any change related to sample geometry, composition etc. We see however that the difference between aligned and non-aligned sample is approximately constant for every value of the integration time for sample B1 and B2, e.g. differences between aligned and non-aligned is constant for a given type of sample. It diminishes as the integration time diminished for sample B3.

The integration time has logically higher impact on the mean image intensity as this parameter is directly proportional to the integration time

6.3.3 Effect of film speed on analysis results

In the last test on the R2R we evaluate the performance of the optical system on a film moving at 50 cm/min. We followed the same procedure as in the other tests, i.e. preparation of sample, acquisition of images as the sample is manufactured and off-line analysis of images. Since the sample is moving at a higher speed than in the other tests, we need to use short integration time in order to freeze the movement of the particles. For this

test, we use an integration time of 100 us. The results of the analysis are shown on Figure 6-13 for sample B1, B2 and B3.

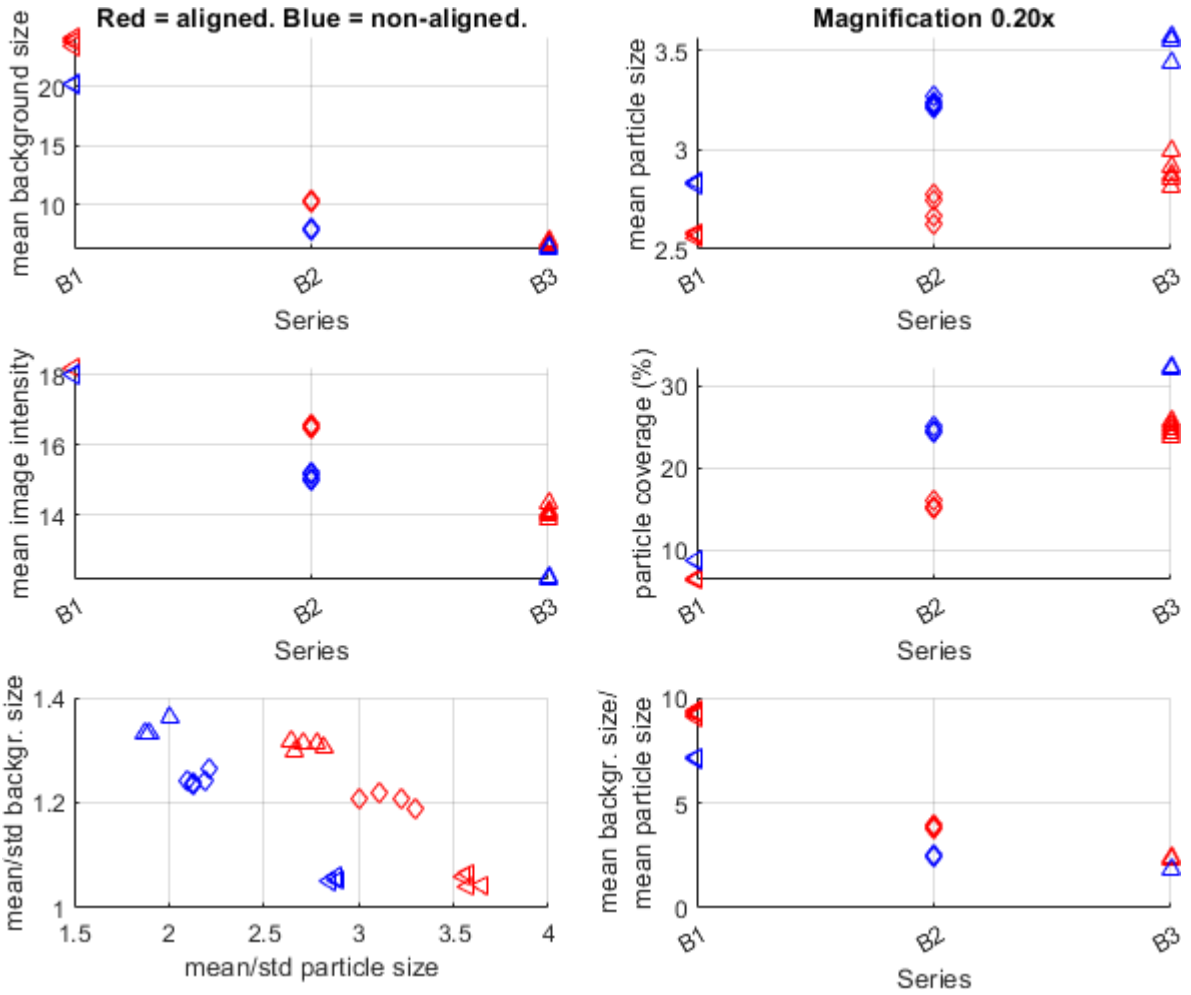

Figure 6-13: Results for high speed test (2020-02-19). Exposure time = 100 us.

The separation between aligned and non-aligned sample is here also good, although we observe a significant dispersion of the results in the bottom left subplots of Figure 6-13. The dispersion is however inferior to the standard deviation in each cloud such that a clear threshold can still be applied for the separation. In the other subplots we observe trends that were also observed in the previous tests. The reason for a larger dispersion of the results in this experiment are not known yet, but it could be a consequence of higher shot noise since we are using a shorter integration time. Variation of the width of the ACF could also be an explanation for the dispersion of the analysis results.

We show on Figure 6-14 to Figure 6-19, raw and segmented images of the film of type B1, B2 and B3, both aligned and non-aligned acquired with 100 us at 50 cm/min. The particles are sharp at ~the pixel level and there does not seem to be traces of blurring due too fast-moving particles or too long exposure times. It seems then that the integration time is short enough to freeze the movement of the particles and thus blurring is not the cause of the dispersion of the measures in the previous figure.

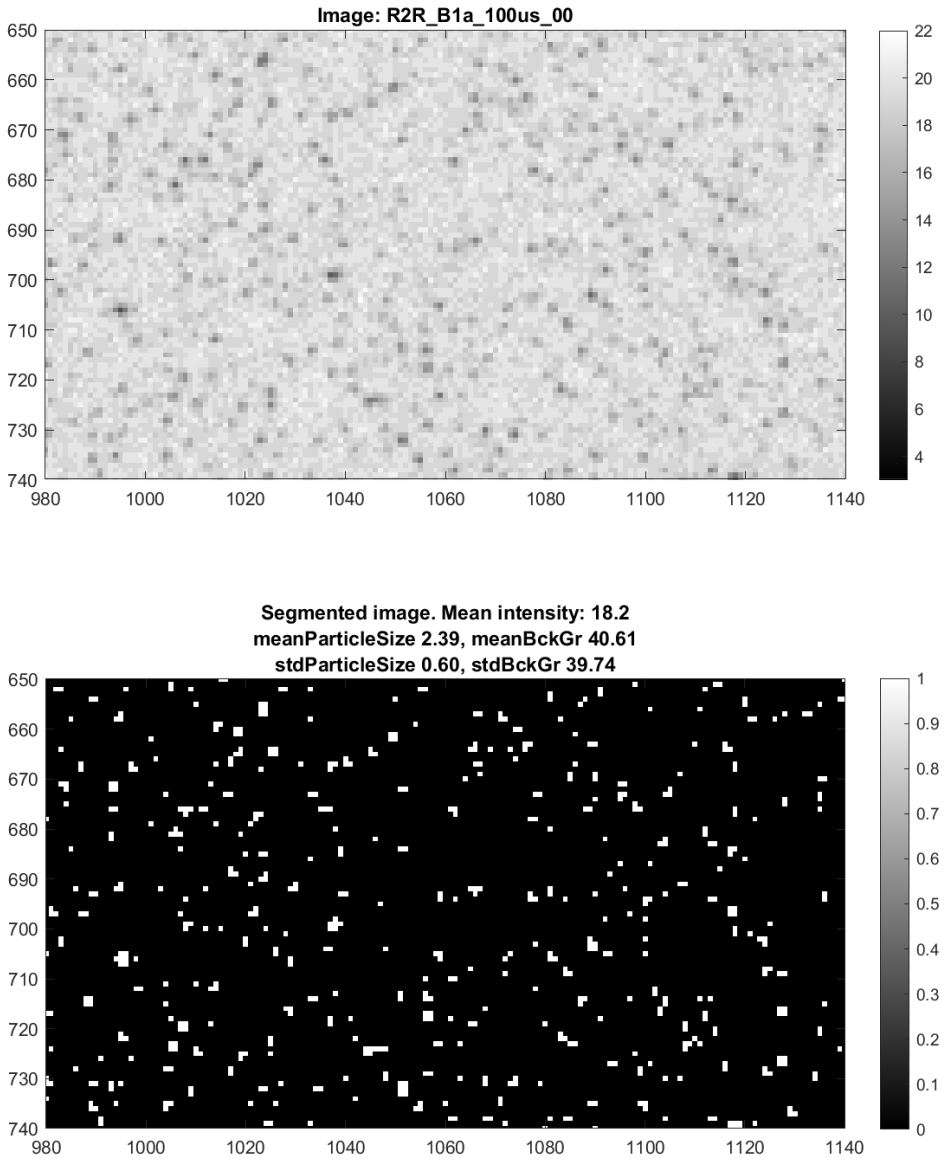

Figure 6-14: Raw and binary images for sample B1 aligned acquired on the R2R with 50 cm/min film speed

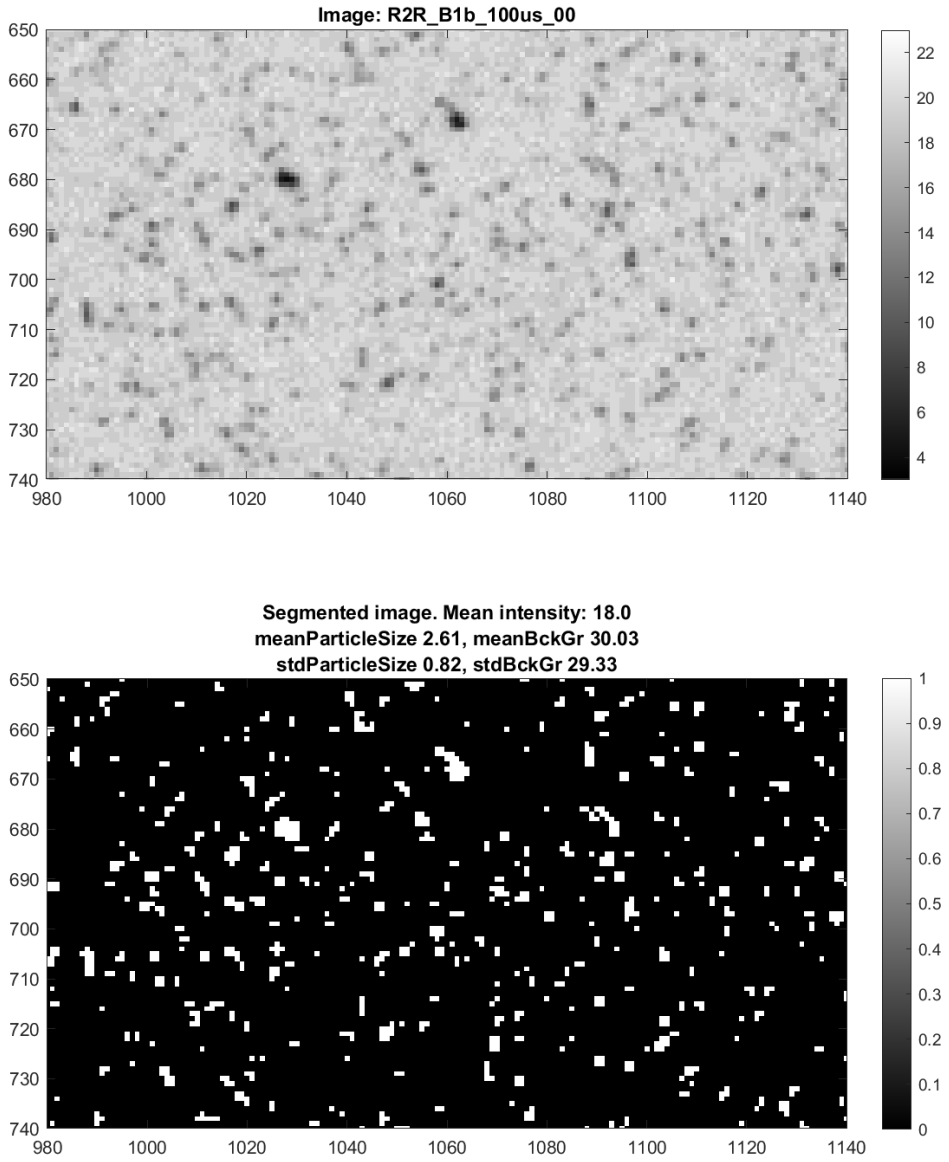

Figure 6-15: Raw and binary images for sample B1 non-aligned acquired on the R2R with 50 cm/min film speed

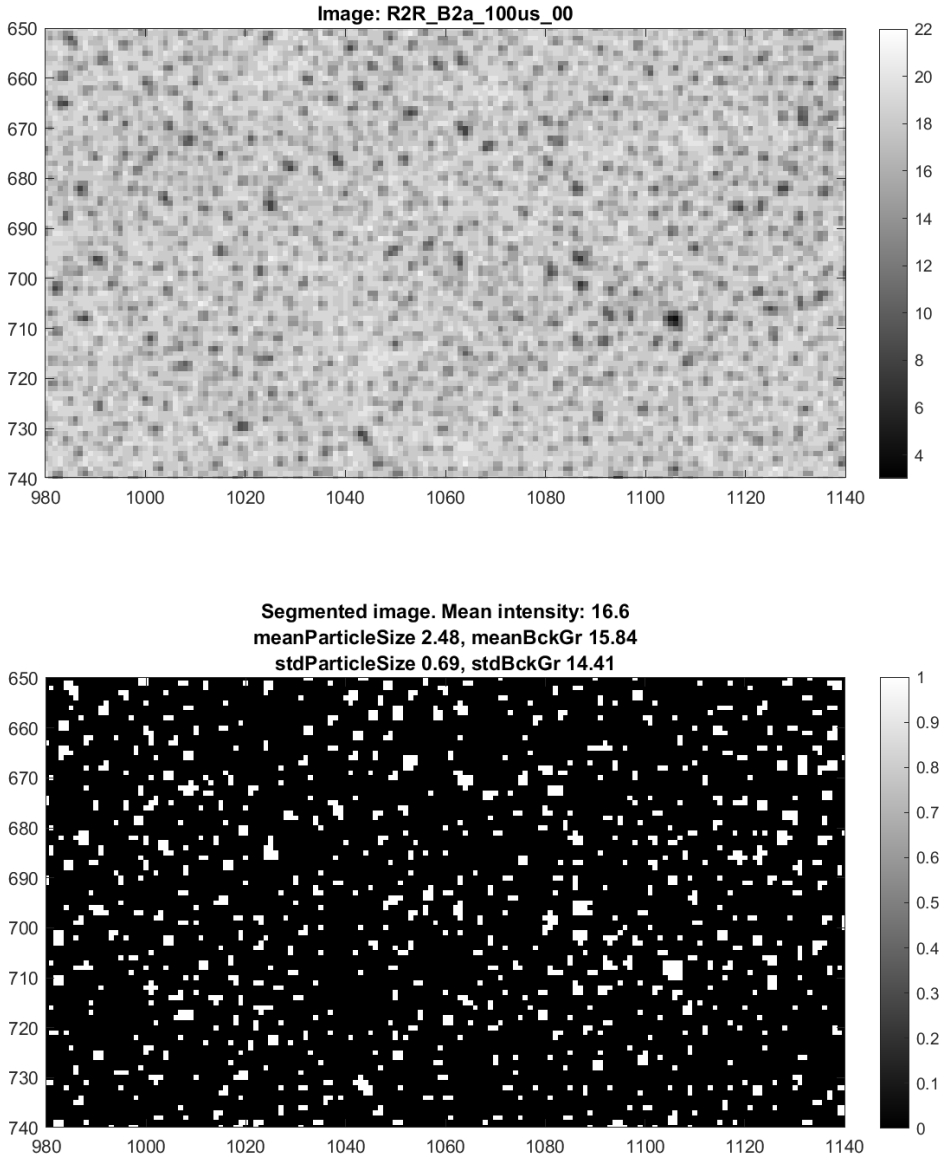

Figure 6-16: Raw and binary images for sample B2 aligned acquired on the R2R with 50 cm/min film speed

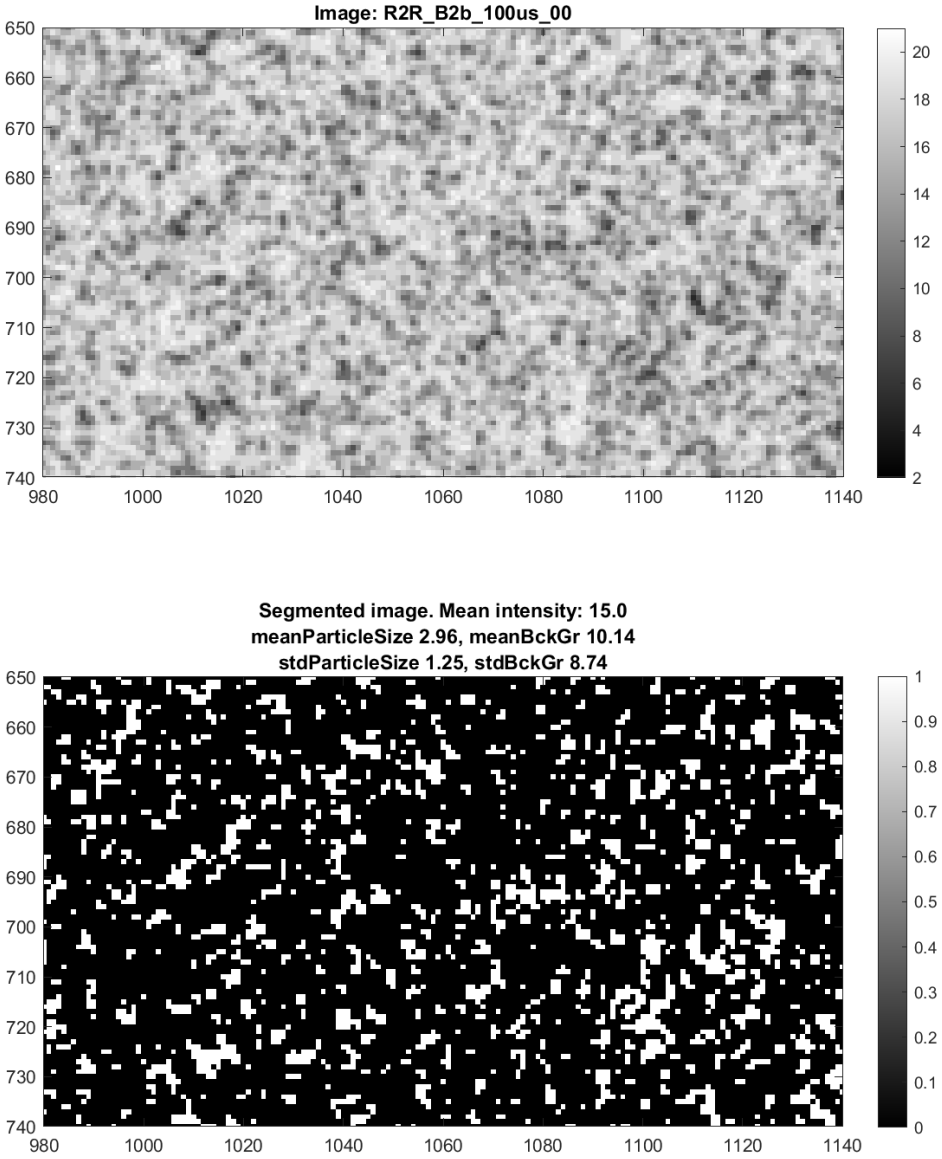

Figure 6-17: Raw and binary images for sample B2 non-aligned acquired on the R2R with 50 cm/min film speed

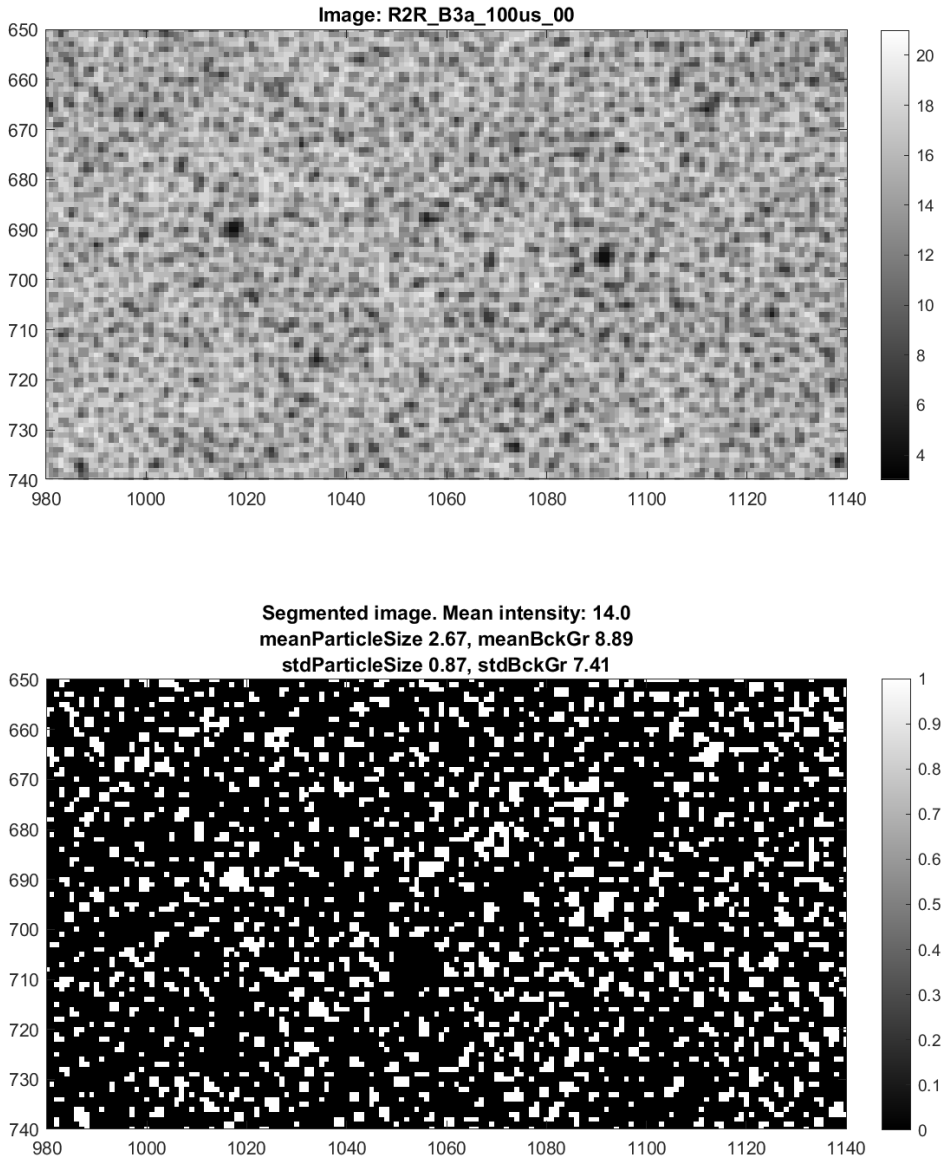

Figure 6-18: Raw and binary images for sample B3 aligned acquired on the R2R with 50 cm/min film speed

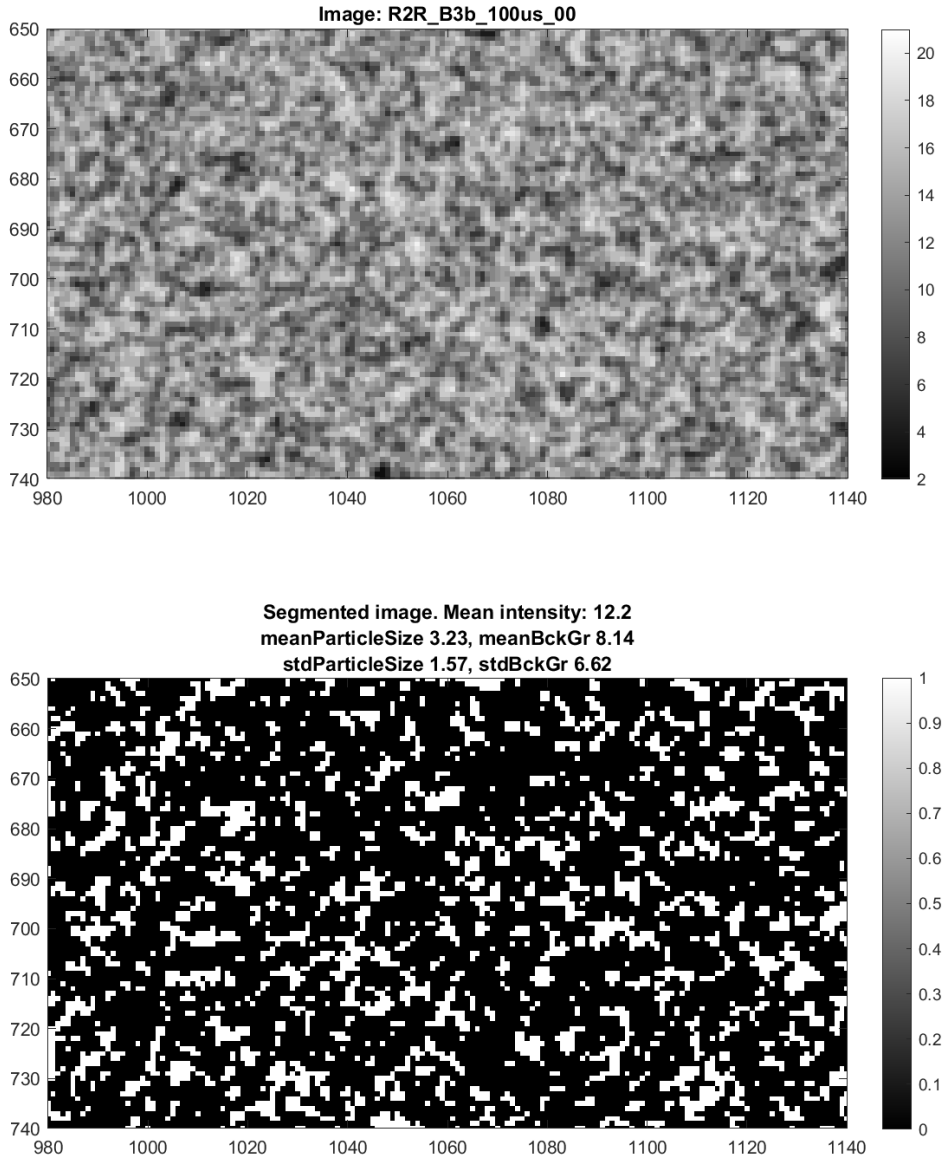

Figure 6-19: Raw and binary images for sample B3 not aligned acquired on the R2R with 50 cm/min film speed

6.4 Discussion

- We have focused in all our analysis on providing binary classification of the alignment, i.e. aligned or not aligned. In a test not summarized here, we also evaluated the effect of electric field parameters known to lead to partial alignment of the particle and could successfully classify the samples in non-aligned, partially aligned and fully aligned sample. This shows that the optical analysis allows measuring the degree of alignment of the particles. The next step is to relate the optical degree of alignment to the conductivity of the sample, the real parameter of interest here. This would allow providing in real time the conductivity of the sample under fabrication. To achieve that we would need to calibrate the inline optical measurements with offline measurement of the conductivity in a way

similar as the calibration performed in 4.4.6.3 on static optical measurement. This can be the subject of a future project.

- In the demonstration, the images were analyzed after they were acquired, but the analysis script can in principle be run simultaneously as the analysis take a few seconds. The analysis and presentation of results could be run as the data are acquired to give real time information about the alignment of the sample.
- The frame rate of the camera is 0.25 Hz at full resolution and the size of the image in the image plane is 4 cm. When the film speed is inferior to 60 cm per minute, there will be redundant information in the image. For higher speed, the analysis will not fully cover the total length of the film and higher frame rate will be necessary.
- High speed application will require higher light source intensity since we have seen that the SNR in images acquired with short integration time are deteriorated by shot noise. This can be achieved by placing several LED beside each other, as the current design make only use of two LED.

6.5 Conclusion

We have installed, tested and demonstrated an optical system for real time monitoring of the spatial organization of micro particle in the R2R of CondAlign. We conducted several tests on samples with various type of particles, A with flakes and B with spherical particles, and showed that the system can separate aligned from non-aligned sample for different particle loadings. We have evaluated the effect of various integration time and film speed on the performance of the optical system to assess its robustness for various processing setting.

7 Conclusion

In this project we have worked with developing a manufacturing process for continuous production of anisotropic conductive films (ACF) for electronics and biomedical applications. We have focused on overcoming two main challenges met in the current R2R process line of CondAlign, i.e.

1. Identify process parameters that influence most the final resistivity of ACF to optimize their production.
2. Establish a method for real time characterization of the manufacturing process of ACF.

In WP2, our Romanian partners have performed simulation of propagation of electromagnetic waves in ACF and identified process parameters (particle size, composition) which influence the absorption of electromagnetic energy.

In WP3, we have manufactured various ACF samples by combining different size of particles and different polymer types. We found that particles with too small diameters, 50 nm, do not lead to conductive samples, presumably due to too high interparticle resistance. As the number of particles increases, the resistance increases proportionally. We decided for the rest of the project to focus on particle with larger diameter, i.e. > 5 µm.

In WP4, we developed measuring tools for characterizing Anisotropic conductive film at various spatial resolution scale and we have established a multivariate model of resistivity.

- We developed and tested a new set-up for measuring the local conductivity of ACF under pressure. This has been used as a reference method for measuring the conductivity both under various pressure and at different location on various type of ACF samples.

- We used SEM to study ACF samples at nanometric resolution. We acquired SEM picture of aligned and non-aligned samples and could verify mechanical contact between particles after the samples had been subjected to electric field and the particles had been aligned. We also could see that particle in chains sometimes meanders when the number of particles times the particles diameter does not match exactly the film thickness.
- We developed an Image analysis algorithm for analysing microscope images to characterize spatial organization of particles chains in ACF. Under electric field, the particles align into chains and organize themselves into very specific pattern in the plan of the film. When the electric field is off, the spatial organization of the chains will be random. The algorithm calculates specific geometric measures related to the spatial distribution of the particles which turns out to have very different value for aligned and non-aligned samples.

We then established a Design Of Experiment (DOE) which is a way to lay out an experiment plan to avoid changing and testing one process parameter at a time. We manufactured ACF samples by varying the identified process parameters and performed resistivity measurements. We then established a statistical model based on the measured resistivity. We found that the most appropriate model of resistivity involves the ratio of the film thickness and the diameter of particles. The higher this ratio the higher the resistivity. A way to understand this result is that again, inter particle contact increases resistivity: the smaller the particle for a given film thickness the higher the number of particles in a chain, the higher the intercontact resistance and the higher the resistivity of the ACF. This model gives simple rules for optimizing process parameters to manufacture ACF samples with low resistivity.
We have also started to establish a correlation between the measured resistivity and the optical measures calculated by the image analysis algorithm. This correlation has been established based on a reduced number of samples and further studies are needed to extend it to a broader range of ACF type.

In WP5, we designed and tested an optical set up for real-time monitoring of the spatial organization of particle chains in a R2R process. The main objective was to achieve a large enough field of view in order to acquire image over the whole width (4 cm) of the R2R film and at the same time have a spatial resolution that is good enough to distinguish > 5 µm particle. We have worked by iteration: we degraded gradually the optical resolution to expand the field of view and checked that the image analysis algorithm still allowed separating aligned from non-aligned ACF samples. We started from a laboratory microscope allowing resolution down to 0.5 µm and 1 mm^2 field of view to an optical system allowing inspection of 4 cm by 4 cm area with an optical resolution of ~13 µm. With this final version of the optical system, we performed measurements on static samples, assessing how robust the optical system is to low light conditions. We could verify that we could separate aligned from non-aligned ACF samples for short exposure time. Short exposure time are needed for freezing the movement of particle in a real R2R process line.

In WP6, the optical system was installed on the R2R and tests were performed over several days, on various type of ACF samples and for various process parameters settings. We demonstrated that we can acquire images in real time, post processed them and successfully differentiate between aligned and non-aligned ACF of various type. We could also demonstrate that the optical system can give indication of partial alignment of ACF, a situation that happens when the process parameters are not optimally set.

8 Further work

At the end of the project we have identified several new research topics.

- Further work is needed to obtain a better correlation between measured resistivity and the optical measures. We have started this work but need further tests combining optical measurements on the R2R with electrical measurements of the resistivity. This will allow establishing a model of the resistivity based on optical measurement that can be transferred to real time measurement on the R2R line.

- Better understanding of the effect of polymer aging on the resistivity of ACF samples and better understanding of conductivity hysteresis for ACF under pressure. This could be established using the conductivity set-up established in this project and extensive test on ACF samples.

- The optical measures are an indication of the spatial order in the sample, but not necessarily an indication of conductivity. For some process parameters, the particles tend to form chains in the plane of the film and not across it. Those samples have bad conductivity but have nevertheless a high degree of spatial organization. These samples would presumably be classified today by the optical system as a "conductive sample". We believe however that a more advanced image analysis algorithm, e.g. using Neural network or other machine learning algorithms, would allow identifying those samples.

- The statistical model of conductivity links the thickness of the film and the diameter of the particles. An optical system allowing in addition the measurement of the film thickness would bring additional information to the image analysis algorithm that could be used for improved measurement of the conductivity of the ACF samples.

- A question that arise during this project is what is the conductivity of a single chain? Measurement of conductivity of a single chain e.g. using Atomic Force Measurement would allow answering this question and help establishing microscopic model of the conductivity of ACF samples.

- Further work is needed to extend the optical analysis to potentially larger film. This can be achieved by tilling several optical measurement units together. As the film width increases, several optical measurement units are needed and the costs for the optical analysis might exceed the cost of the R2R. Scanning the field of view of the optical unit is a possible low-cost alternative.

9 References

[1] M. Buchanan, E. Svasand, M. Knaapila and G. Helgesen, "The process feed for making an anisotropic conductive layer and a resulting generated object," *Norway Patent NO333507B1, 22 06,* 2009.

[2] T. Jones, Electromechanics of particles, ABSTRA, 1995.

[3] A. J. Kadaksham, P. Singh and N. Aubry, "Dielectrophoresis of nanoparticles," *Electrophoresis,* pp. 3625-3632, 2004.

[4] M. Mohammadimasoudi, Z. Hens and K. Neyts, "Full alignment of dispersed colloidal nanorods by alternating electric fields," *RCS Advances,* p. 55736, 2016.

[5] A. K. Agarwal and A. Yethiraj, "Low-Density Ordered Phase in Brownian Dipolar Colloidal Suspensions," *PHYSICAL REVIEW LETTERS,* pp. 198301-1, 2009.

[7] G. Belijar, S. Diaham and Z. Valdez-Nava, "Online optical and dielectric monitoring of anisotropic epoxy/BaTiO3 composite formation tailored by dielectrophoresis," *J. Phys. D: Appl. Phys,* 2016.

[8] A.-S. B. Vardøy, A. Garcia, D. Wright, B. D. Belle, M. M. V. Taklo, O. Hagel, L. Xie, M. Danestig and T. Eriksson, "Soldering of components onto a smart tag – an evaluation of the process window," in *NordPac*, Gøtbeborg, 2017.

[9] NIST/SEMATECH e-Handbook of Statistical Methods, 2017.

[10] B. J. P. Goos, Optimal design of experiments: a case study approach, A John Wiley & Sons Ltd, 2011.

[11] A. K. A. a. A. Yethiraj, "Low-Density Ordered Phase in Brownian Dipolar Colloidal Suspensions," *PHYSICAL REVIEW LETTERS,* 2009.

[12] J. S. Park and D. Saintillan, "Electric-field-induced ordering and pattern formation in colloidal suspensions," *PHYSICAL REVIEW E,* 2011.

A Dielectrophoresis

The CondAlign patented technology is based on dielectrophoresis, wherein an external electric field is used to orient and organize filler particles in polymeric resins. After exposure to the electric field, the polymer is cured, fixing the position of the particles. The dielectric force on a dielectric sphere is given by:

$$F_{dep} = 4\pi a^3 \epsilon_0 \epsilon_m \beta \vec{E} \cdot \vec{\nabla}\vec{E}$$

where a is the particle radius, ϵ_m is the permittivity of the polymeric matrix, ϵ_0 is the permittivity of free space, E is the electric field, and β is the real part of the Clausius Mosotti factor, given by

$$\beta(\omega) = Re\left(\frac{\epsilon_p^* - \epsilon_m^*}{\epsilon_p^* + 2\epsilon_m^*}\right)$$

Here, ϵ_p^* and ϵ_m^* are the complex permittivities of the dielectric particle and the medium respectively [3]. We see that the dielectric force depends on both the size of the particle, the strength of the electric field, and the contrast in permittivity between the particle and polymer. It is also proportional to the gradient of the electric field. In our process, however, we employ uniform electric fields across the sample. The particles are therefore not accumulating on one electrode; rather it is the dielectrophoretic interactions between induced dipoles in the particles that are causing the alignment. If the particles are non-spherical, the electric field will also induce a torque on the particles that act to change their orientation. The result is a rotation of the particles such that their long axis is preferentially aligned parallel to the electric field [4].

B Modeling and Simulation of Nanoparticles Dispersion for the Realization of ACFs

Contributor: Romeo Cristian Ciobanu, Senior Member IEEE, Marius Andrei Olariu, George-Andrei Ursan, Mihaela Aradoaei, Olga Plopa for University of Iasi and All Green AS

B.1 INTRODUCTION

THE actual technology of direct use of ACF presumes that a thermosetting resin, containing conductive particles, is first deposited on a base substrate, by either a lamination, or a dispensing process. A secondary substrate is then placed over the base substrate and the two parts are pressed together to be bonded, process presuming exposure to temperatures close to casting and some pressure. The conductive particles are trapped between predefined areas, such as electrodes, thereby creating an electrical connection between the areas. The other particles remain insulated within the thermosetting resin. The process is hard to control and not very energy/cost efficient in high volume manufacturing. However, improved results were obtained in small scale manufacturing. The proposed innovation pushes ACF technology beyond the one particle barrier, which is the main limitation of traditional ACFs. Existing solutions tested to achieve high pitch is based on small monodispersed particles, making the films very thin and unsuccessful. This makes the ACF fragile by reducing adhesion, and not suitable for flexible devices. Traditional anisotropic conductive films typically use homogenously monodispersed particles in compound bulk, whereas the project intends to develop a technology of nanostructured anisotropic conductive films with tailored architecture under electromagnetic field. Consequently, it is possible to work with particles less differentiated as sizes and shapes, since they are aligned in chains and only the chain features matter. The electric fields used to define, structure and align the chains, permit the use of a much wider range of nano/micromaterials as ingredients, comparing to a potential homologue technology of using magnetic fields for the same purpose, that are limited only to the use ferri/ ferromagnetic materials. Other benefits are related to the significant reduction of the amount of filler particles required to achieve similar conductive properties, comparing to homogenously monodispersed films (up to 10 times, with clear cost and quality advantages. The potential application areas identified so far are: ECG electrodes, anisotropic conductive / thermally conductive films for printed electronics. Modeling and simulation with specialized software is the starting point for achieving the proposed objectives of the process, which comprises: homogenous dispersion of certain nano/microparticles, chain generation

under electromagnetic field and polymer curing for particle locking.

B.2 Analysis of Material Parameters with Inserts/Particles for the Realization of ACFs

Simulation of a generic PE / PP composite with a nanoconductive powder corresponding to a parallelepiped sample was performed. In the substrate material (polymer matrix), a number of different material elements were inserted to form the nanoconductive powder particles Eelements are considered, uniform / random spatial positioning.

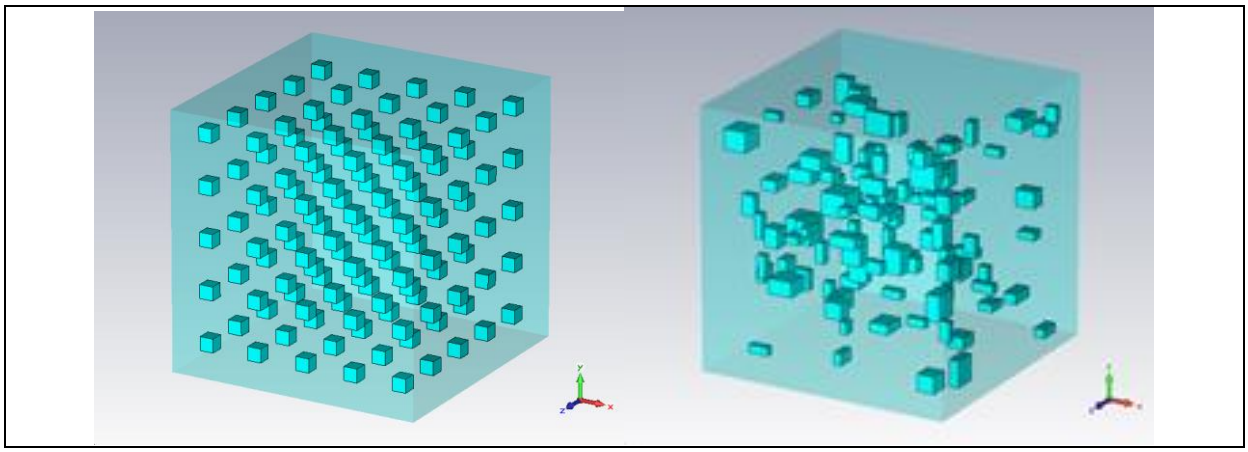

Figure 9-1: Typical structures analyzed for the realization of ACFs.

The phenomenon investigated was primarily the absorption of electromagnetic energy in the sample. Any use of such material is related to energy absorption analysis and transformation into heat. For this reason, analyzes were made on the calculation of SAR - Specific Absorption Rate - which is defined as the rate at which energy is absorbed by the mass unit of material exposed to electromagnetic radiation. SAR is defined, in time, of the energy (dW) absorbed by the mass (dm) contained in volume (dV) in the known density (p) element. SAR is expressed in W / kg. Absorption total rates (which allow for the thickness / quantity of material needed to remove a certain amount of electromagnetic energy) and the peak local value of this rate (Peak Point SAR) have been calculated as an indication of the uniformity of energy absorption in the material. The analyzes were carried out in two stages: only the substrate material and the substrate material with powder inserts, the difference between the two situations allowing the elimination of the influence of the own characteristics (frequency / size range) of the models used in the simulation.

Table 9-1: Characteristics of material used for modelling and simulation

Material	Density ρ[g/cm³]	relative permittivity ε_r	tan δ	Specific heat [J/kg/K]	Thermal conductivity [W/K/m]
Substrate (PP / LDPE-HDPE)	0.93	2.25	0.012	1900	0.4
Inserts Category A	5.18	7	0.05	734	9.7
Inserts Category B	5.18	12	0.09	734	9.7

Volumetric concentration for different densities of the substrate material and mass concentrations of the mixture are presented in next tabel.

Table 9-2: VOLUMETRIC CONCENTRATION FOR DIFFERENT DENSITIES

MR[%]	VR(P_S)						
	0.9	**0.91**	**0.92**	**0.93**	**0.94**	**0.95**	**0.96**
10%	1.89%	1.91%	1.94%	**1.96%**	1.98%	2.00%	2.02%
7%	1.29%	1.31%	1.32%	**1.33%**	1.35%	1.36%	1.38%
3%	0.53%	0.54%	0.55%	**0.55%**	0.56%	0.56%	0.57%

B.3 Analysis of Field Results, Local Behavior

The effect of insertions on the phenomena of absorption of electromagnetic energy into the material can be investigated by analyzing power losses, energy transfer through material, and specific absorption rate.

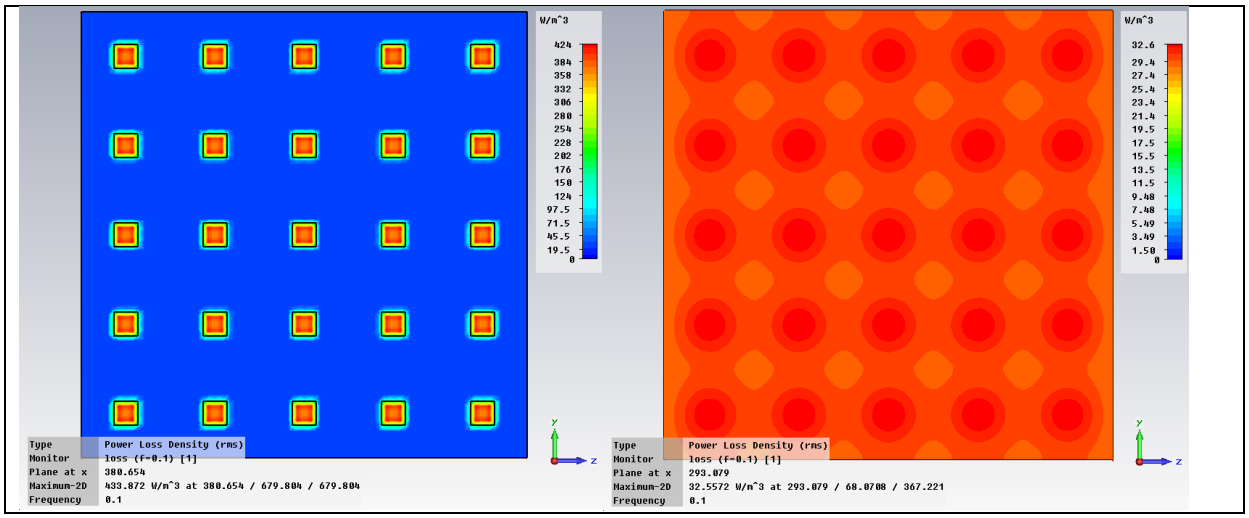

Figure 9-2: . Volumetric density of the absorbed power, MR = 10%, R = 25µm, f = 0.1GHz, uniform distribution, Type A inserts, insertion plan and plane between inserts

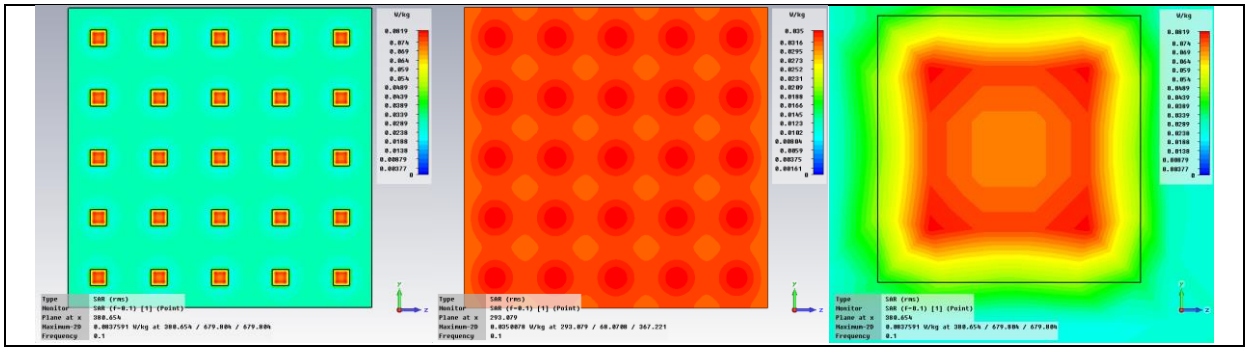

Figure 9-3: Local SAR, MR = 10%, R = 25µm, f = 0.1GHz, uniform distribution, Type A inserts in the plane of the inserts, in a plane between inserts and detail around an insertion.

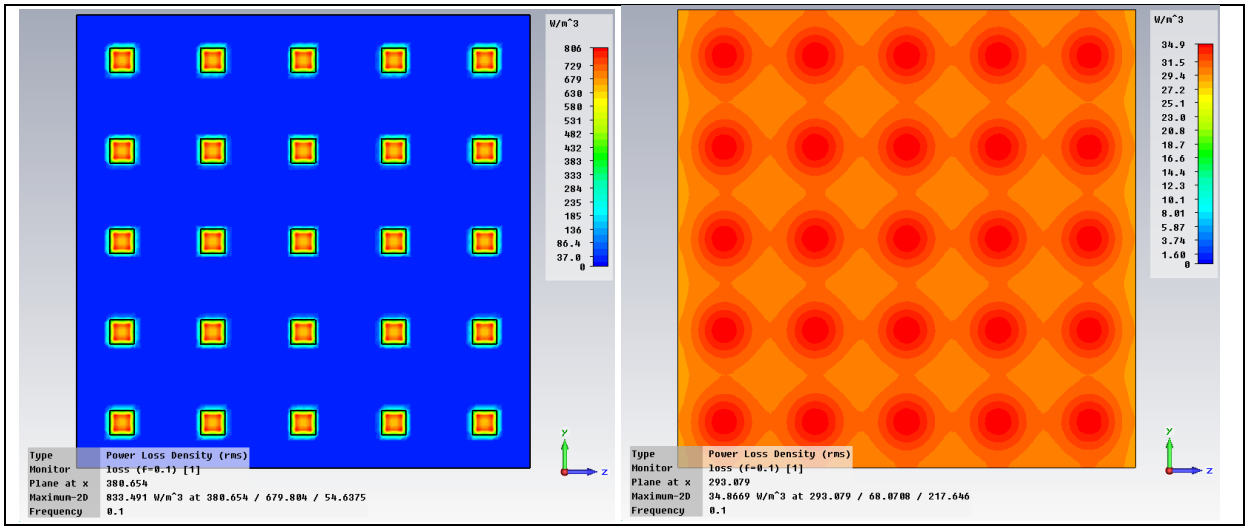

Figure 9-4: Volumetric density of the absorbed power, MR = 10%, R = 25µm, f = 0.1GHz, uniform distribution, Type B inserts, insertion plan and plane between inserts.

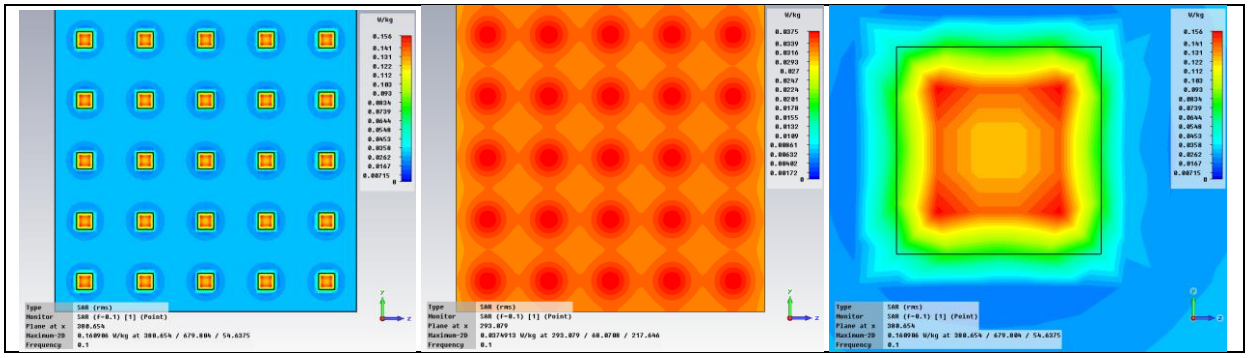

Figure 9-5: Local SAR, MR = 10%, R = 25µm, f = 0.1GHz, uniform distribution, Type B inserts in the plane of the inserts, in a plane between inserts and detail around an insertion.

It is observed by comparison for Type B inserts (and similar for Type A inserts) that the presence of inserts characterized by high loss results in the realization of electromagnetic energy dissipation "centers": compared to the situation present in the plane between the inserts, where we find uniformity of the energy dissipation, there is an increase in the concentration of electromagnetic energy around the inserts. Due to the dielectric characteristics of the material corresponding to type B inserts, especially in the plane of the inserts, we have an increased energy dissipation (806 W / m3 versus 424 W / m3 and 0.156 W / kg versus 0.082 W / kg).

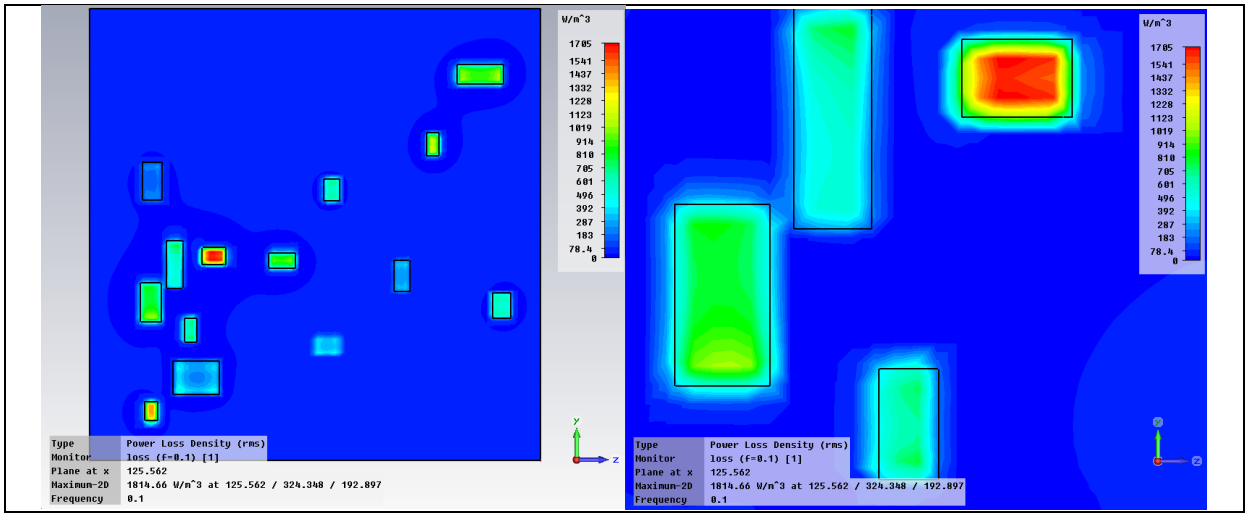

Figure 9-6: Volumetric density of the absorbed power, MR = 10%, R = 25µm, f = 0.1GHz, random distribution, type B inserts and detail around an insertion.

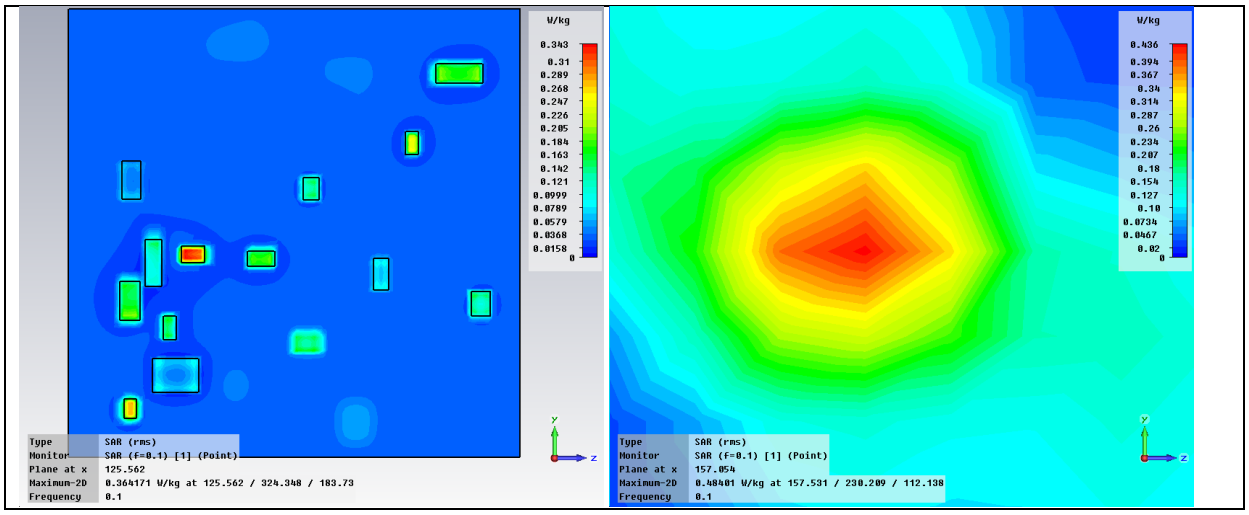

Figure 9-7: Local SAR, MR = 10%, R = 25µm, f = 0.1GHz, uniform distribution, Type B inserts, and detail around an insertion.

The figures show the situation in the case of random particle distribution. There is an increase in the maximum power dissipation and SAR levels over the uniform distribution. The explanation for this can be given by following the Poynting vectors for the two spatial distributions involved.

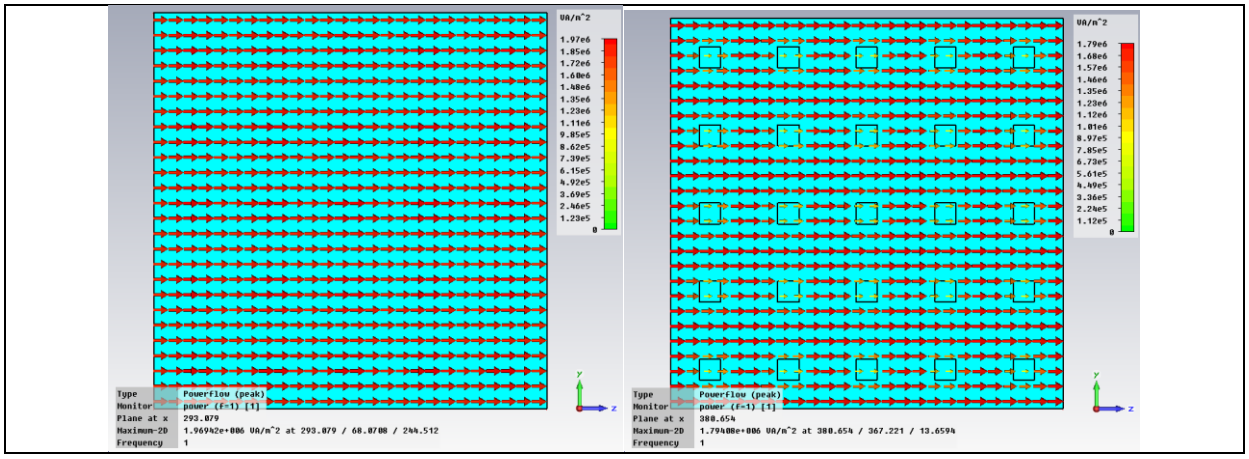

Figure 9-8: Poynting vectors, MR = 10%, R = 25µm, f = 0.1GHz, uniform distribution, type B inserts, in a plane between the inserts and the insertion plane.

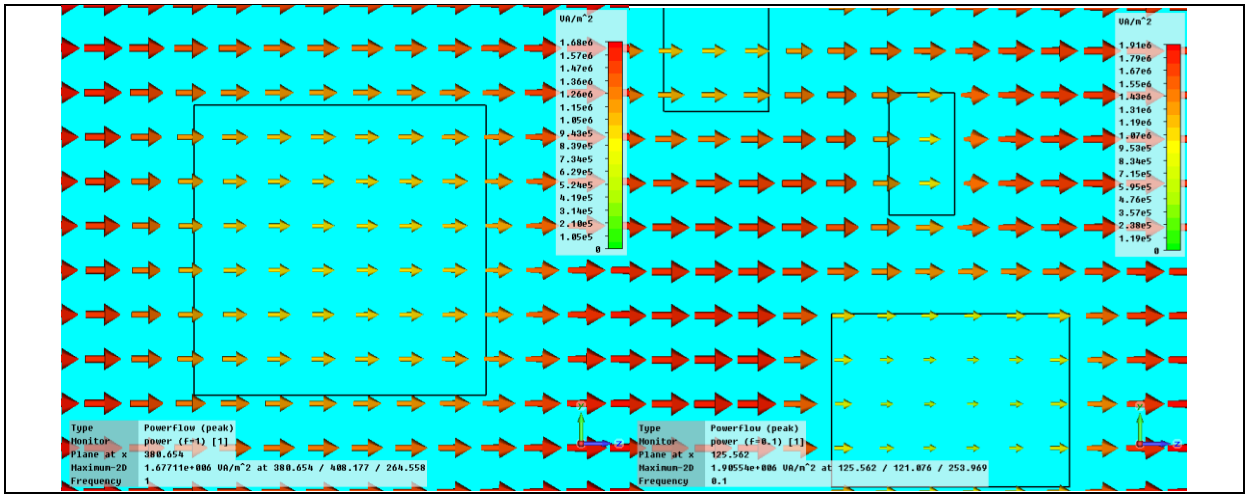

Figure 9-9: Poynting vectors, MR = 10%, R = 25µm, f = 0.1GHz, Type B inserts, uniform and random distribution, in the vicinity of insert.

In the case of uniform distribution, the electromagnetic energy transfer finds a low loss path (among the inserts). In the case of random distribution, such a pathway is more unlikely, so overall we expect the results of random distribution to be characterized by higher losses than homogeneously distributed (MR, R, type of inserts) equivalent models.

B.4 Synthesis of Comparative Analysis at the 1 MHz Frequency

Major differences are observed between sample results with a random distribution of inserts, of the same size and different size, difficult to evaluate in this way at the micro-scale. For a more accurate evaluation, it is necessary to analyze the field results, which provide local information and general explanations for micro-scale phenomena. The integration of these results over the whole volume analyzed provides a characterization of the entire material, from a macroscopic point of view, useful in designing the systems.

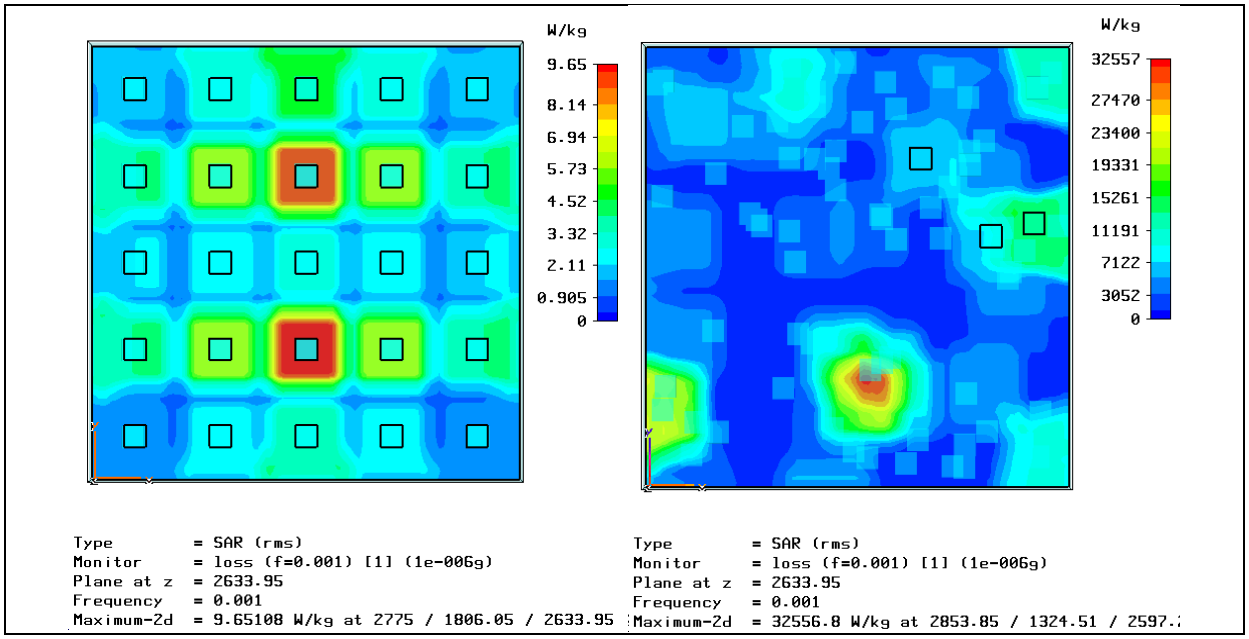

Figure 9-10: Local SAR, MR = 10%, R = 25µm, f = 1MHz, uniform and random distribution of inserts, type B inserts.

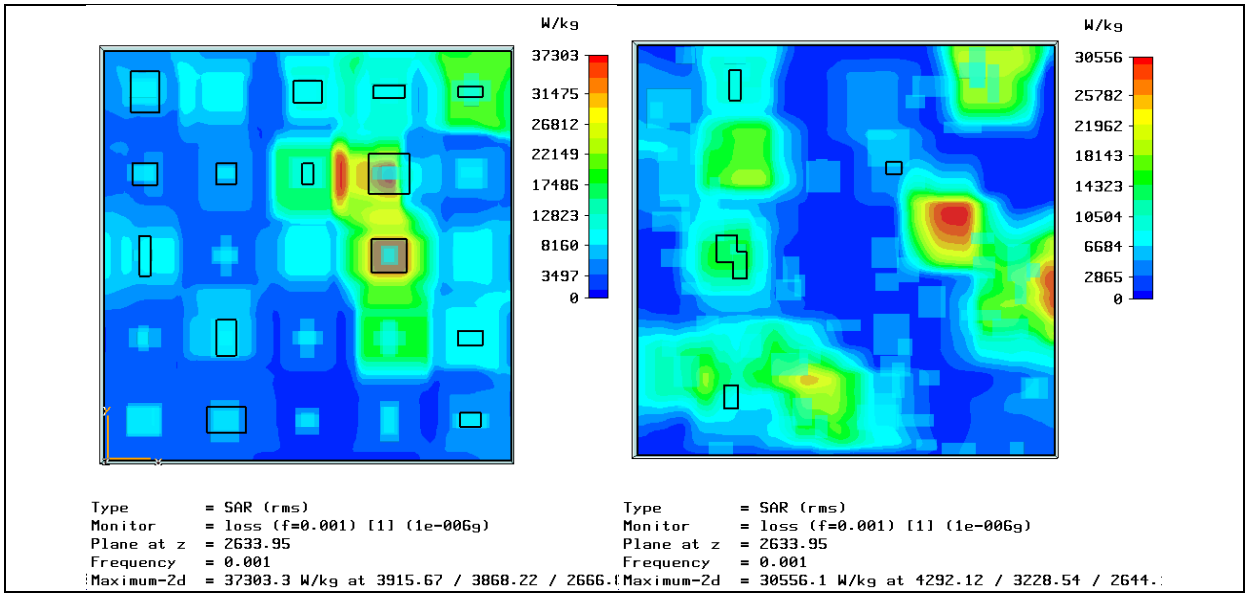

Figure 9-11: . Local SAR, MR = 10%, R = 25µm, f = 1MHz, random distribution of inserts, the same size and different sizes, B-type inserts.

B.5 Investigating the Effect of Particle Size and Particles Concentration (MR)

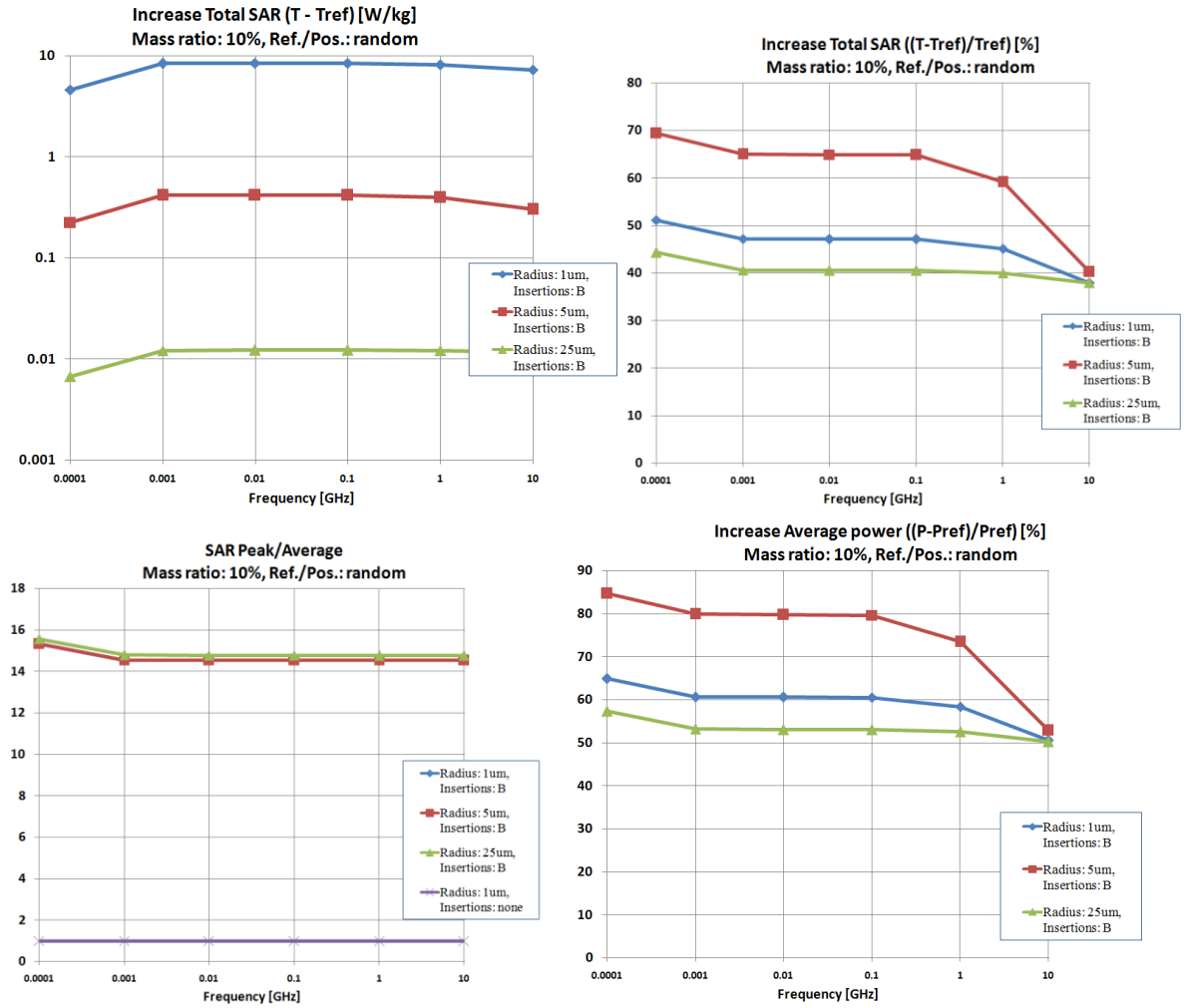

Figure 9-12: Particle size effect, MR = 10%, random distribution

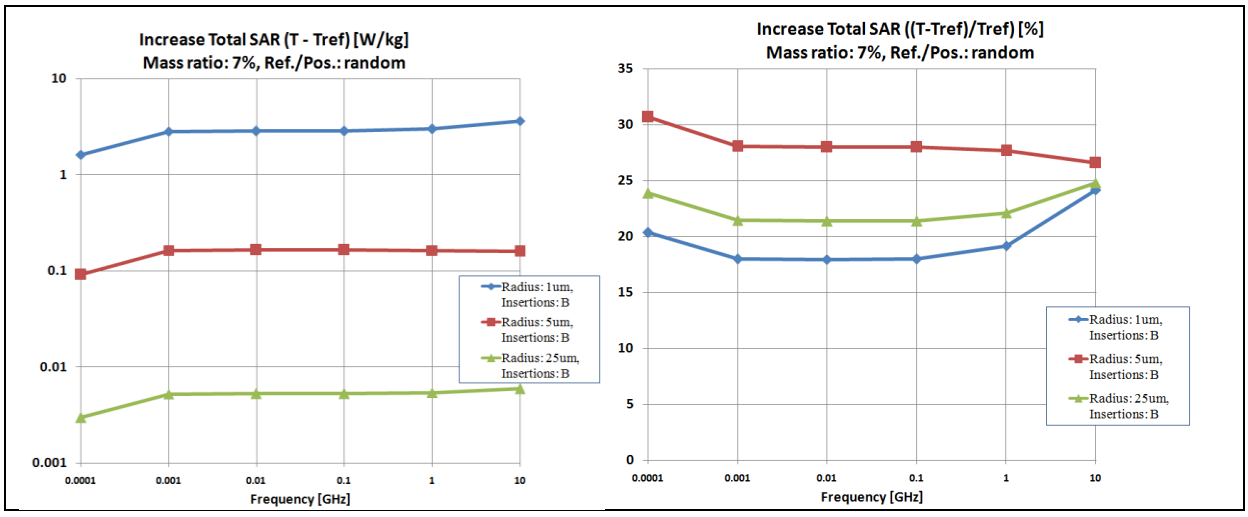

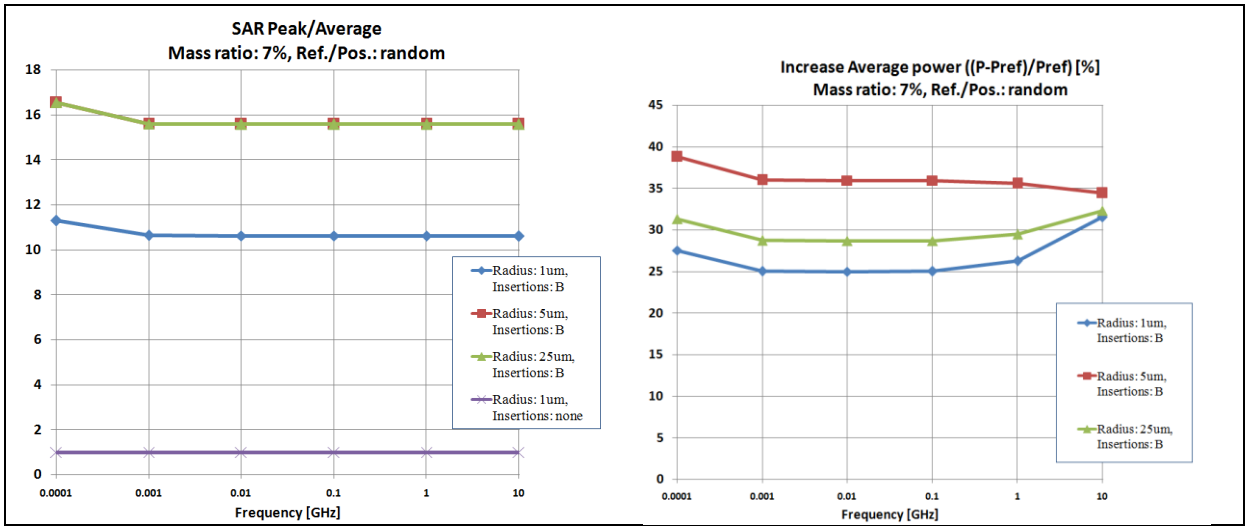

Figure 9-13: Particle size effect, MR = 7%, random distribution

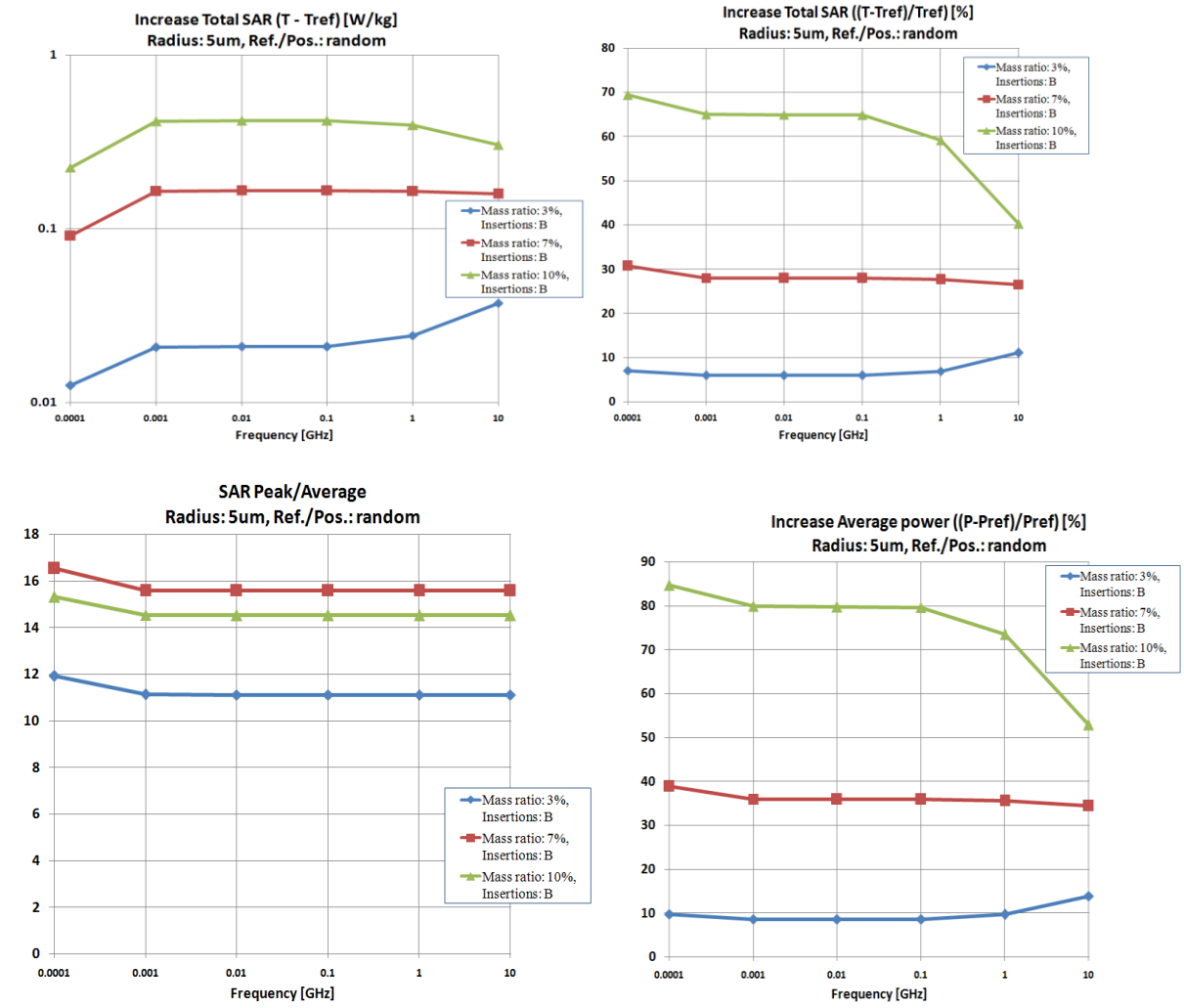

Figure 9-14: The efect of particles concentration , particles with R = 5µm.

B.6 Conclusions

From the results obtained we can see the beneficial effect of the inserts on the absorption capacity of the substrate material. An increase of up to 80% of the average dissipated power is observed (concentration-dependent, but all concentrations tested benefit from increased energy dissipation).

The material used for inserts is of particular importance, with materials with the highest permittivity and with the greatest possible losses being recommended. In the cases analyzed, Type B inserts ($\varepsilon r = 12$, $\tan \delta = 0.09$) have a double efficacy compared to the inserts type A ($\varepsilon r = 7$, $\tan \delta = 0.05$) at any particle size.

A lower mass concentration (e.g. MR = 3%) has a larger particle size (25µm), while at a high concentration a smaller particle size (5µm) gives a more pronounced increase in energy absorption.

B.7 References

[1] Ghodgaonkar D.K., Varadan V.V., Varadan V.K., "Free-Space Measurement of Complex Permittivity and Complex Permeability of Magnetic Materials at Microwave Frequencies", *IEEE Transactions on Instrumentation and Measurement*, 39(2), 1990, pp. 387-394.

[2] CST GmbH, *Application Note, Photonic Crystal Simulation,* Article ID: 296, 2007 - http://www.cst.com.

[3] R. Ciobanu, R.F. Damian, I. Casian Botez, Electromagnetic Characterization of chiral auxetic metamaterials for EMC applications, Computer Standards & Interfaces, Volume 32, Issue 3, March 2010, Pages 101-109.

[4] Agilent E4991A RF Impedance/Material Analyzer, Operation Manual, Ninth Edition, 2012.

[5] IEEE Std C95.1™-2005, "IEEE Standard for Safety Levels with Respect to Human Exposure to Radio Frequency Electromagnetic Fields, 3 kHz to 300 GHz", 2005.

[6] Federal Communications Commission, "Evaluating Compliance with FCC Guidelines for Human Exposure to Radiofrequency Electromagnetic Fields", OET Bulletin 65 (Edition 97-01). Supplement C (Edition 01-01), 2001.

[7] L. Ramajo, A. Cristóbal, P. Botta, J. Porto López, M. Reboredo, M. Castro, ”Dielectric and magnetic response of Fe3O4/epoxy composites”, Composites: Part A 40 (2009) 388–393.

C Image analysis algorithm

Segmentation results and histograms of average background and particle size for all image series taken with RGB microscope are shown on Figure 9-15 to Figure 9-20. The upper row shows the original images, the second row shows the segmented image (with each colour channel segmented independently to make a new RGB image), the third row shows histograms of the background size (black regions in the segmented images) and the bottom row shows histograms of the particle size (white regions in the segmented images).

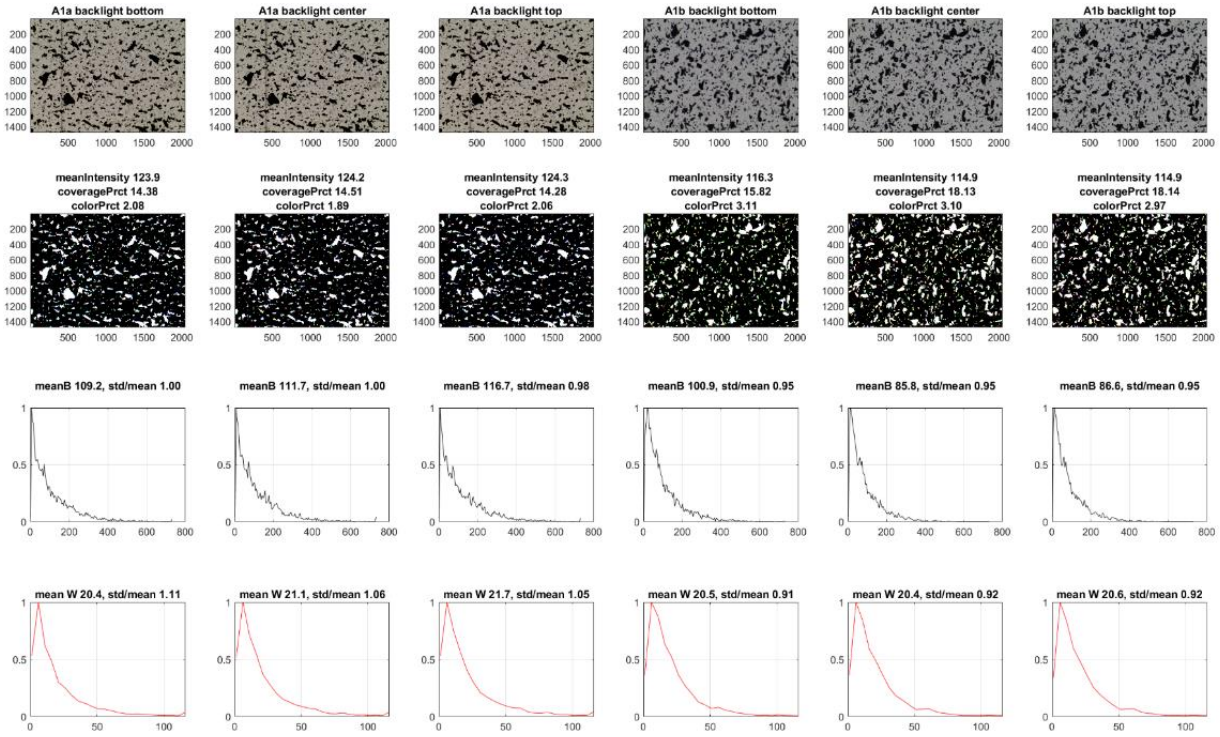

Figure 9-15 Film A1

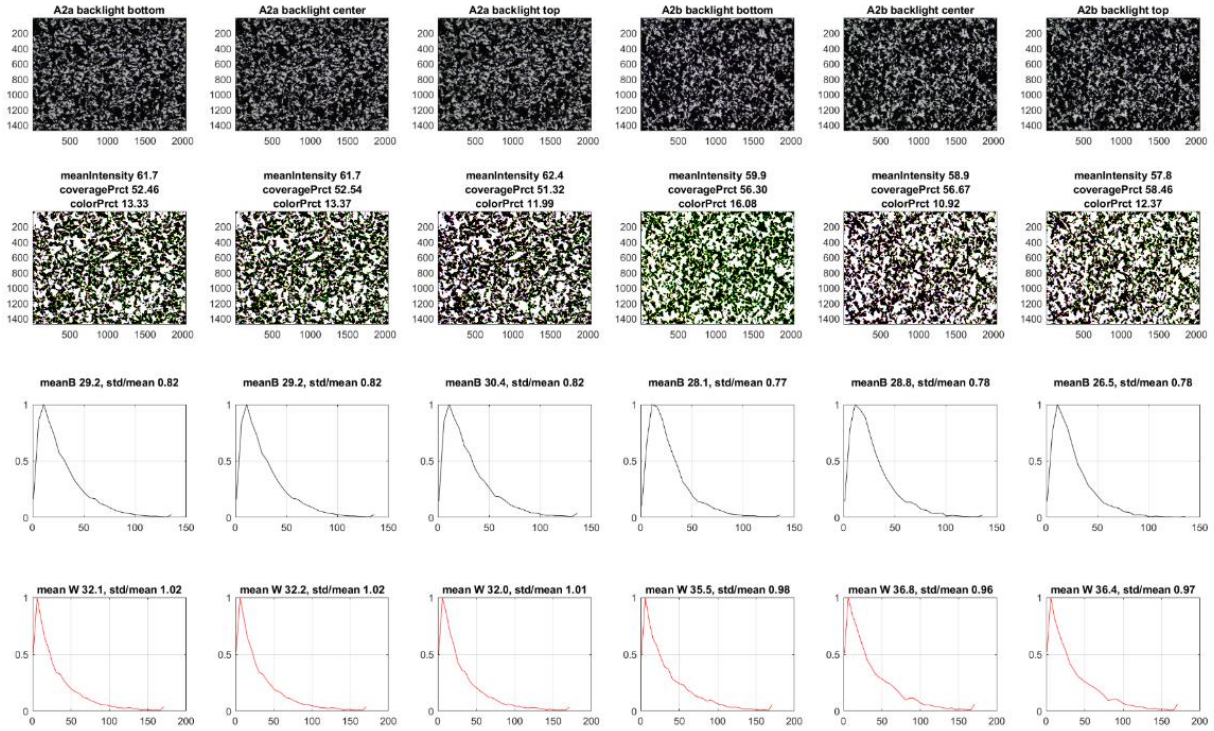

Figure 9-16 Film A2

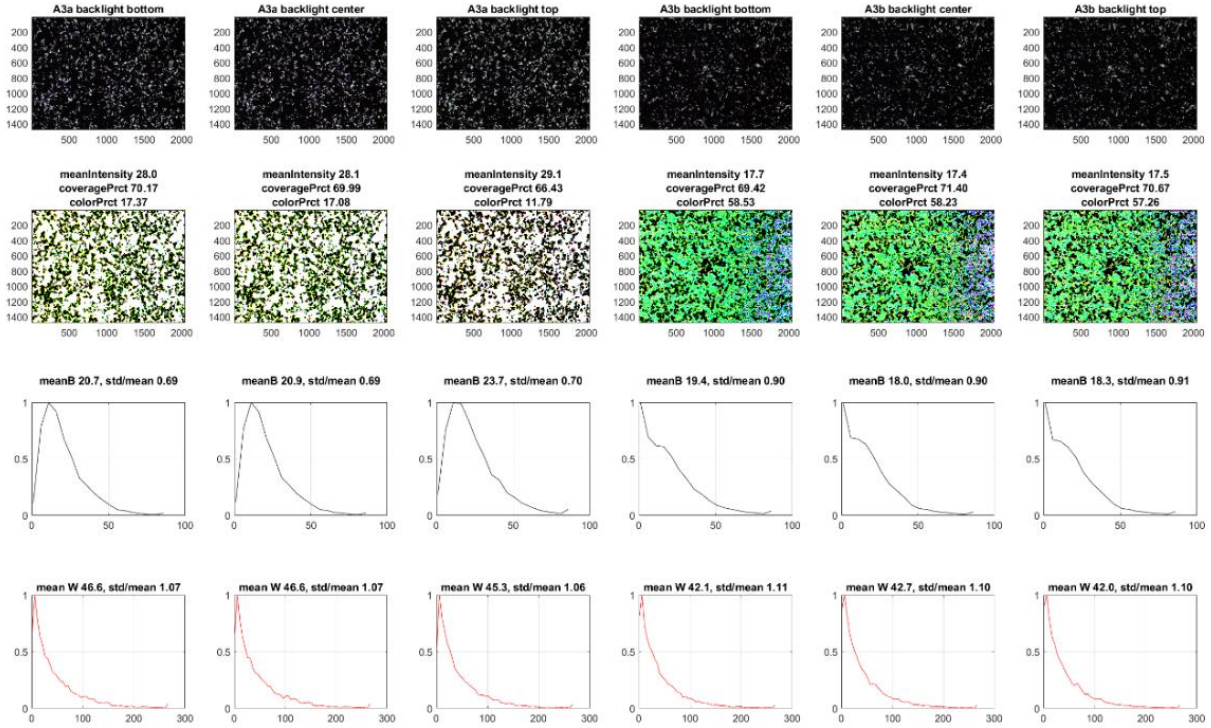

Figure 9-17 Film A3

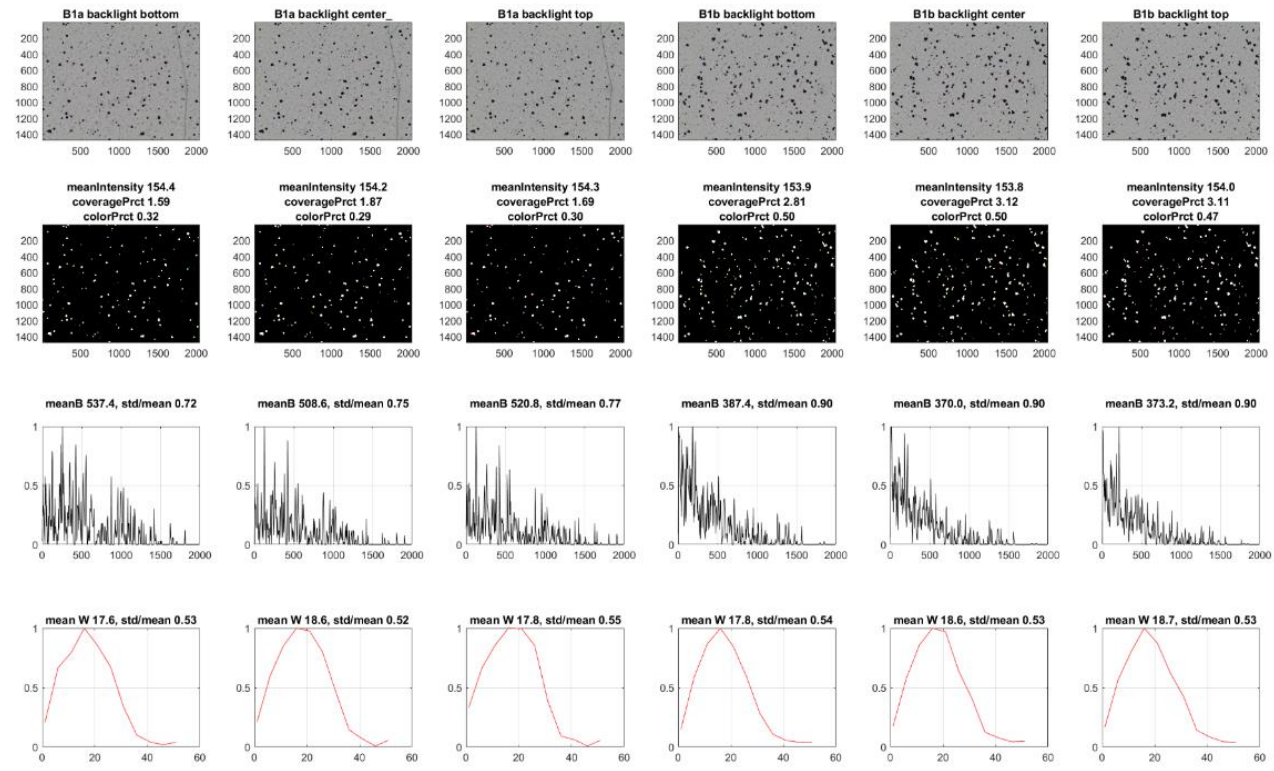

Figure 9-18 Film B1

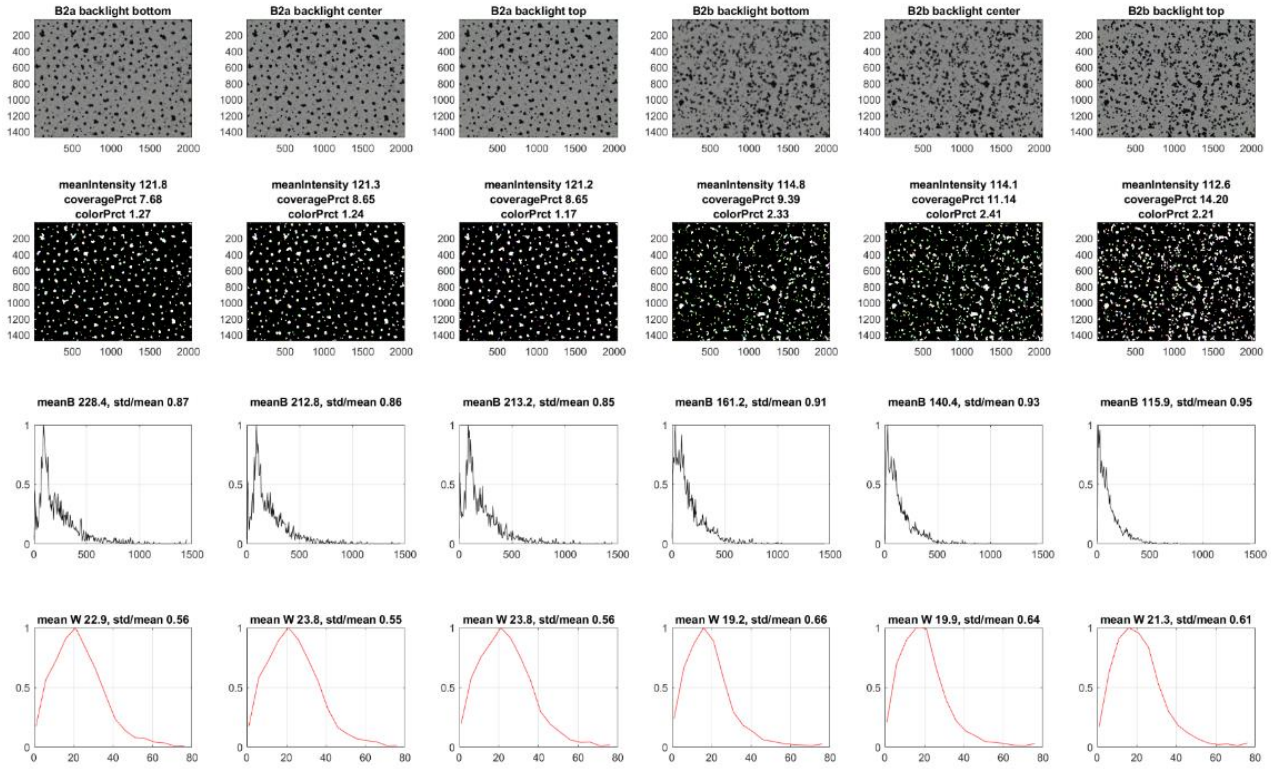

Figure 9-19 Film B2

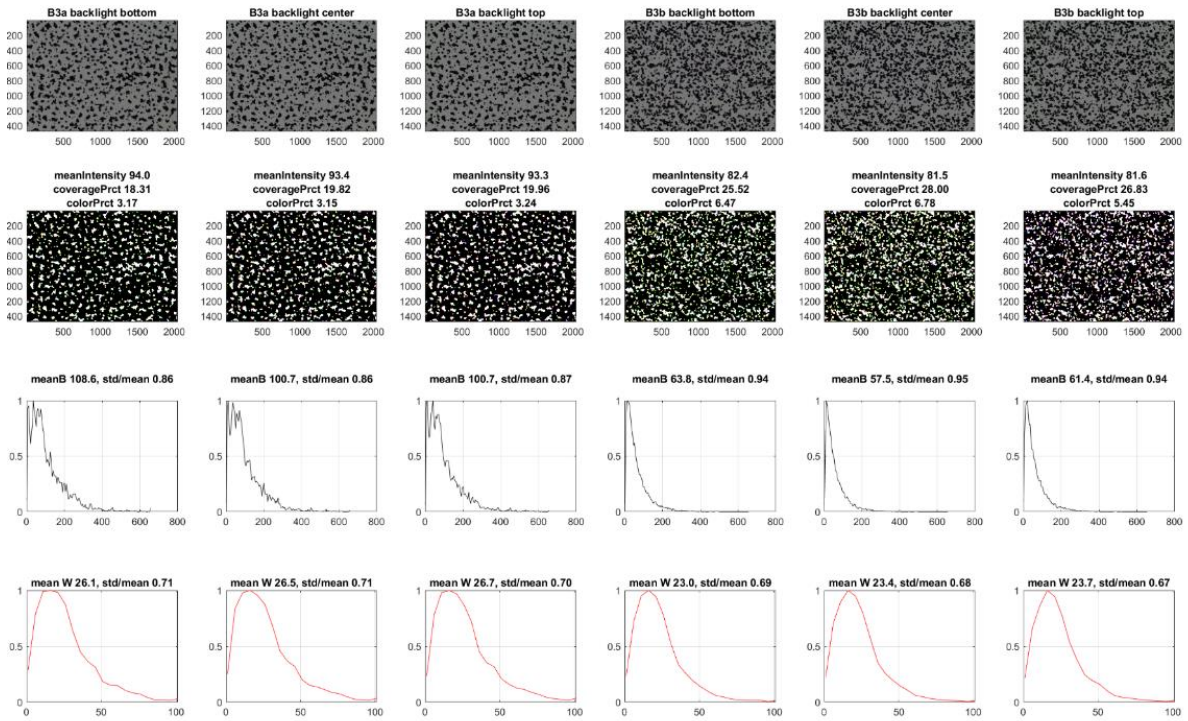

Figure 9-20 Film B3

Table 9-3 Mean value and standard deviation of all measures after and before alignment.

	mean after	mean before	std after	std before	difference % of summed std
B2-g1					
mean particle size	35.2	31.04	15.91	13.7	0.1
mean background size	350.18	195.65	188.77	109.35	0.5
std particle size	12.83	12.61	0.5	0.5	0.2
std background size	194.83	119.06	15.36	10.4	2.9
max background size	1582	953.5	2.83	68.59	8.8
coveragePrct	7.84	12.6	1.03	1.94	1.6
coloredPrtc	1.15	2.18	0.1	0.2	3.4
imQual	3.28	4.37	1.46	1.99	0.3
meanInt	121.4	112.85	0.35	0.24	14.4
imColorsumMean	2.99	2.98	0	0.01	1
B2-g2					
mean particle size	35.33	30.89	15.9	13.57	0.2
mean background size	363.46	205.54	195.26	113.95	0.5
std particle size	12.72	12.61	0.45	0.48	0.1
std background size	200.52	124.16	14.47	10.44	3.1
max background size	1582	1002.5	2.83	4.95	74.5
coveragePrct	7.58	11.96	0.99	1.83	1.6
coloredPrtc	1.15	2.17	0.09	0.2	3.4
imQual	2.9	4.08	1.33	1.88	0.4
meanInt	121.4	112.86	0.35	0.24	14.5
imColorsumMean	2.99	2.98	0.01	0.02	0.5
B2-g4					
mean particle size	35.11	30.89	15.75	13.58	0.1
mean background size	400.17	238.95	212.74	130.71	0.5
std particle size	12.46	12.98	0.41	0.42	0.6
std background size	218.6	139.85	13.07	9.97	3.4
max background size	1585.5	1006.5	3.54	2.12	102.4
coveragePrct	6.74	10.25	0.88	1.56	1.4
coloredPrtc	1.04	1.94	0.09	0.2	3.1

imQual	2.35	3.49	1.09	1.61	0.4
meanInt	121.4	112.86	0.35	0.24	14.5
imColorsumMean	3	2.99	0	0.02	0.4
A1					
mean particle size	21.09	20.5	0.64	0.09	0.8
mean background size	112.52	91.09	3.79	8.48	1.7
std particle size	22.64	18.82	0.22	0.09	12.1
std background size	111.89	86.63	2.79	8.12	2.3
max background size	1043.67	733	0.58	38.97	7.9
coveragePrct	14.39	17.36	0.11	1.34	2
coloredPrtc	2.01	3.06	0.11	0.08	5.7
imQual	5.64	3.98	0.28	0.19	3.5
meanInt	124.14	115.37	0.19	0.8	8.9
imColorsumMean	4.04	3	0.08	0.01	11.2
A2					
mean particle size	32.12	36.24	0.08	0.64	5.7
mean background size	29.6	27.81	0.72	1.16	1
std particle size	32.64	35.22	0.22	0.3	4.9
std background size	24.19	21.57	0.56	0.91	1.8
max background size	239	227	12.12	2.65	0.8
coveragePrct	52.11	57.15	0.68	1.16	2.7
coloredPrtc	12.9	13.12	0.79	2.66	0.1
imQual	7.03	6.88	0.08	0.35	0.3
meanInt	61.92	58.85	0.38	1.08	2.1
imColorsumMean	3.04	3	0.02	0.02	1.1
A3					
mean particle size	46.18	42.29	0.76	0.35	3.5
mean background size	21.77	18.53	1.68	0.74	1.3
std particle size	49.32	46.64	1.04	0.46	1.8
std background size	15.17	16.77	1.31	0.63	0.8
max background size	157	162.33	20.81	15.95	0.1
coveragePrct	68.86	70.5	2.11	1	0.5

coloredPrtc	15.41	58.01	3.15	0.66	11.2
imQual	4.73	2.86	0.05	0.14	9.9
meanInt	28.38	17.52	0.6	0.19	13.7
imColorsumMean	3.16	3.24	0.03	0.03	1.2
B1					
mean particle size	18.02	18.39	0.54	0.47	0.4
mean background size	522.27	376.87	14.43	9.25	6.1
std particle size	9.59	9.8	0.21	0.22	0.5
std background size	391.12	339.21	9.79	7.4	3
max background size	1878.67	1855	56.89	2	0.4
coveragePrct	1.71	3.01	0.14	0.17	4.1
coloredPrtc	0.3	0.49	0.01	0.02	5.8
imQual	1.85	1.88	0.24	0.03	0.1
meanInt	154.29	153.86	0.12	0.1	2
imColorsumMean	3.02	3.01	0	0.01	0.8
B2					
mean particle size	23.46	20.12	0.53	1.08	2.1
mean background size	218.17	139.18	8.88	22.67	2.5
std particle size	13.08	12.76	0.22	0.14	0.9
std background size	187.79	128.8	9.08	17.99	2.2
max background size	1656	985.33	135.1	71.99	3.2
coveragePrct	8.32	11.58	0.56	2.43	1.1
coloredPrtc	1.23	2.31	0.05	0.1	6.9
imQual	2.27	2.9	0.21	0.21	1.5
meanInt	121.42	113.84	0.32	1.15	5.1
imColorsumMean	3	3	0.01	0.02	0.1
B3					
mean particle size	26.41	23.4	0.31	0.35	4.6
mean background size	103.31	60.88	4.57	3.19	5.5
std particle size	18.7	15.88	0.16	0.09	11.4
std background size	89.66	57.42	3.68	2.64	5.1
max background size	831.33	504.33	10.97	13.58	13.3

coveragePrct	19.36	26.78	0.91	1.24	3.4
coloredPrtc	3.19	6.23	0.05	0.7	4.1
imQual	2.95	3.98	0.19	0.23	2.5
meanInt	93.58	81.82	0.36	0.5	13.7
imColorsumMean	3	2.99	0	0.02	0.3

D Optic instrumentation

Four versions of a high-resolution imaging optical set-up have been established during the project. Several modifications have been made to reach a set-up optimized for a final application to the R2R line of CondAlign. The modifications consist in:

- Evolving from CCD cooled down camera to low cost CMOS industrial camera
- Expanding the field of view of the optical and reducing optical resolution.

The first version of the optical system is a conventional RGB microscope (D.1). The second version is an industrial camera-based microscope (D.2). The third version makes used of an industrial camera with improved resolution (D.3). In the fourth version, we expand the field of view by making use of a telecentric lens (D.4). Eventually, the last version has been installed on the R2R line of CondAlign. The various versions are described in the following sub-chapter.

D.1 RGB microscope

The RGB microscope use for these studies is an Olympus BX60F5 Upright Metallurgical Microscope with Motorized Stage. Images were acquired in transmission and reflectance mode.

Figure 9-21: RGB Olympus BX60F5 Upright Metallurgical Microscope

D.2 Industrial based microscope version 0

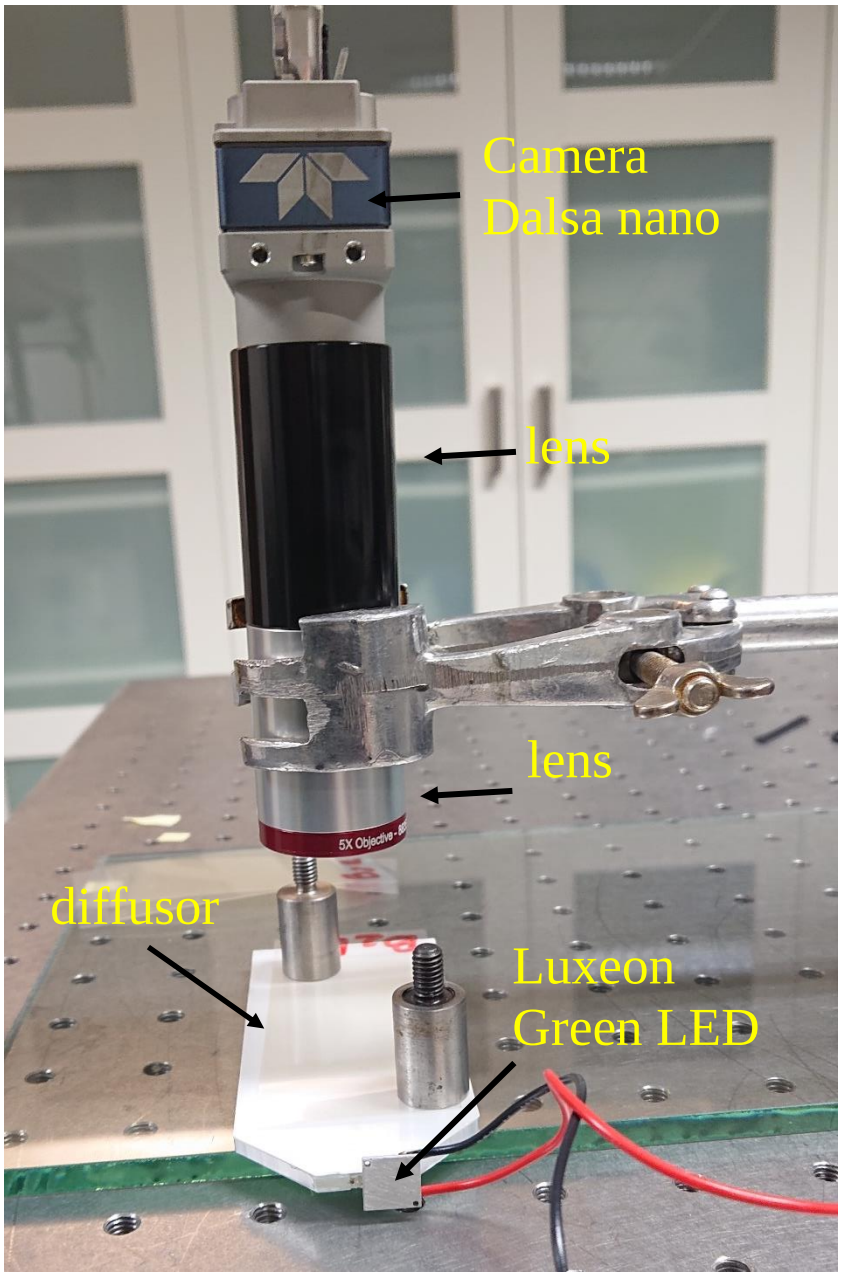

Figure 9-22: The industrial camera-based imaging system comprises a Dalsa nano camera, an imaging lens from Edmunds optic and a modified LED backlight module from Adafruit. The Dalsa nano camera has 1984 by 1264 pixels. The pixels are 4.8 µm. The objective lens are diffraction limited objective or relay lenses from Edmunds optic.

The industrial camera-based imaging system comprises a Dalsa nano camera, an imaging lens from Edmunds optic and a modified LED backlight module from Adafruit. The Dalsa nano camera has 1984 by 1264 pixels with 4.8 µm by 4.8 µm pixels. Important camera specifications are given in Table 9-4.

Table 9-4: Dalsa nano camera G3-GM12-M1930

Camera parameters	Value
Full well capacity	10000 phe
Format	8-10 bit
Min Exposure time	87 us
Resolution	1920x1200
Pixel size	4.8 um

The objective lens are diffraction limited objective and relay lenses from Edmunds optic. Three magnifications are available x1, x2 and x5.

The light sources were white LED backlight module from Adafruit and modified one to allow utilization of more powerful Luxeon Green LED with central wavelength 567 nm. In the modified one, the Luxeon LED is glued on one side of the waveguide, see Figure 9-23. The 3.5 mm thick acrylic strip diffuse light and provides near-uniform lighting. One flat side of the strip has a reflector on it to increase the reflection in one direction only.

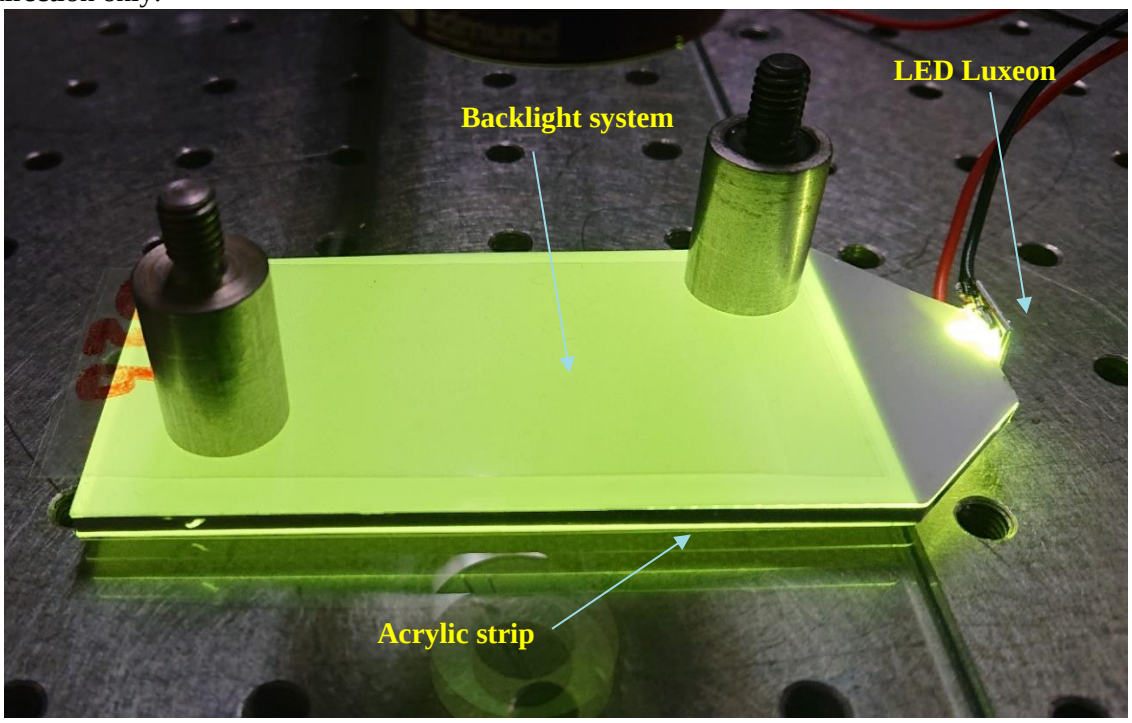

Figure 9-23: Modified LED backlight system. The original LED has been removed and a Luxeon LED is glued on the side and light coupled into the acrylic stripe. A non-aligned sample (B2b is positioned on the diffusor.

D.3 Industrial microscope version 1

A 20 Mpixels camera from FLIR, blackfly model BFS-U3-200S6M-C, is used for acquisition of images. The pixel size is 2.4 um, the saturation capacity 14794 e- and the read noise 3.26 e-. The main characteristics of the camera are listed in Table 9-5. By increasing the resolution to 20 Mp, we increase the spatial resolution of the system by a factor of two in comparison to the previous model. The camera and lenses are fixed to a rotation stages and two linear translation stages. The rotation stage allows varying the angle between the central axis of the field of view and the direction perpendicular to the plane of the film. In that way, we can observe the particle chains from various angle. We can translate the optical system horizontally and vertically using the linear translation stages. This open for scanning of the film and acquiring images at various position and various distances from the film.

Both Black and White and RGB camera have been evaluated. Similarly, to version 0, the objective lens are diffraction limited objective and relay lenses from Edmunds optic.

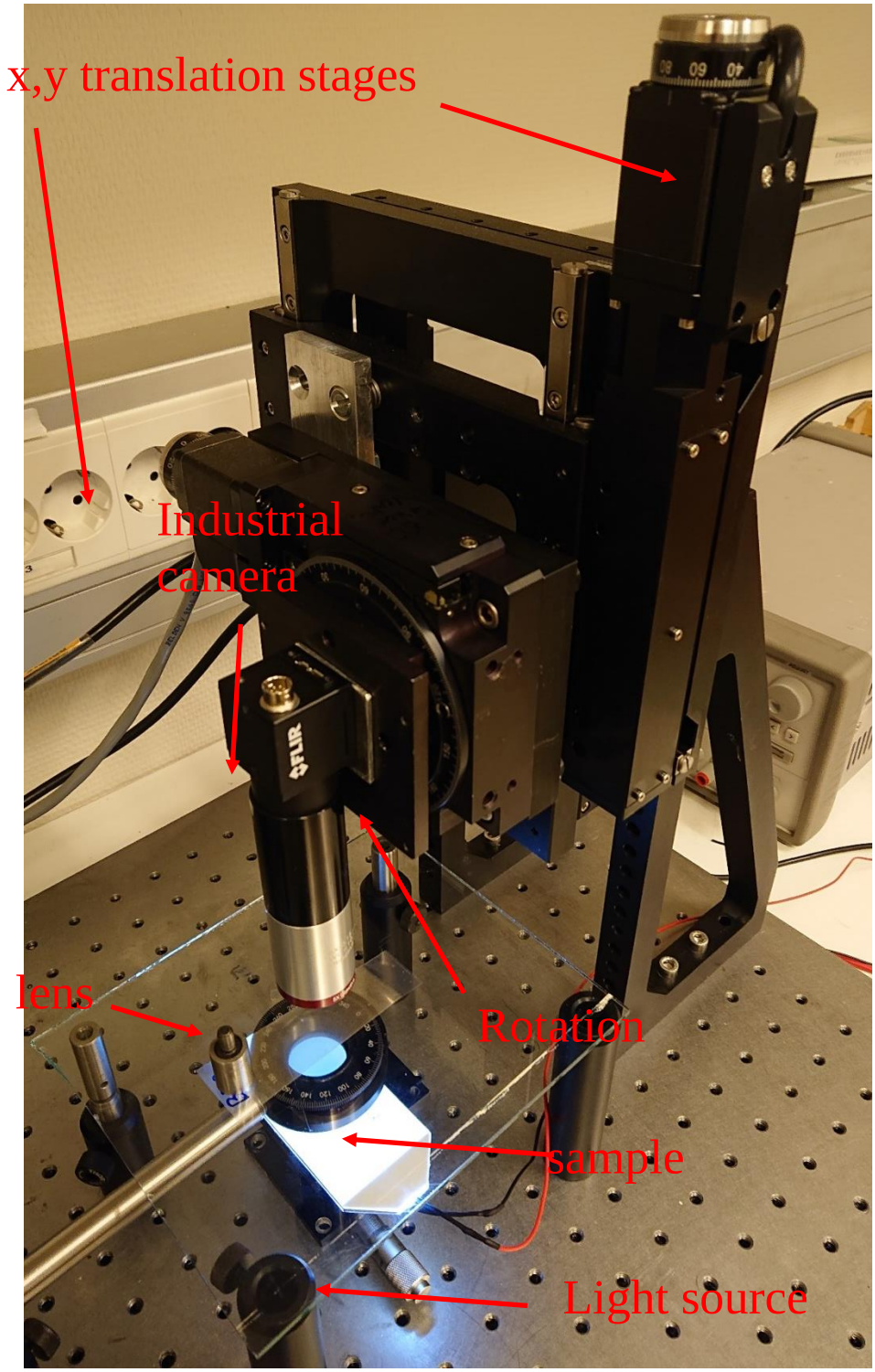

Figure 9-24: Industrial microscope version 1.

Table 9-5: characteristics of the industrial camera FLIR blackfly model

Camera parameters	Value
Full well capacity	14794 phe
Format	10-12 bit
Min Exposure time	67 us
Resolution	5472x3648
Pixel size	2.4 um
Temporal dark noise	3.26 e-
Quantum efficiency at 525 nm	79 %
Frame rate	18

Several light sources have been evaluated with this version of the optical system, i.e. a white and green LED backlight module as in the previous systems (see Figure 9-24) but also a new illumination source which provide higher light intensity and more efficient homogenous illumination of the sample. This last version is made of two Luxeon Green LED whose illumination pattern is shaped and homogenized by a 3D printed white diffuser, see Figure 9-25. On top of the 3D printed device, plastic diffusor with various grain concentration are utilized to further diffuse the light in 2pi steradian.

Figure 9-25: Light source of Industrial microscope version 1

D.4 Industrial microscope version 2

The 20 Mp Black fly camera is selected for the in-line optical system to be installed on the R2R line. A telecentric lens from Edmunds optic, 0.25X 2/3" GoldTL™ (Figure 9-26), is used to image a ~4 cm by 4 cm region from the ACF film onto the sensor of the camera. The lens magnification is ~0.2. The light source is identical to the version 1.

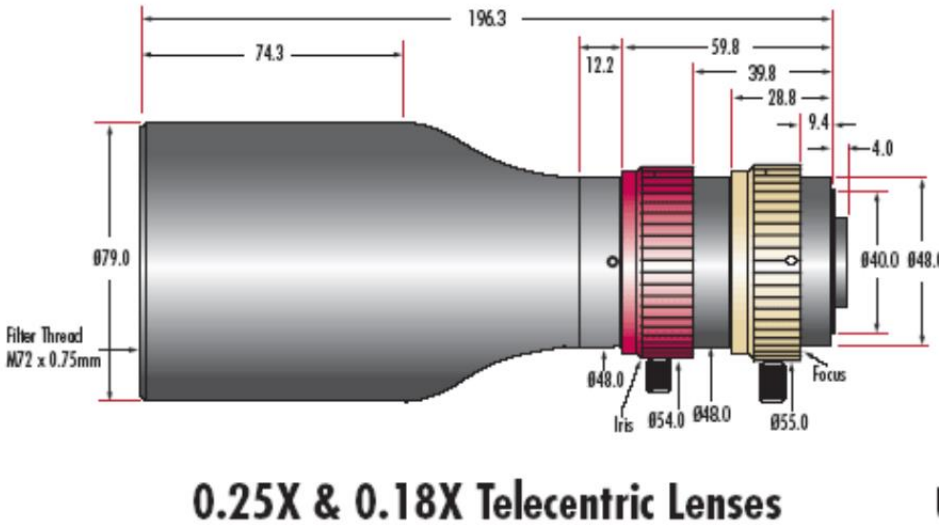

Figure 9-26: Telecentric lens for large field of view imaging

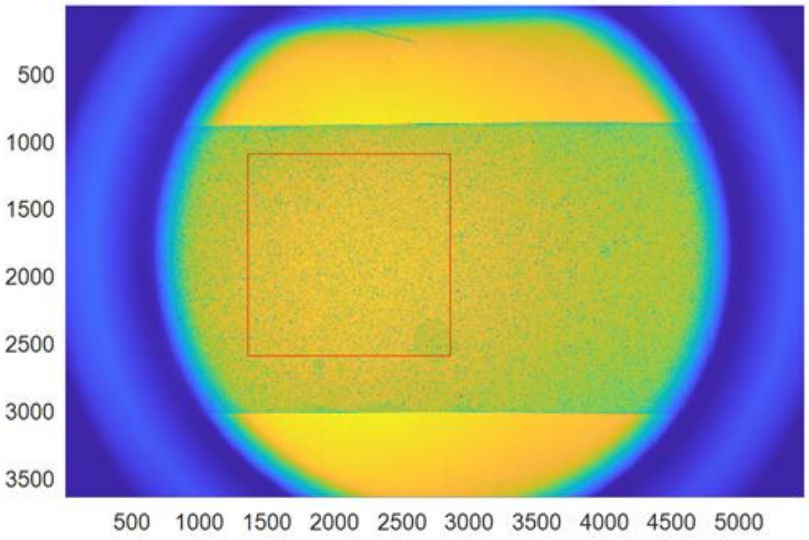

Figure 9-27: Example of image of one of the sample acquired by the optical system version 2. The field of view in the image plan is larger than the aperture of the lens. The effective field of view is a circle with a Ø~4 cm

E Spectral transmission investigation

Transmission spectroscopy is performed in the visible (VIS) from 300 nm to 800 nm.

E.1 Set up

The set up consists in an Ocean Optics spectrometer (OO), a sample holder and a halogen lamp. The halogen lamp provides illumination over a broad wavelength range (Detectable over 450 nm to 1000 nm by the OO spectrometer). The measurement set up is illustrated on Figure 9-28. The light attenuated by the samples is measured as function of wavelength by the spectrometer.

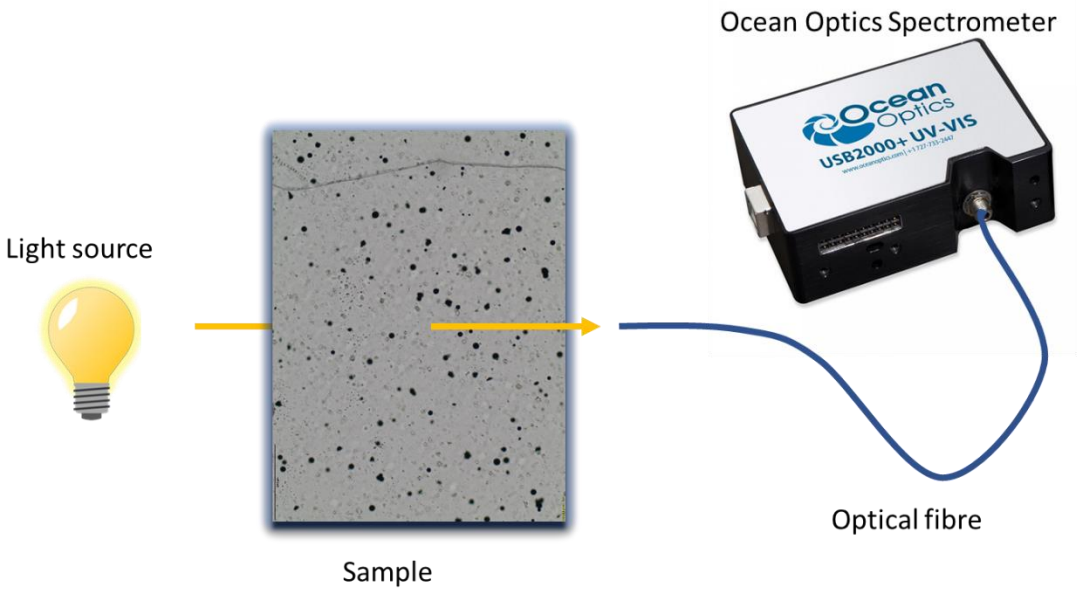

Figure 9-28: Set up for measuring spectral transmission in CondAlign polymer sample

E.2 Measurement method

Spectra are acquired at various position in the sample. Reference measurement (without sample) and black measurement (with light source off) are acquired beforehand. The spectra are corrected both for the dark and the reference, i.e.

$$S(\lambda) = \frac{S_{raw}(\lambda) - S_{ref}(\lambda)}{S_{dark}(\lambda)}$$

The acquisition time for a single spectrum is 30 ms. We take 10 Spectra for each sample and position. The mean over 10 spectra is used for study and presentation. For each sample, three positions are investigated.

E.3 Transmission results

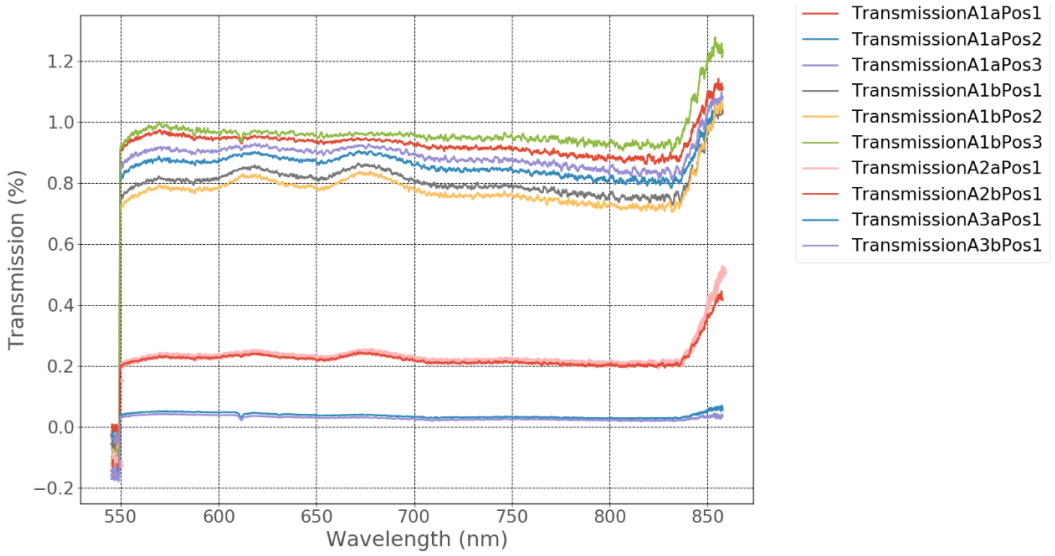

Figure 9-29: Transmission spectra of CondAlign sample with different particle loading

Figure 9-29 show the corrected transmission spectra for sample A1 to A3. The spectra are mostly flat, and no wavelengths presents really advantages over the other when it comes to transmission strength. Within one sample, there can be up to 20 % variations for the transmission from one position to another (sample A1 b). Inspection of the sample reveals that the density of particles is distributed in homogeneously in the transverse direction. Position with higher loading alternates with position with lower loading.
Figure 9-30 shows the transmission averaged over all the wavelength as function of particles loadings for all the samples. We see that the mean transmission over the sample is inversely proportional with the particle loadings. There is a difference factor of around 90 % between the sample presenting the highest transmission and the sample presenting the lowest.

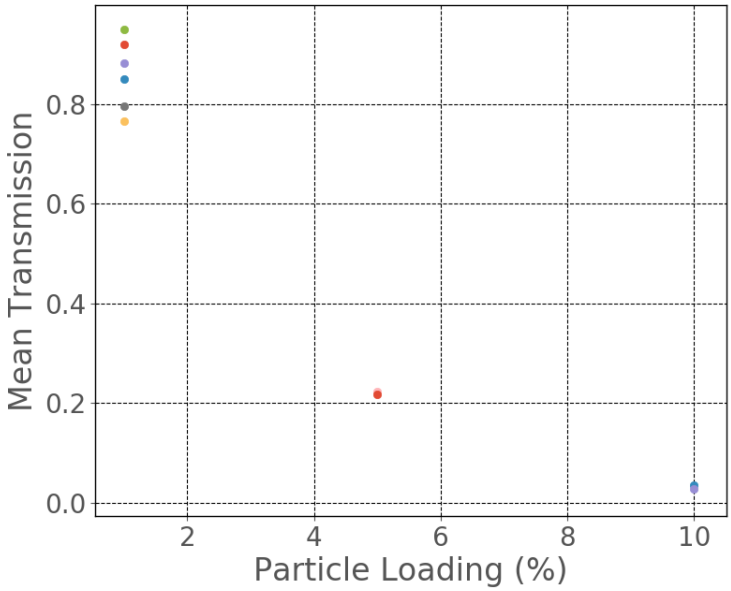

Figure 9-30: Averaged transmission versus particle loading

Conclusion:

- No spectral window giving a better transmission
- Samples with high particle loading can have up to 90 % less transmission than sample with low loading

F Manufacturing sample for Design Of Experiment

The procedure for preparing the sample for the Design Of Experiment are presented in two power point presentation, one for the first design of experiment (F.1) and the second one for the second design of experiment (F.2).

F.1 Sample manufacturing procedure in first DOE

CondAlign+
conductive alignment

DOE
Samples making
WP3- WP4
2019-03-19

Confidential

F.2 Sample manufacturing procedure in second DOE

CondAlign+
conductive alignment

2nd DOE
Samples making
WP3- WP4
2019-06-11

Confidential

G Analysis of grey scale images from industrial camera-based system

The images of series B2 that were acquired with the Dalsa camera were analysed according to the algorithms described in 4.3. Due to the lower resolution of these images, small objects were not removed. Several features were again evaluated on the segmented images, but since the images were monochrome, we could not evaluate any colour features.

The results for the different magnifications are shown in Figure 9-31, **Figure 9-32** and **Figure 9-33**. We see that the results are good for 1x, whereas there is some overlap at 2x and 5x. This is because some of the images at 2x and 5x were out of focus. To overcome this problem, it may be necessary to take images at a few different focus distances to ensure that one of the images is properly focused even if the film moves slightly up or down relative to the ideal position. The edge-based image quality measure (titled imQual in the figures) can be used to decide which image to use for analysis (larger measure = better focus). When the defocused images are left out from the analysis, we get similar results for 2x and 5x as for 1x (**Figure 9-34** and **Figure 9-35**). The two remaining outlier values at 2x (mean particle size 4 pixels instead of 3.5 pixels and coverage percentage > 10) are due to images with too high exposure time leading to saturated pixel values. This gives inaccurate segmentation because the true background level is not known when too many pixels are saturated. In practical use this can be avoided by setting a suitable exposure time at the beginning of a film series or by adjusting the exposure time iteratively based on the acquired images.

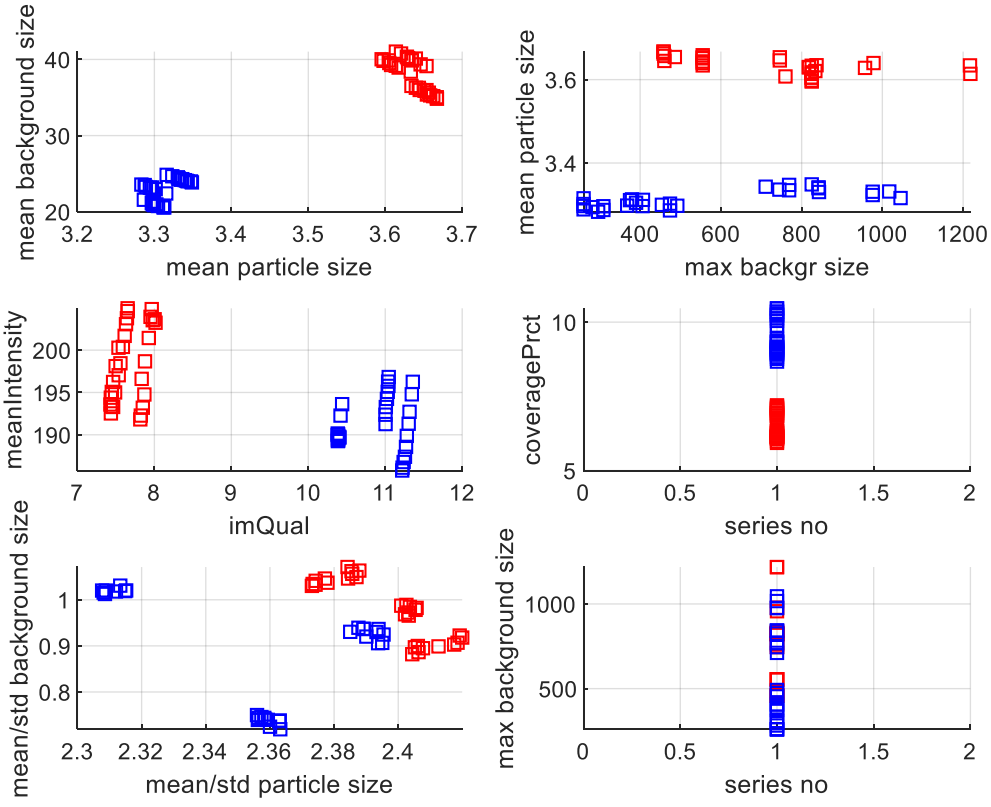

Figure 9-31 Analysis results for film B2 (in pixels and percentages) at 1x magnification. All images at 1x were in focus. Images taken before alignment are shown with blue markers, and after alignment are shown with red markers.

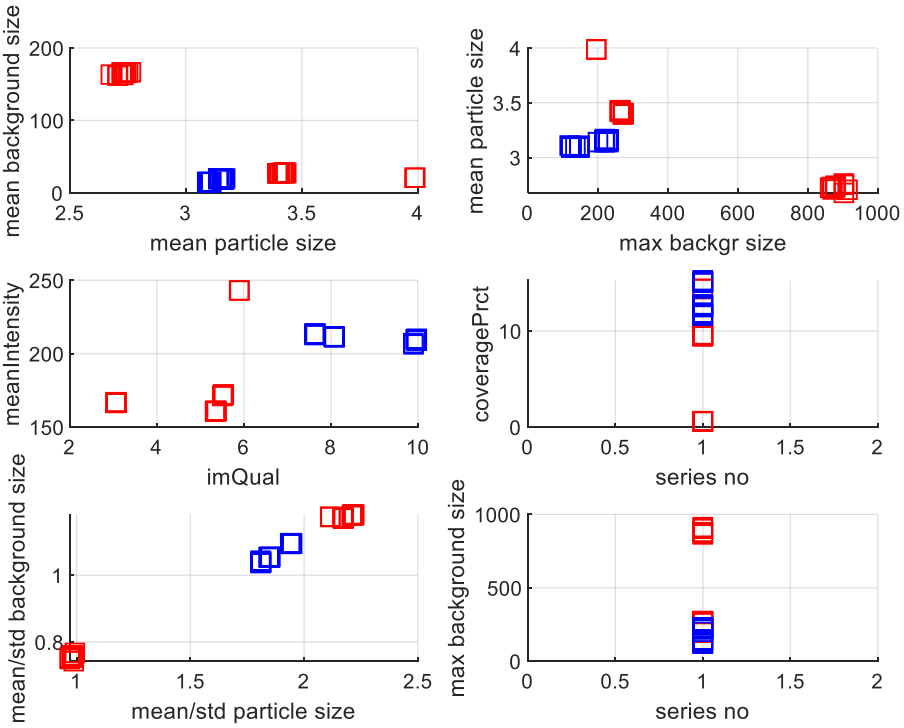

Figure 9-32 Analysis results for film B2 (in pixels and percentages) at 2x magnification with defocused images included. Images taken before alignment are shown with blue markers, and after alignment are shown with red markers.

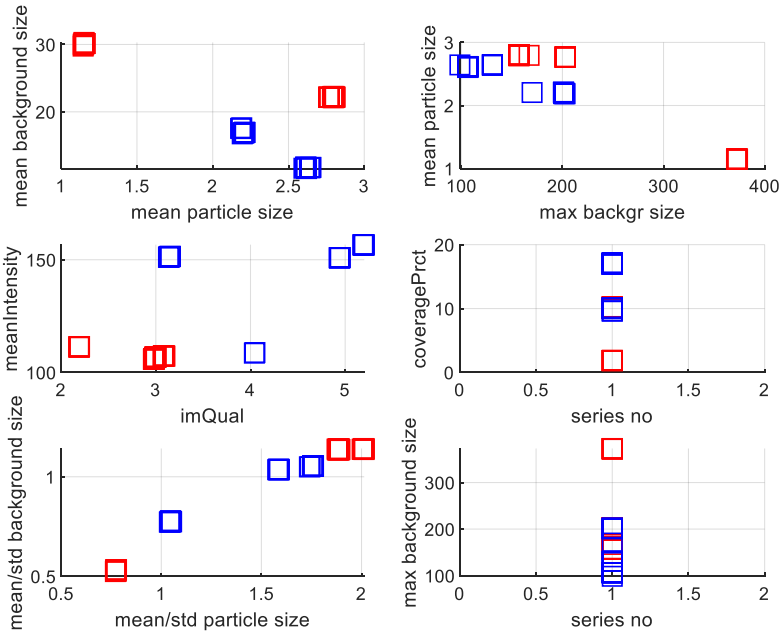

Figure 9-33 Analysis results for film B2 (in pixels and percentages) at 5x magnification with defocused images included. Images taken before alignment are shown with blue markers, and after alignment are shown with red markers.

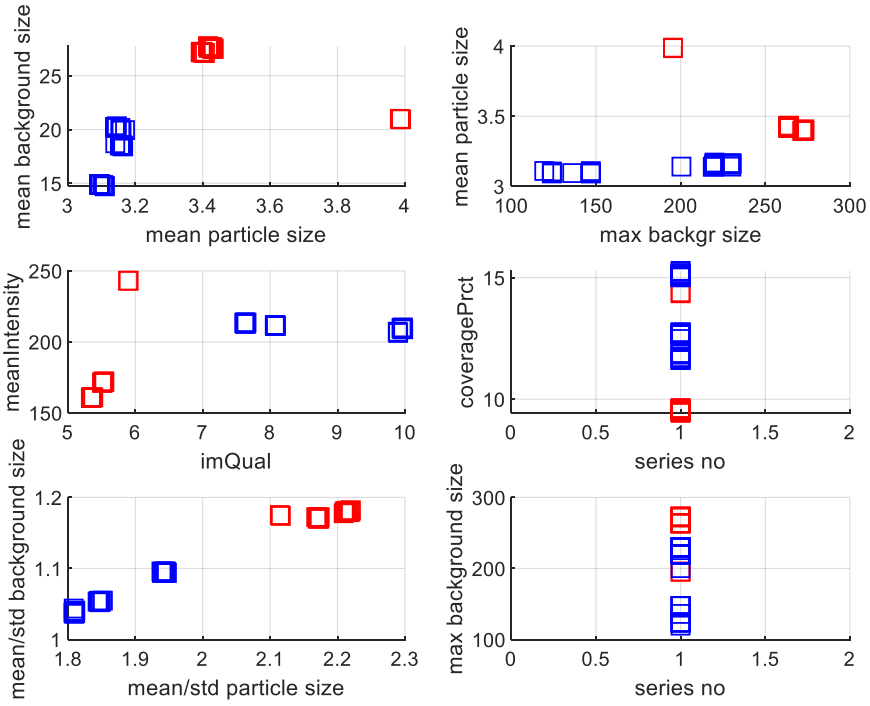

Figure 9-34 Analysis results for film B2 (in pixels and percentages) at 2x magnification with defocused images removed.

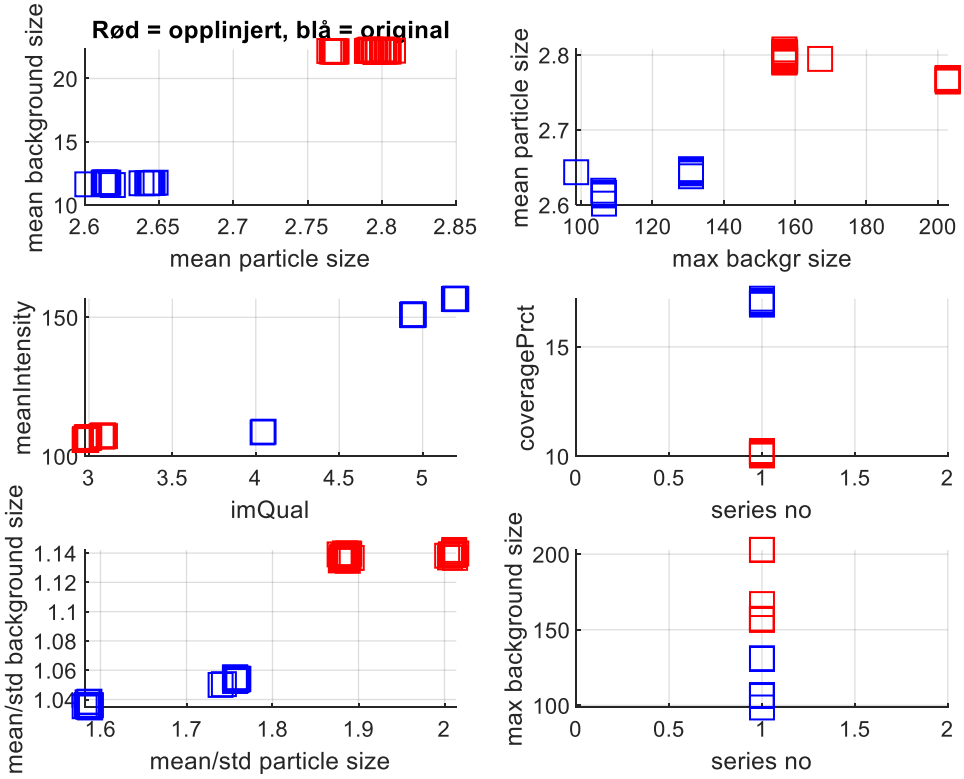

Figure 9-35 Analysis results for film B2 (in pixels and percentages) at 5x magnification with defocused images removed.

Technology for a better society

www.sintef.no